The Role of Amphibole in the Evolution of Arc Magmas and Crust: the Case from the Jurassic Bonanza Arc section, Vancouver Island, Canada

by

Jeffrey Paul Larocque

B.Sc., McGill University, 2005

A Thesis Submitted in Partial Fulfillment of the

Requirements for the Degree of

MASTER OF SCIENCE

In the School of Earth and Ocean Sciences

University of Victoria

The Role of Amphibole in the Evolution of Arc Magmas and Crust: the Case from the Jurassic Bonanza Arc section, Vancouver Island, Canada

by

Jeffrey Paul Larocque

B.Sc., McGill University, 2005

Supervisory Committee

Dr. Dante Canil, (School of Earth and Ocean Sciences)

Supervisor

Dr. Laurence Coogan, (School of Earth and Ocean Sciences)

Departmental Member

Dr. Kevin Telmer, (School of Earth and Ocean Sciences)

Departmental Member

Supervisory Committee

Dr. Dante Canil, Supervisor (School of Earth and Ocean Sciences)

Dr. Laurence Coogan, Departmental Member (School of Earth and Ocean Sciences)

Dr. Kevin Telmer, Departmental Member (School of Earth and Ocean Sciences)

ABSTRACT

Exposed on Vancouver Island, British Columbia, the Jurassic Bonanza arc is believed to represent the southerly continuation of the Talkeetna arc. Small bodies of mafic and ultramafic cumulates within deeper plutonic levels of the arc constrain the fractionation pathways leading from high-MgO basalt to andesite-dacite compositions. The removal of amphibole from the most primitive non-cumulate compositions controls the compositions of mafic plutons and volcanics until the onset of plagioclase crystallization. This removal is accomplished by the intercumulus crystallization of large amphibole oikocrysts in primitive olivine hornblendite cumulates. Experimental hornblende compositions that crystallize from high-MgO basalts similar to primitive basalts from the Bonanza arc show a good correlation between octahedral Al in hornblende and pressure, and provide a means of estimating crystallization pressures during differentiation of primitive arc basalt. Application of an empirical barometer derived from experimental amphibole data ($P = Al(6)/0.056 – 0.143$; $r^2 = 0.923$) to natural hornblendes from this study suggests that crystallization of primitive basalts took place at 470-880 MPa. Two-pyroxene thermometry gives a result of 1058 +/- 91 ºC for the only olivine hornblendite sample with both pyroxenes. Lever rule calculations require the removal of 30-45 % hornblende

from the most primitive basalt compositions to generate basaltic andesite, and a further 48% crystallization of hornblende gabbro to generate dacitic compositions. Hornblende removal is more efficient at generating intermediate compositions than anhydrous gabbroic fractionating assemblages, which require up to 70% crystallization to reach basaltic andesite from similar starting compositions. There are no magmatic analogues to bulk continental crust in the Bonanza arc; no amount of delamination of ultramafic cumulates will push the bulk arc composition to high-Mg# andesite. Garnet removal appears to be a key factor in producing bulk continental crust.

TABLE OF CONTENTS

Chapter 3

Bibliography

Appendices

List of Tables

List of Figures

Acknowledgments

Firstly, I would like to thank Dante for all of his support during my time at UVic. He gave me plenty of space to pursue my own ideas, but was always there when I needed guidance. What more could I ask for. Secondly, thank you to Robyn, for pushing me when it was needed. Thanks as well to Laurence, who suggested many useful papers, as well as helping me through my analytical difficulties. Gary Pearson and Perry Heatherington were instrumental in getting the project off the ground, providing funding as well as local expertise – thank you both very much. Funding for field and analytical work was also provided by Geoscience BC. I would also like to thank Holly Steenkamp for her assistance in the field. I benefited greatly from working under the tutelage of Graham Nixon at the BCGS. Thank you Graham for your input, and for showing me how proper field work is done. Lastly, thanks to those people who made my windowless office space a pleasant place: Dave, Abi, Jody, Jason, Zhihuan, Angela, Sussi, and Kimberly.

Chapter 1

INTRODUCTION

The mechanism whereby Earth's continental crust has been generated remains a first-order problem in geology. Important geochemical similarities between bulk continental crust and arc magmas, namely positive mantle-normalized Pb and negative Nb-Ta anomalies (Arculus, 1999; Rudnick & Gao, 2003; Hawkesworth & Kemp, 2006 and references therein), require that arc magmas have been a key component in the generation of the continents. Primary arc basalt is believed to be generated in the mantle wedge overlying the subducting plate, due to the influence of hydrous fluids released during dehydration of the oceanic lithosphere on the peridotite solidus (Grove *et al*., 2003; Ulmer, 2001).

Given that most primary arc magmas are basaltic (DeBari, 1997), and that basalts appear to be the most common extrusive rock type in arc environments (Arculus, 1981; Rudnick, 1995), one would expect that the continents should have a basaltic bulk composition. The best estimate of the composition of the bulk continental crust, however, is andesitic (Rudnick & Gao, 2003).

The generation of intermediate magmas (andesite *sensu lato*) can be accomplished in different ways. One long-held hypothesis conceives of felsic magmas as representing the residual liquids from the crystallization of more mafic compositions (e.g. Bowen, 1928; Grove & Kinzler, 1986; Prouteau & Scaillet, 2003). The problem of identifying the large volumes of cumulate rocks which must accompany such protracted crystal fractionation has led to models in which evolved magmas are viewed as the results of partial melting of pre-existing crust (e.g. Huppert & Sparks, 1988). Indeed, the close correspondence between many felsic magma compositions and the eutectic point in simple analogues of the crust provides support for the

crustal anatexis model (Arculus, 1999). Intermediate compositions could therefore arise either from some degree of fractionation, or mixing of felsic and mafic end-member magmas, or a hybrid of the two processes (e.g. Eichelberger *et al*., 2006; Annen *et al*., 2006). Regardless of which process is invoked, the compositional gap between arc contributions from the mantle and bulk continental crust persists.

The presence of mafic and ultramafic cumulate rocks in arc terranes suggests that crystal fractionation plays an important role in arc petrogenesis. The question of which mineral(s) constitute the fractionating assemblage driving the evolution of liquid compositions in arcs from primary basalt to andesite remains a source of disagreement. Phenocryst assemblages in arc volcanics have been used as a constraint on possible fractionation assemblages (e.g. Cawthorn & O'Hara, 1976 and references therein), and this has led to a widespread appeal to a gabbroic mineral assemblage consisting of olivine – augite – plagioclase – magnetite (Gill, 1981). The abundance, however, of amphibole-bearing cumulate rocks, both as plutons and as cognate xenoliths in arc lavas, suggests that amphibole plays an important role in the differentiation of many arc suites (e.g. Cawthorn *et al*., 1973; Arculus & Wills, 1980). Recent work using Dy/Yb ratios from individual arc volcanoes worldwide has shown that in many cases, amphibole must be involved in the differentiation of primitive arc basalt to yield more evolved compositions (Davidson *et al*., 2007).

The relative importance of mafic and ultramafic cumulates in arc settings can be investigated where uplift and erosion have exposed arc crustal cross-sections, including both the plutonic and volcanic sequences. These exhumed arc sections provide direct field evidence pertaining to the mechanisms of differentiation of island arc crust. This in turn may shed light on

the relationship between island arc crust and the bulk composition of the continental crust (eg. Burns, 1985; Greene *et al*., 2006; Jagoutz *et al*., 2006).

Exposed on Vancouver Island, the Jurassic Bonanza arc is believed to represent the southerly continuation of the Talkeetna arc (DeBari *et al*., 1999; Clift *et al*., 2005). The arc section preserves both deep plutonic roots and sub-aerial volcanics and volcaniclastics, offering a window into the processes and products of differentiation at depth beneath the arc. Within the deeper plutons, hornblende-rich mafic to ultramafic cumulates are preserved which provide constraints on the mechanisms and P-T conditions of the differentiation of island arc basalt.

Thesis Overview

This thesis is organized as one large comprehensive paper to be submitted to the Journal of Petrology. The paper is authored by myself and Dante Canil, on the petrogenesis of the exhumed Bonanza arc as exposed on southern Vancouver Island. The exposure of cogenetic cumulates, plutons and volcanics provides an excellent opportunity to assess the geochemical relationship between magmas which have crystallized at depth within the crust and those which have ascended to the surface. For example, is there a difference in mineral assemblage between plutonic and volcanic rocks of similar composition? What proportion of cumulates are required to explain the observed geochemical trends in the more evolved magmas, and is such a relationship even possible?

The paper outlines the regional geology, the field area geology and previous work on the Bonanza arc, before describing sample petrography and geochemistry. The discussion focuses on the geochemical relationships between the various lithologies and the implications of petrographic textures with a view towards addressing the role of amphibole in the differentiation of basic arc magmas. The overall goal is to add to our understanding of the formation and

changes in composition of island arc crust via igneous differentiation deep in the crust, in order to better understand the relationship between arc magmatism and the origin and composition of continental crust.

Methods

The fieldwork which forms the basis for this study was undertaken over seven weeks in the summer of 2006 in the area, and on smaller fieldtrips between Port Renfrew and Cowichan Lake on southern Vancouver Island (figure 3). The field area has been mapped previously at varying scales by Federal and Provincial Geological survey teams. My field assistant and I mapped the southern portion of the field area at 1:20 000 scale using the network of logging roads. The northern portion of the area was previously mapped by N. Massey of the BC Geological Survey in the mid-1980s. We mapped this northern portion at 1:50 000 scale. Over 100 samples were taken during the course of our mapping, in an attempt to sample the Bonanza arc both spatially and compositionally. Care was taken to sample the least-altered parts of a given outcrop. In the case of plutonic samples, we attempted to sample homogeneous areas, and often took several samples from distinctive lithologies within a single outcrop.

Of the 100+ samples taken in the field, approximately 60 were chosen for whole rock and petrographic analyses. These were chosen based on sample freshness, as well as to best reflect the range of compositions encountered. Samples were prepared for whole-rock analysis by first cutting away all weathered surfaces and alterations. These pieces were then run through a jaw-crusher, before being milled in agate-lined cups. Rock powders were then sent for major and trace element analysis by X-Ray Fluorescence (XRF) at McGill University. In addition, the sample powders were dissolved by acid dissolution and analyzed for trace elements by ICPMS at the University of Victoria.

Each sample was examined petrographically in order to determine mineralogy, textural relationships, and the degree of alteration as a measure of the rock's geochemical reliability. A subset of thin sections, predominantly cumulate samples, were selected for microprobe analysis at UBC to determine mineral chemistry.

Four samples were taken for U-Pb geochronological analysis but are not described in this thesis. These samples confirmed rocks in the area had ages belonging to the Bonanza arc and are being used for a regional synthesis of southern Vancouver Island geology which is beyond the scope and not the purpose of my study, which concerns the petrogenesis of the rocks.

Chapter 2

The Role of Amphibole in the Evolution of Arc Magmas and Crust: the Case from the Jurassic Bonanza Arc section, Vancouver Island, Canada

INTRODUCTION

Earth is unique in our solar system in having a predominantly sialic, high-standing crust (Rudnick, 1995). The origin of the continental crust and the processes which gave rise to it is a long-standing problem in geology. One theory holds that net crustal growth has, at least since Phanerozoic time, taken place at both island and continental arcs. This idea stems from important geochemical similarities between bulk continental crust and arc magmas (Arculus, 1999; Rudnick & Gao, 2003; Hawkesworth & Kemp, 2006 and references therein), requiring that the latter must have been a key component in the generation of the continents. There is now a general consensus that the majority of arc magmas are generated in the mantle wedge overlying the subducting plate, due in part to the influence of hydrous fluids released during dehydration of the oceanic lithosphere on the peridotite solidus (Grove *et al*., 2003; Ulmer, 2001).

Field studies of modern arcs show that the majority of magmas erupted in this setting are basaltic, suggesting a basaltic parental melt (Arculus, 1981; Rudnick, 1995). For this reason, one would expect that the continents should have a basaltic bulk composition. The best estimate of the composition of the *bulk* crust, however, is andesitic (Rudnick & Gao, 2003) leaving a paradox (eg. Lee *et al*., 2007; Behn & Kelemen, 2006; Arculus, 1999; Rudnick, 1995).

The generation of intermediate magmas can be accomplished by different mechanisms, including simple crystal fractionation from parental mafic magmas (e.g. Bowen, 1928; Pichavant

& Macdonald, 2007; Prouteau & Scaillet, 2003), or mixing of those magmas with felsic crustal melts (e.g. (Annen *et al*., 2006). Regardless of which process is invoked, the compositional gap between arc contributions from the mantle and bulk continental crust persists.

The mineral assemblage and eqilibria driving the evolution of liquid compositions in arcs from primary basalt to andesite remains a source of disagreement. Phenocryst assemblages in arc volcanics have been used as a constraint on possible fractionation assemblages (e.g. Cawthorn & O'Hara, 1976 and references therein), leading to widespread appeal to a gabbroic mineral assemblage consisting of olivine – augite – plagioclase – magnetite (Gill, 1981). There is, however, a danger in this approach. For example, the fractionation of clinopyroxene is required to explain MORB glass trends, yet clinopyroxene phenocrysts in MORB lavas are rare (Francis, 1986). This 'pyroxene paradox' was overcome with the realization that sub-liquidus phases can be effectively fractionated by the return of interstitial liquids from crystallization zones back to the main magma body (Langmuir, 1989). Therefore, the absence of a phenocryst phase from arc lavas need not preclude its involvement in controlling differentiation trends.

The abundance of amphibole-bearing cumulate rocks, both as plutons and as cognate xenoliths in arc lavas, suggests that amphibole plays an important role in the differentiation of many arc suites (e.g. Cawthorn *et al*., 1973; Arculus & Wills, 1980). The fractionation of amphibole is required to explain the Dy/Yb ratios in many arc volcanic suites (Davidson *et al*., 2007). The scarcity of amphibole phenocrysts in arc lavas can be attributed to its instability at low pressures (e.g. Rutherford & Devine, 1988; Romick *et al*., 1992), its effect on magma crystallinity, and therefore eruptability (Barclay & Carmichael, 2004), or a process of interstitial liquid fractionation similar to that mentioned above for MORB, leaving the possibility for amphibole fractionation at mid-crustal depths to influence the evolution of arc magmas.

Phase equilibria of H_2O-bearing basalts show that pressure, f_{O2}, and f_{H2O} are the dominant controls on liquidus mineralogy (Yoder & Tilley, 1962; Holloway & Burnham, 1972; Anderson, 1980; Allen & Boettcher, 1983; Grove *et al*., 2003). For oxygen fugacities relevant to the arc environment (~NNO-0.5 – NNO+2, Carmichael, 1991; where NNO is the Nickel-Nickel Oxide oxygen buffer), the suppression of plagioclase occurs with increasing pressure and/or f_{H2O} (Grove & Kinzler, 1986). At pressures above 700 MPa and at elevated $f_{H2O,}$ hornblende can appear on the liquidus in alkali-rich basalts (Anderson, 1980; Grove *et al*., 2003; Barclay & Carmichael, 2004). Garnet appears on the liquidus at lower-crustal pressures in basaltic systems (Allen & Boettcher, 1983; Rapp & Watson, 1995). Crustal thickness should therefore exert a strong influence on fractionation pathways for arc magmas, by determining the depth at which magmas saturate in different phases while ascending from the mantle to pond and undergo the first stage of crystallization (see Davidson *et al*., 2007; Macpherson, 2008).

The lack of subsurface exposure at modern-day island arc volcanoes means that processes occurring at depth can only be inferred, with little information regarding the composition, distribution, and proportions of plutonic lithologies. There are, however, cases where uplift and erosion have exposed arc crustal cross-sections, including both the plutonic and volcanic sequences. These exhumed arc sections provide direct field evidence pertaining to the bulk composition of the continental crust (eg. Burns, 1985; Greene *et al*., 2006; Jagoutz *et al*., 2006). The Talkeetna (south-central Alaska) and Kohistan (northwest Pakistan) arcs preserve sections spanning from the top of the crust to below the Moho (DeBari & Coleman, 1989; Hacker *et al*., 2008; Jagoutz *et al*., 2006, and references therein). Detailed work on the former has provided important constraints on the bulk composition of arcs and the P-T conditions at which various lithologies last equilibrated in the crust (DeBari & Sleep, 1991; Greene *et al*., 2006; Hacker *et*

al., 2008). These studies show that a significant portion (25-85%) of the plutonic section is missing, based on calculated pressures in the plutonic lithologies (DeBari & Coleman, 1989; Hacker *et al*., 2008), and petrologic modeling (Greene *et al*., 2006). Depending on assumptions regarding the composition and proportions of the missing arc crust, the bulk composition of the Talkeetna arc is constrained to lie between 51-58 wt% SiO_2 (DeBari & Sleep, 1991; Hacker *et al*., 2008). The nature of the process by which such large portions of arc crust have been removed remains controversial. The apparent loss of considerable thicknesses of crust may occur by structural thinning during accretion or by subsequent tectonic activity. Structural thinning cannot, however, change the true bulk composition of arc crust, although it can change the apparent bulk composition of exposed crust. Alternatively, the foundering and loss of a dense lower crustal cumulate layer into the mantle may explain the discrepancy between the calculated and actual proportions of plutonic lithologies (e.g. DeBari & Sleep, 1991; Behn & Kelemen, 2006; figure 1). Such a model provides a potential solution to the compositional quandary of primary basaltic island arc magmas and andesitic continental crust: the removal of ultramafic components from primary island arc magma will drive the bulk composition of the arc (and by extension new continental crust) towards more silica-rich compositions.

Exposed on Vancouver Island, British Columbia, the Jurassic Bonanza arc is believed to represent the southerly continuation of the Talkeetna arc (DeBari *et al*., 1999; Clift *et al*., 2005) but differs by having been emplaced into a substrate of Paleozoic island arc and a Mesozoic oceanic plateau. The latter are not represented in the Talkeetna section. The Bonanza arc section preserves both deep plutonic roots and sub-aerial volcanics and volcaniclastics, offering a window into the processes and products of differentiation at depth beneath the arc.

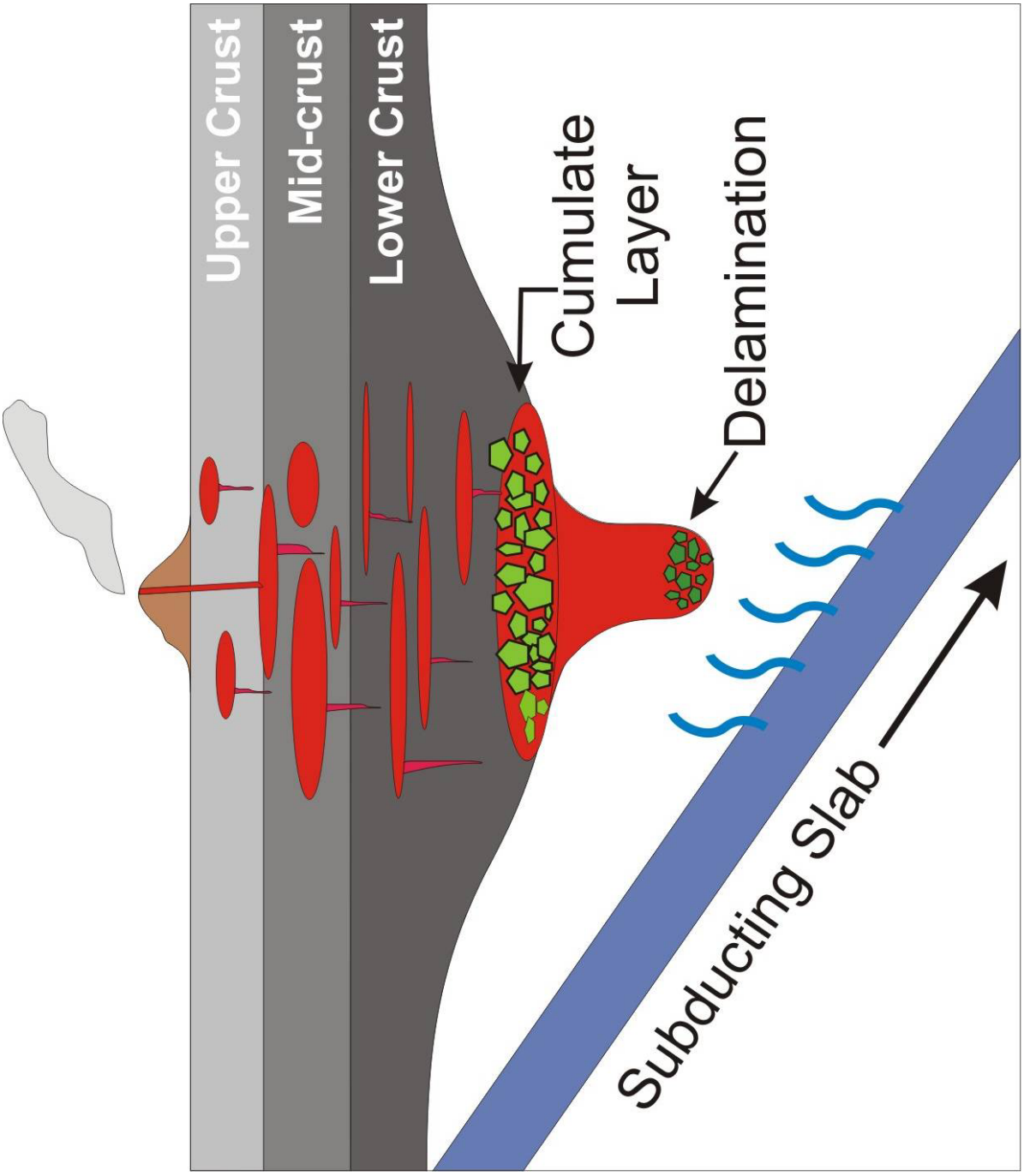

Figure 1. Schematic subduction zone diagram showing relative positions of upper, mid- and lower crust, hypothetical cumulate layer at the base of the crust, and idealized delamination of dense cumulates. Plutons are shown as red ellipses. Blue curves emanating from subducting slab indicate dehydration of oceanic crust.

In this study a combination of field mapping, petrography, and whole rock, trace element and mineral chemistry are used to constrain the P-T conditions and pathways along which the magmas that fed the Bonanza arc evolved, with a view towards better understanding how arc magmatism gives rise to the composition of continental crust. The exposure of cogenetic plutons and volcanics provides an excellent opportunity to assess the geochemical relationship between magmas which have crystallized at depth in the crust and those which have ascended to the surface. For example, is there a difference in mineral assemblage between plutonic and volcanic rocks of similar composition? What proportion of cumulates are required to explain the observed geochemical trends in the more evolved magmas, and is such a relationship even possible? The overall goal is to add to our understanding of the formation and changes in composition of island arc crust via igneous differentiation deep in the crust, in order to better understand the relationship between arc magmatism and the origin and composition of continental crust.

GEOLOGIC SETTING

Regional Geology

The Canadian Cordillera is broadly divisible into three parts: an eastern foreland domain, a central Intermontane domain, and an Insular domain (Johnston, 2008). The western portion of the Insular domain is dominated by Wrangellia, a tectonic terrane which extends along the western coast of North America from Vancouver Island, through the Queen Charlotte Islands, and into the Wrangell Mountains of southern Alaska, whence it takes its name (Jones *et al*., 1977).

The Sicker Group forms the basement to Wrangellia on Vancouver Island, and consists of Devonian arc volcanics and volcaniclastics, overlain by Permian epiclastic and carbonate sediments (Massey & Friday, 1987). Unconformably overlying the Sicker Group are the Triassic

Karmutsen basalts, a thick (~6000 m) sequence of subaqueous pillow lavas, pillow breccia, and subaerial flows (Nixon *et al*., 1993) and references therein). Conformably overlying the Karmutsen basalts is the Quatsino Formation, a thin (< 75 m) sequence of micritic limestone deposited during the late Triassic (Massey & Friday, 1987). The Karmusten and Quatsino Formations comprise the Vancouver Group, and are the diagnostic stratigraphic features of Wrangellia (Jones *et al*., 1977). The Vancouver Group is itself conformably overlain by thinly bedded sediments of the late Triassic Parson Bay Formation (Massey & Friday, 1987; Nixon *et al*., 1995). Minor arc volcanics and volcaniclastics within the Parson Bay are interpreted as representing the earliest phase of activity of the Late Triassic to Middle Jurassic Bonanza island arc, (Nixon & Orr, 2007).

Rocks of the Bonanza arc have been divided into three units (figure 2). The Westcoast Crystalline Complex (WCC) is the deepest level, and consists of variably deformed gabbro to diorite plutons and amphibolites. (Isachsen, 1987; DeBari *et al*., 1999). Cumulate rocks consisting of hornblende gabbro and variably-serpentinized olivine pyroxenite have been mapped as a subunit of the WCC (Isachsen, 1987; DeBari *et al*., 1999) and references therein). Where exposed, the country rocks to the WCC plutons appear to be Sicker Group lithologies (DeBari *et al*., 1999).

The Island Plutonic Suite (IPS) represents the upper plutonic levels, and consists of plutons ranging in composition from diorite to granite that intrude the Vancouver Group as well as the coeval Bonanza Group volcanics. The rocks of the WCC and IPS have traditionally been differentiated by the lack of deformation textures in the latter (Muller *et al*., 1981). The erupted equivalents of the IPS and WCC are known as the Bonanza volcanics, which cap the stratigraphic section for the Bonanza arc on Vancouver Island. The Bonanza volcanics consist of

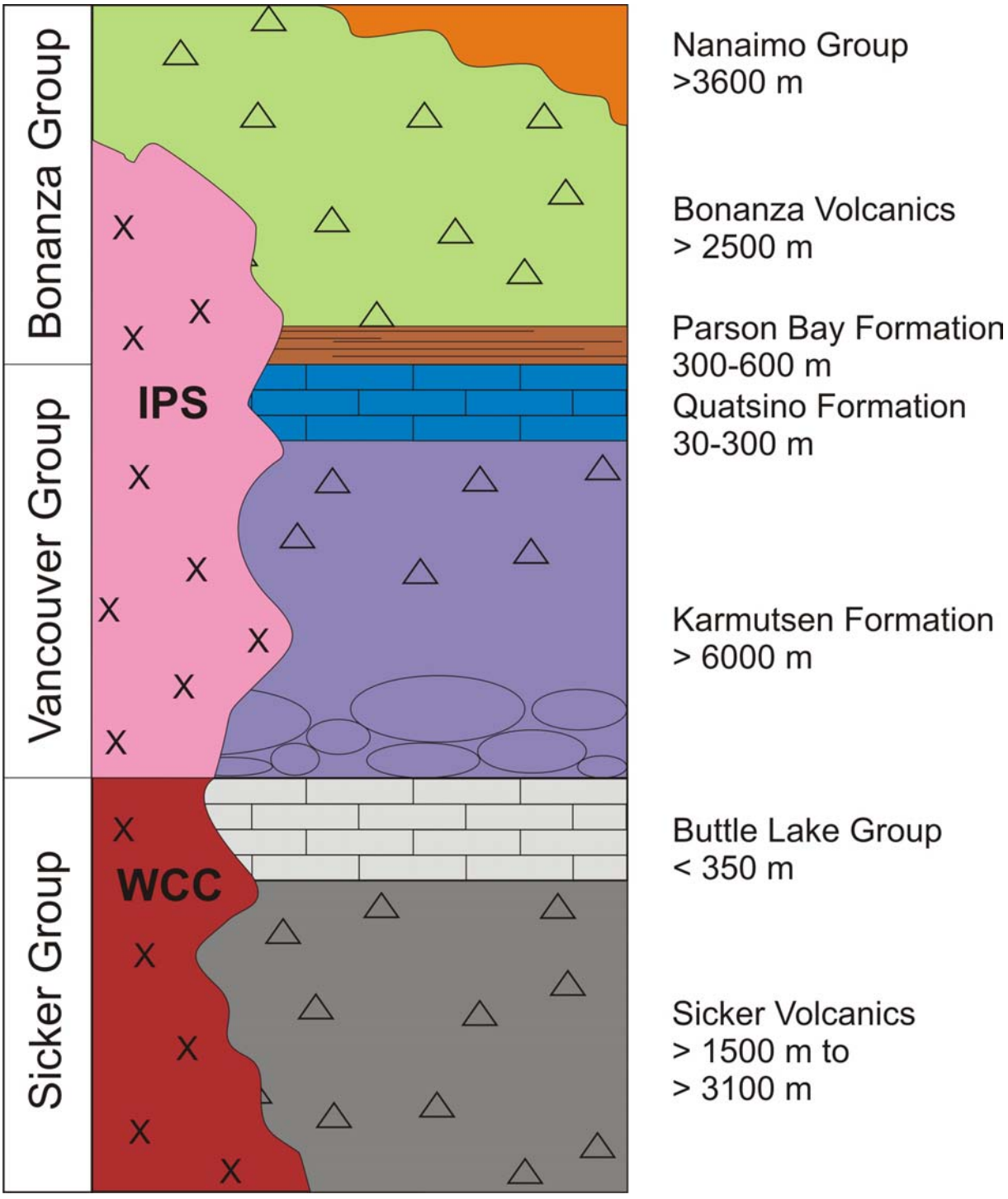

Figure 2. Simplified schematic stratigraphic section for southern Vancouver Island. WCC- West-coast Crystalline Complex: IPS- Island Plutonic Suite. Thickness estimates from Muller *et al*., (1981); Massey & Friday, (1987); England & Calon, (1991); Nixon & Orr, (2007).

interbedded basaltic to rhyolitic subaerial flows and flow breccias, with minor dacitic to rhyolitic tuff beds. The base of the volcanics is dominated by epiclastic deposits interbedded with crystal and lapilli tuffs (Massey & Friday, 1987; Nixon & Orr, 2007). Wrangellia is unconformably overlain by the Cretaceous Nanaimo Group, a fining-upwards sequence of pebble conglomerates, sandstones, and black argillite (Massey & Friday, 1987).

Geochronology and geochemical data support a co-magmatic origin for the three igneous subunits of the Bonanza Group (Isachsen, 1987; DeBari *et al*., 1999). U-Pb zircon ages indicate that the Bonanza arc was active from approximately 200 Ma to 167 Ma. Conodonts and bivalves recovered from epiclastic deposits interbedded with volcanics within the Parson Bay formation suggest that arc volcanism began as early as the Norian stage (~215-203 Ma) of the late Triassic (Nixon & Orr, 2007). These ages overlap with those determined from U-Pb zircon geochronology within the Talkeetna arc (205-156 Ma), leading to the suggestion that the Bonanza arc represents an along-strike correlation of the Talkeetna arc (DeBari *et al*., 1999; Clift *et al*., 2005). DeBari *et al.* (1999) offer an excellent overview of the geology, geochemistry, and geochronology of the Bonanza arc, mostly in central Vancouver Island. Their study did not, however, address the overall thickness of the arc section, or examine the differentiation history of the arc in detail, which are the goals of the present work.

The Port Renfrew Area

We examined a crustal section of the Bonanza arc exposed on southern Vancouver Island in the region surrounding Port Renfrew (figure 3). The southern boundary of the field area is marked by the San Juan Fault, which separates Wrangellia to the north from the Pacific Rim terrane to the south, a sequence of Jurassic-Cretaceous pelites metamorphosed from chlorite to staurolite

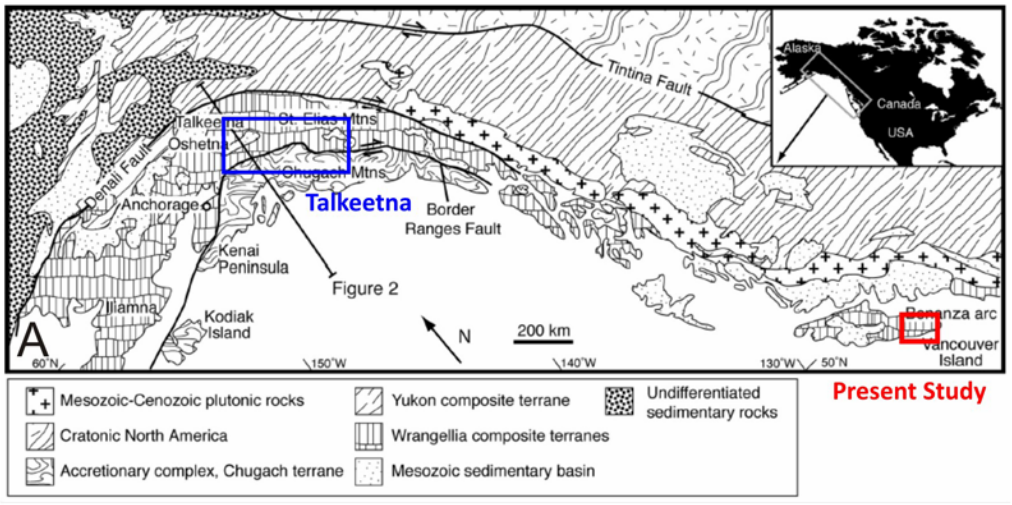

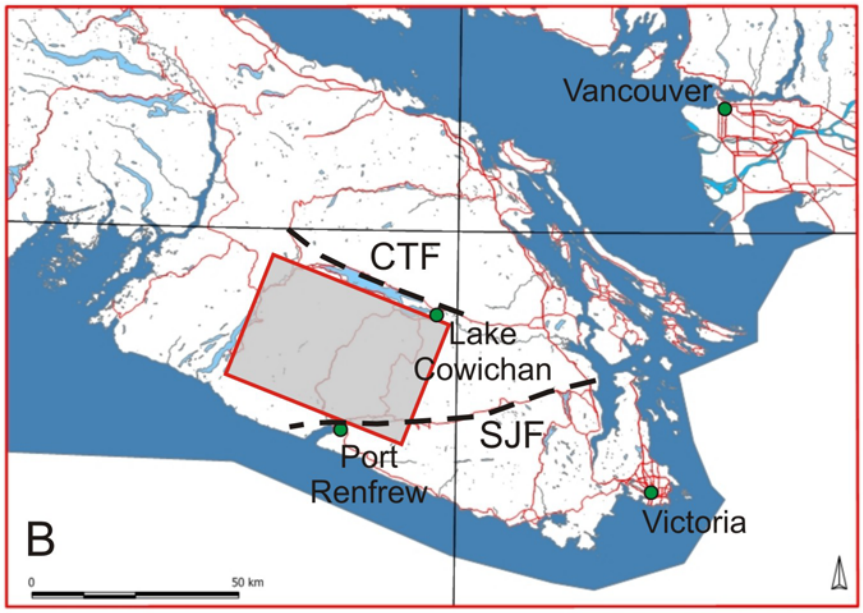

Figure 3. Location of field area surrounding Port Renfrew on southern Vancouver Island. Location of B is shown in red inset of A. Figure A adapted from Clift *et al.* (2005). CTF: Cowichan thrust fault; SJF: San Juan fault

grade. The field area is bound to the north by the Horne Lake – Cowichan Uplift, a west-verging thrust fault which exposes the Sicker Group north of Cowichan Lake (Massey & Friday, 1987).

Excellent exposures of all three subunits of the Bonanza Group are present throughout the field area (figure 4). The WCC is restricted to the southern parts of the area, and is dominated by melanocratic to leucocratic quartz diorite and gabbro containing varying amounts of hornblende, biotite, and Fe-Ti oxides. WCC plutons are quite heterogeneous on the outcrop (meter) scale, and locally display a well-develop gneissosity (figure 5a). Although Sicker Group country rock has been reported by DeBari *et al.* (1999), plutonic margins in the WCC have not been recognized in the present study area, possibly owing to limited exposure. Foliations within the WCC, defined by planar fabric of hornblende, biotite and/or plagioclase, strike southeast and dip 60-75 degrees to the southwest. Shear zones having the same orientation cut across the WCC. The common orientation and sense of shear (tops to NE) for these shear zones suggest the WCC was emplaced as a series of thrust-faulted panels, the easternmost one of which has been thrust onto the Karmutsen basalts.

Ultramafic rocks occur as discreet bodies within the WCC, ranging in size from a meter to several tens of meters. Contact relationships between the ultramafic bodies and the main gabbro-diorite phase of the WCC are quite variable: olivine-bearing cumulate bodies show either abrupt, undeformed contacts with their hosts (Figure 5b), or are present as sheared pods and discontinuous layers; larger bodies of cumulate hornblende gabbro grade into the main gabbro-diorite phase of the WCC. In outcrop, the olivine-bearing ultramafic bodies can be difficult to recognize, owing to their strongly weathered character (Figure 5c).

IPS plutons range in composition from quartz diorite to alkali feldspar granite. They range in size from <1km to several tens of km across, and occur as large irregular bodies having

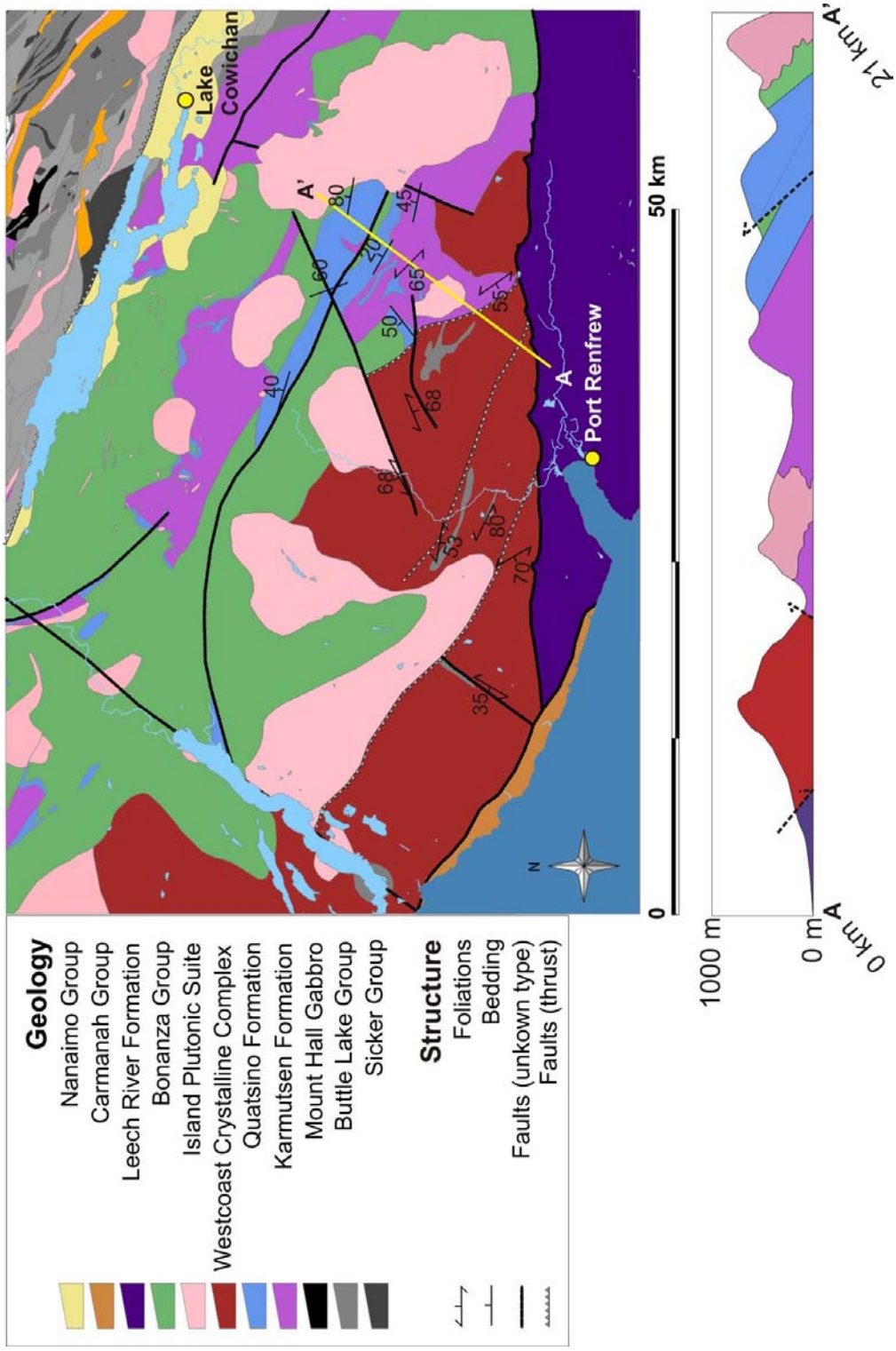

Figure 4. Geology map of field area determined by 1:25,000 scale mapping. Transect for cross section denoted by line marked A-A'. Dashed arrows in cross section denote inferred thrust faults.

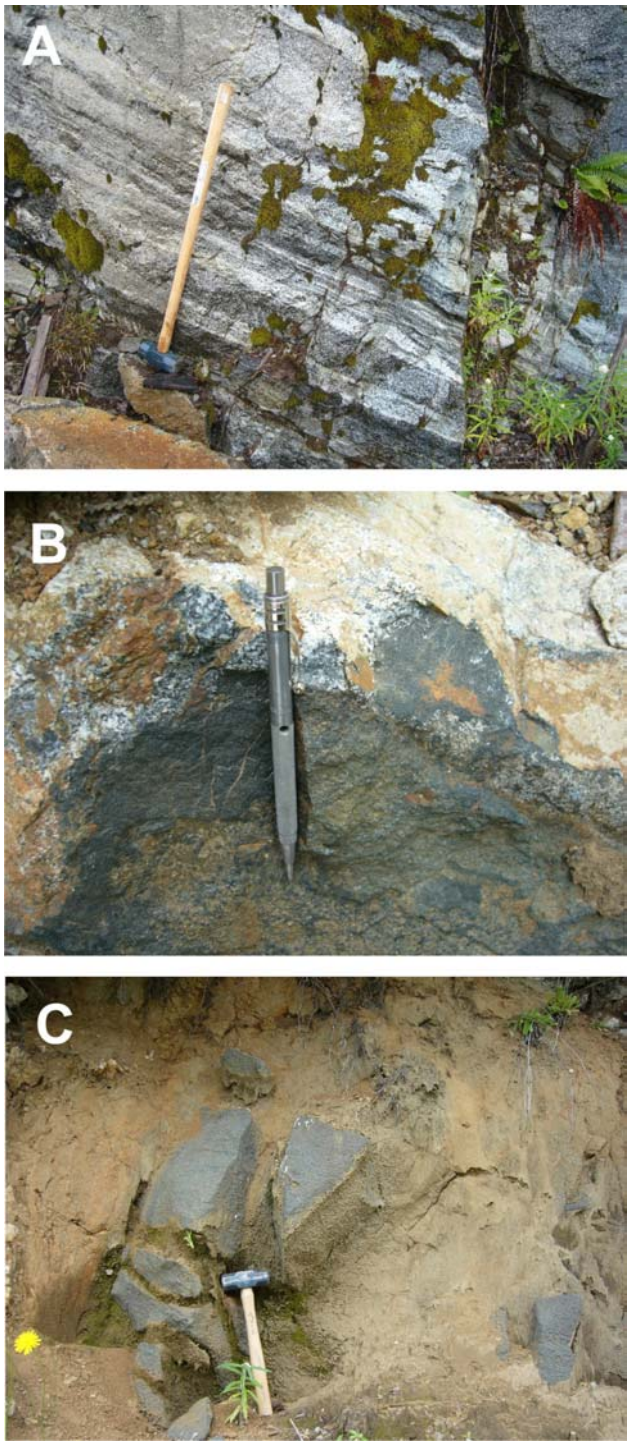

Figure 5. Field exposures of WCC and olivine cumulate in outcrop. A) gneissic layering in WCC diorite. B) contact between olivine cumulate inclusion and the WCC gabbro-diorite host. C) Strongly weathered olivine cumulate outcrop (JL06-106).

no deformational fabric. Except where faulted, the contact between the Island Plutonic Suite and the Westcoast Crystalline Complex is not well defined.

The Bonanza Group volcanics vary in composition from basalt to rhyolite. Aphanitic to plagioclase-, pyroxene-, and rare hornblende-phyric basalt to basaltic andesite is the dominant erupted composition. In addition to massive flows, the Jurassic volcanics are also encountered as flow breccias. Lesser pyroclastic deposits are also present, including banded and air fall tuffs. Aphyric mafic dykes cut across the Vancouver Group and the plutonic sections of the Bonanza Group, and are interpreted to represent the feeder dykes to volcanic centres.

PETROGRAPHY

Petrographic descriptions for each sample are listed in Table 2. Metamorphic alteration is on the whole very minor, with typically less than 10% secondary minerals by mode. Metamorphism is expressed through the alteration of plagioclase to sericite and epidote, and the partial replacement of biotite and hornblende by chlorite and epidote. Where present, cumulus olivine is partially serpentinized. Volcanic rocks contain quartz, chlorite, epidote, calcite and actinolite as amygdaloidal assemblages. Plagioclase and biotite are the most likely phases to be pervasively altered.

Westcoast Crystalline Complex

The rocks of the WCC may be subdivided into two main groups distinguished by the presence or absence of quartz. Quartz-free rocks can be further divided into those containing (1) cumulus olivine, and (2) cumulus plagioclase.

Olivine hornblendites

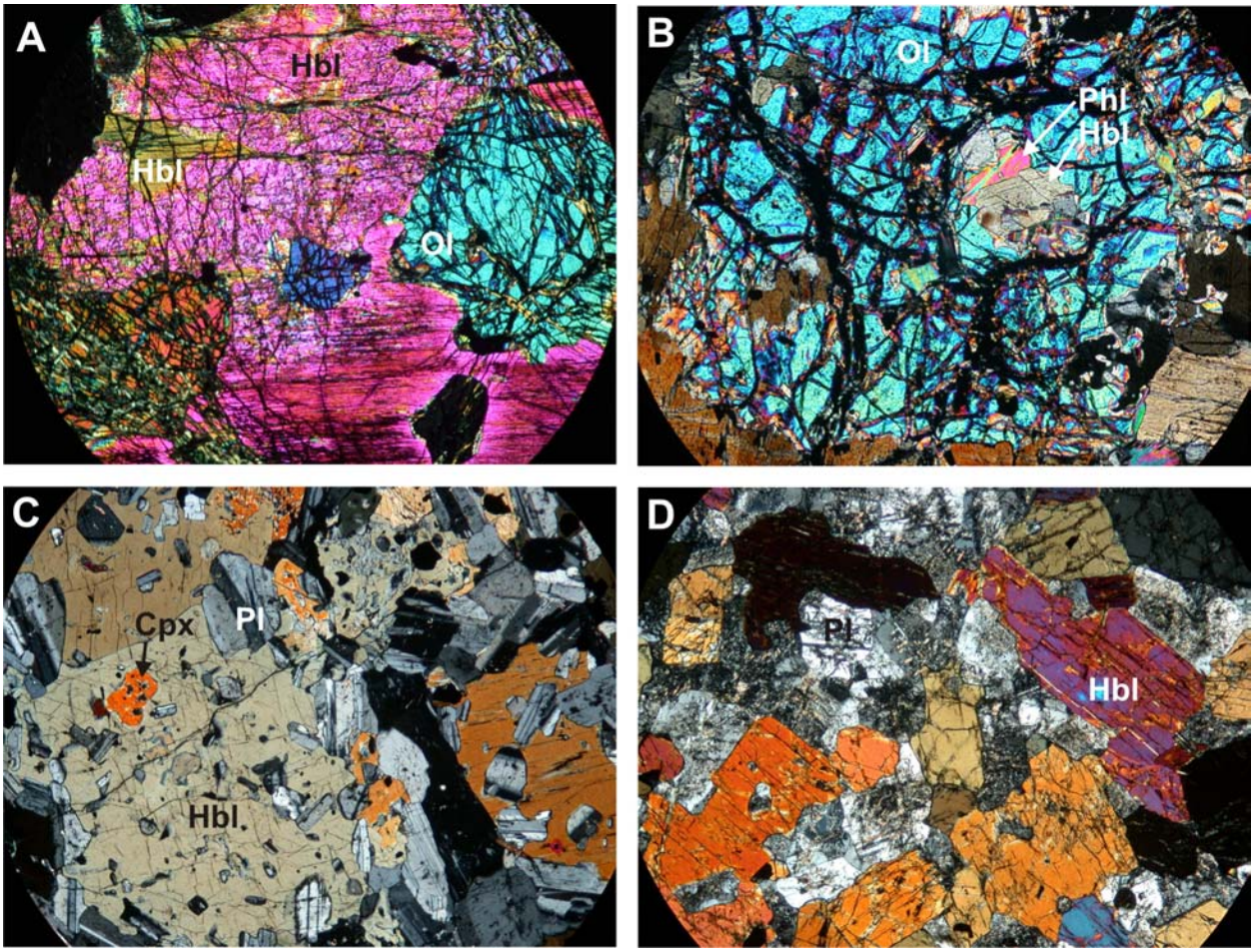

Figure 6. Photomicrographs showing textures in cumulates. A) Olivine hornblendite. (field of view 4mm) B) Hornblende and phlogopite included in olivine (field of view 2mm) C) Pyroxene-bearing poikilitic hornblende gabbro D) Hornblende gabbro with cumulus hornblende and plagioclase. Ol – olivine; Hbl – hornblende; Phl – phlogopite; Cpx – clinopyroxene; Pl – plagioclase

Olivine hornblendites display a heteradcumulate texture, with variably-serpentinized olivine poikilitically enclosed either by amphibole or orthopyroxene, or rarely phlogopite (Figure 6a). Spinel, clinopyroxene, plagioclase and magnetite are present in minor amounts in some samples.

Olivine is always rounded and embayed, suggesting a reaction relationship with the surrounding phase. Clinopyroxene is rarely present, as ragged anhedral grains surrounded by amphibole, making it difficult to ascertain whether it was originally a cumulus phase. Plagioclase is present as an intercumulus phase in two samples, and is usually pervasively altered to clay, epidote, chlorite and/or sericite. In one sample (JL-031), euhedral plagioclase is a cumulus mineral. Plagioclase and olivine are never in contact, and are separated by a corona of amphibole surrounding olivine. Euhedral phlogopite is present in varying quantities in almost all samples. It may rarely form a poikilitic texture, enclosing olivine. Large amphibole oikocrysts commonly show exsolution lamellae of ilmenite, and may have originally been Ti-rich (kaersutitic). Olivine may contain inclusions of spinel, and in two samples, orthopyroxene, amphibole, and/or phlogopite. Euhedral orthopyroxene may contain inclusions of olivine and amphibole.

Hornblende gabbros and gabbronorites

The rocks from this group never contain any olivine. Most samples display a heteradcumulate texture where poikilitic amphibole encloses plagioclase, clinopyroxene, magnetite and/or orthopyroxene. Some samples contain euhedral cumulus amphibole, and lack pyroxene. Euhedral magnetite is present in all but two samples (JL-068 and JL-105), and is found included in all other phases; it may rarely contain plagioclase inclusions. Plagioclase commonly contains inclusions of subhedral amphibole and clinopyroxene, although when orthopyroxene is present, plagioclase generally only contains magnetite inclusions. Both pyroxenes tend to be strongly anhedral, with corroded margins. Isolated, rounded pyroxene grains within amphibole oikocrysts

often display optical continuity. Where present, orthopyroxene contains inclusions of all other phases. Relict clinopyroxene is never in contact with plagioclase, magnetite, or orthopyroxene, but is always surrounded by amphibole. Euhedral biotite is present in most samples in minor amounts.

Quartz-bearing samples

This group constitutes the main gabbro-diorite phase of the WCC. All samples contain abundant amphibole and plagioclase, with minor biotite and quartz. Magnetite, K-feldspar, and titanite are also present in some samples. Coarse grained samples typically show strongly zoned subhedral plagioclase, euhedral to subhedral amphibole, euhedral biotite with variable chlorite alteration, and interstitial quartz and potassium feldspar. Finer grained samples contain prismatic amphibole and plagioclase laths, with a finer groundmass of subhedral amphibole and feldspar clusters. Where present, magnetite occurs as a phase included in both amphibole and plagioclase.

Island Plutonic Suite

The Island Plutonic Suite samples are all quartz-bearing, having a similar mineralogy to the quartz-bearing WCC samples, but contain more quartz and potassium feldspar and less amphibole. Plagioclase shows marked zoning and tends to be euhedral-subhedral.

Bonanza Group Volcanics

All volcanic samples contain plagioclase phenocrysts, with some samples also containing euhedral zoned clinopyroxene as well as Fe-Ti oxide phenocrysts. Relic olivine phenocrysts are present in two samples (JL-027, JL-093), having been replaced by talc and chlorite+calcite, respectively. Several basaltic samples preserve rounded amphibole phenocrysts or clinopyroxene pseudomorphs after amphibole (JL-092, JL-027, JL-090).

GEOCHEMISTRY

Analytical methods

All major elements, along with selected trace elements, were analyzed by a Philips PW2440 4kW automated XRF spectrometer at McGill University. Major elements, as well as the trace elements Ba, Co, Cr, Cu, Ni, Sc and V, were analyzed using 32mm diameter fused beads prepared from a 1:5 sample: lithium tetraborate mixture. Accuracy for Si is within 0.5%, while for other major elements it is within 1%. Trace element accuracy is within 5%. Overall precision is within 0.5%.

Trace elements were analyzed by solution nebulisation ICPMS at the University of Victoria, using a Thermo X-series II (X7) instrument. Samples were dissolved using concentrated HF- HNO_3 mixtures in 25 mL Teflon beakers, dried to a gel, and then refluxed with HNO_3 and redried. Each sample was then redisolved in HNO_3, and diluted with de-ionized water to which an internal standard is added prior to analysis. The dissolution procedure and subsequent data deconvolution procedures were based on the method of (Eggins *et al*., 1997). Certified reference materials were run as unknowns along with the samples. Accuracy and precision for reference materials are listed in Appendix 1.

The Rb-Sr and Sm-Nd isotope ratios of ten samples where analyzed by Thermal Ionization Mass Spectrometry (TIMS) at the University of Alberta (Table 1). Descriptions of methods are given in Unterschutz *et al*. (2002), Creaser *et al*. (2004), and Schmidberger *et al*. (2007).

Major Elements

The question of element mobility is central to a geochemical interpretation of any igneous suite. Pearce element ratios (PER) have been used to determine the extent of element mobility in

igneous suites (e.g. Beswick & Soucie, 1978), but their application in our study is complicated by the amphibole-bearing phase assemblages of the Bonanza arc. Stoichiometric uncertainty due to site vacancies, as well as the fact that few elements are truly incompatible in amphibole, make PER analysis unreliable. Alternatively, mobile elements K and Rb show very coherent behaviour throughout the range of compositions, with minor scatter in the volcanics presumably due to amydaloidal alterations. This, and petrographic observations showing only minor alteration, leads us to conclude that element mobility is not a significant factor in our study. The complementary geochemical behavior of the Westcoast Crystalline Complex, the Island Plutonic Suite, and the Bonanza Group volcanics has been noted previously (Isachsen, 1987; DeBari *et al*., 1999). Non-cumulate rocks within the arc define a typical calc-alkaline trend, ranging in composition from basalt to rhyolite with the majority of samples falling in the basalt to basaltic-andesite range (figure 7). The IPS samples define the high-SiO_2 end of the compositional spectrum, with minor overlap with the WCC at intermediate compositions. The majority of the volcanic samples are shifted towards more mafic compositions, and have SiO_2 concentrations which are indistinguishable from the WCC samples (figure 8). Cumulate rocks comprise the low-SiO_2 end of the spectrum.

On all Harker diagrams, plotted in cation units (normalized to 100 cations) in order to better show the mineralogic controls on trends (figure 9), the WCC, IPS and Bonanza volcanic samples define a linear array, with the gabbroic cumulates clustering at the low-Si end of the array, and the olivine cumulates extending on a vector towards olivine. The olivine cumulates lie on a tie-line connecting olivine and hornblende, the two modally dominant phases in these rocks. Concentrations of Ti, Al and Ca are highest in the gabbroic cumulates, and decrease with increasing Si.

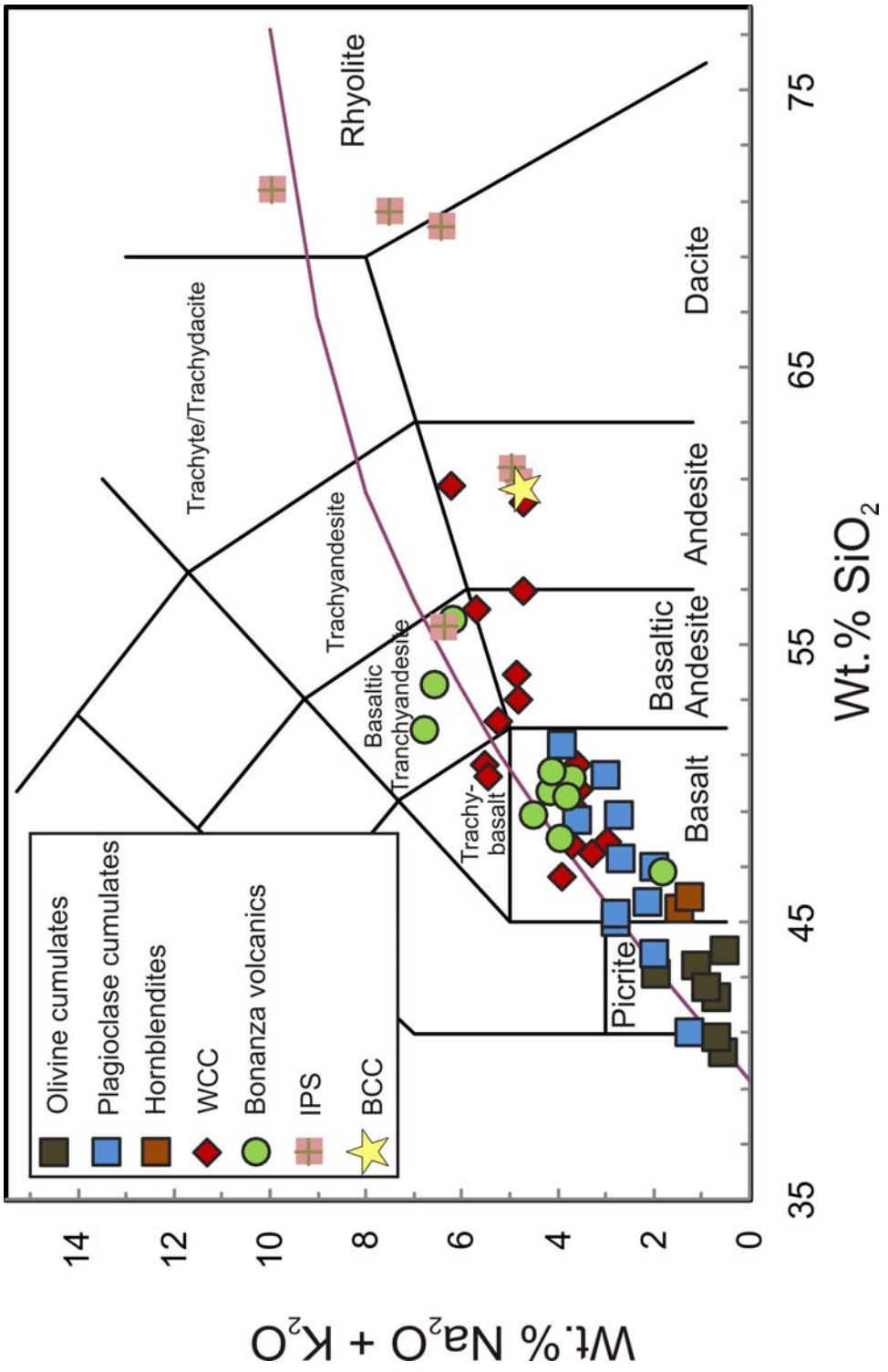

Figure 7. Total alkali-silica plot for all Bonanza arc lithologies. Bulk continental crust (BCC) from Rudnick and Gao (2003).

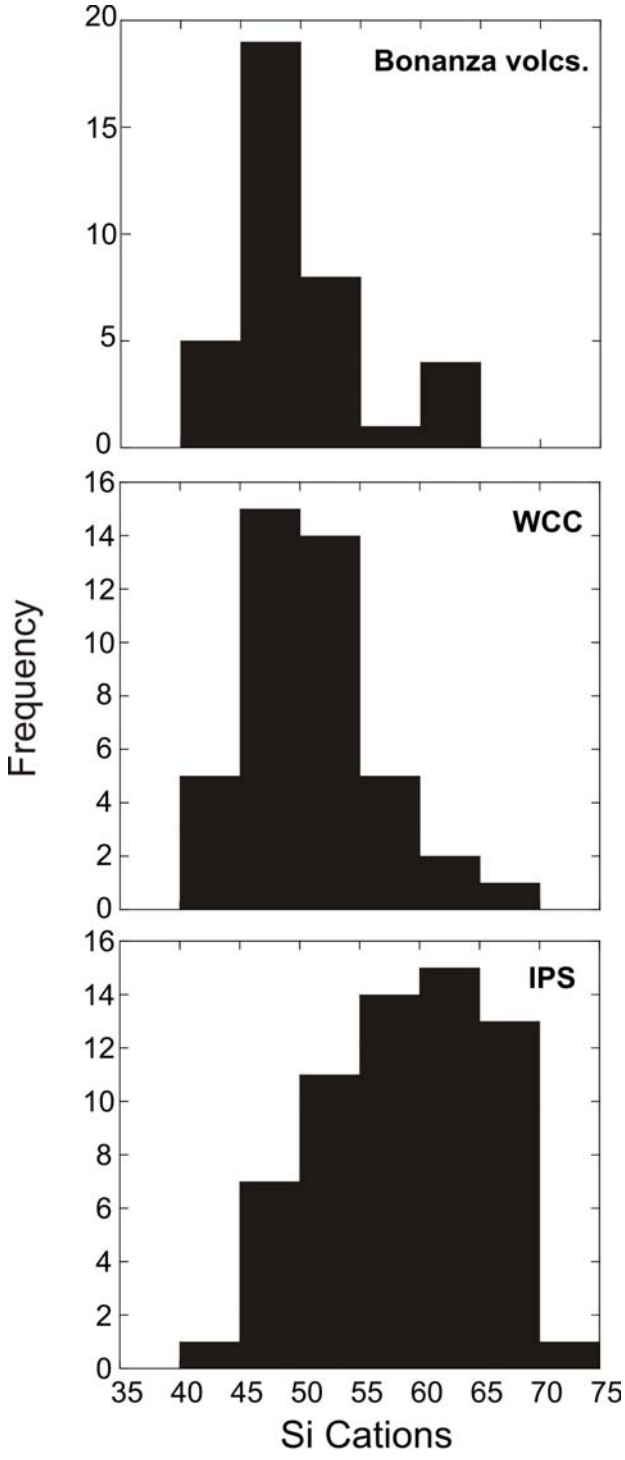

Figure 8. Histogram plot of the Si cation (normalized to 100) concentrations of Bonanza arc subunits: WCC- West Coast Complex: IPS- Island Plutonic Suite. Note the overlap of the WCC plutons and Bonanza volcanics.

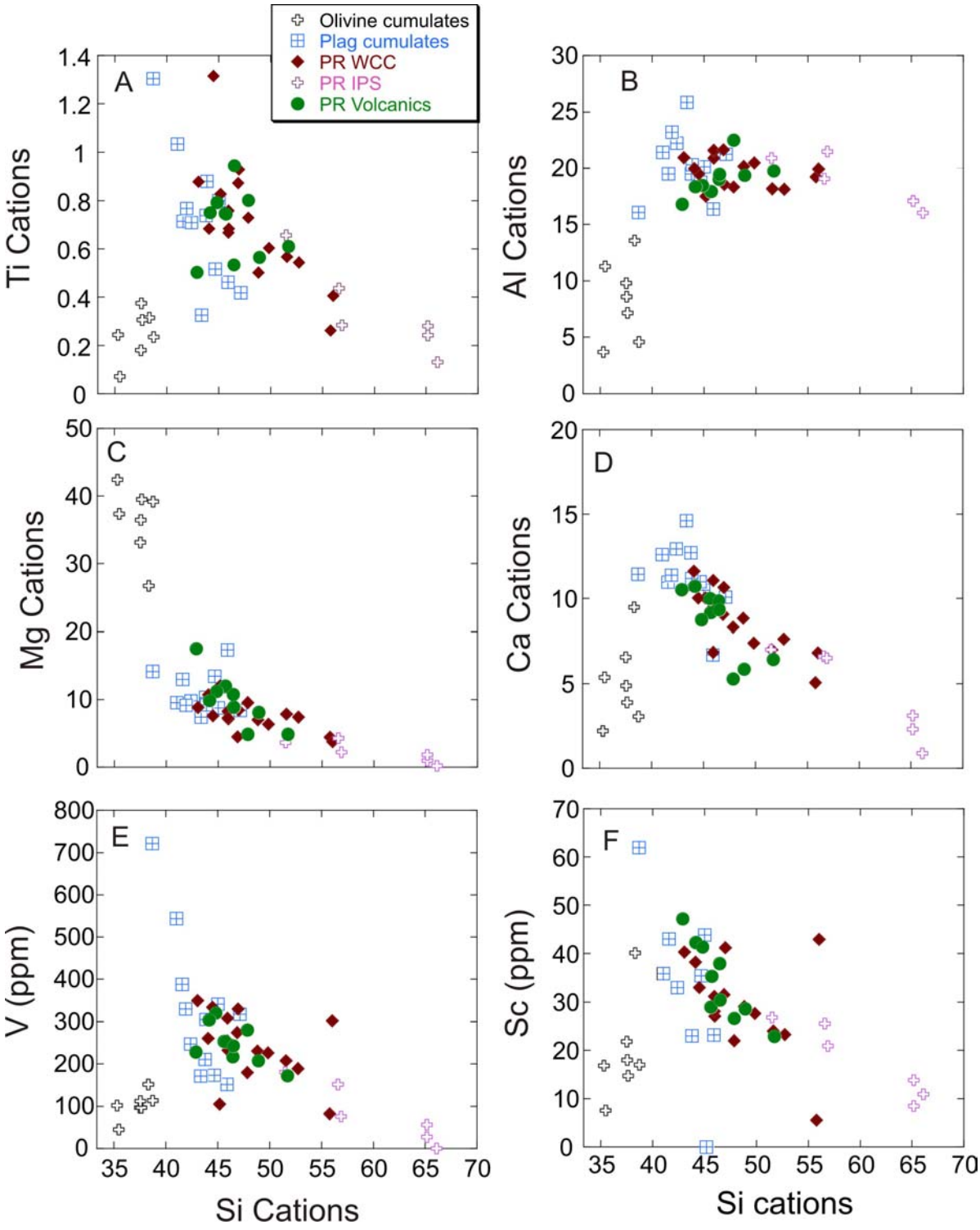

Figure 9. Harker diagrams plotted in cation units (normalized to 100) for all Bonanza arc lithologies from the Port Renfrew (PR) area. WCC- West Coast Complex: IPS- Island Plutonic Suite

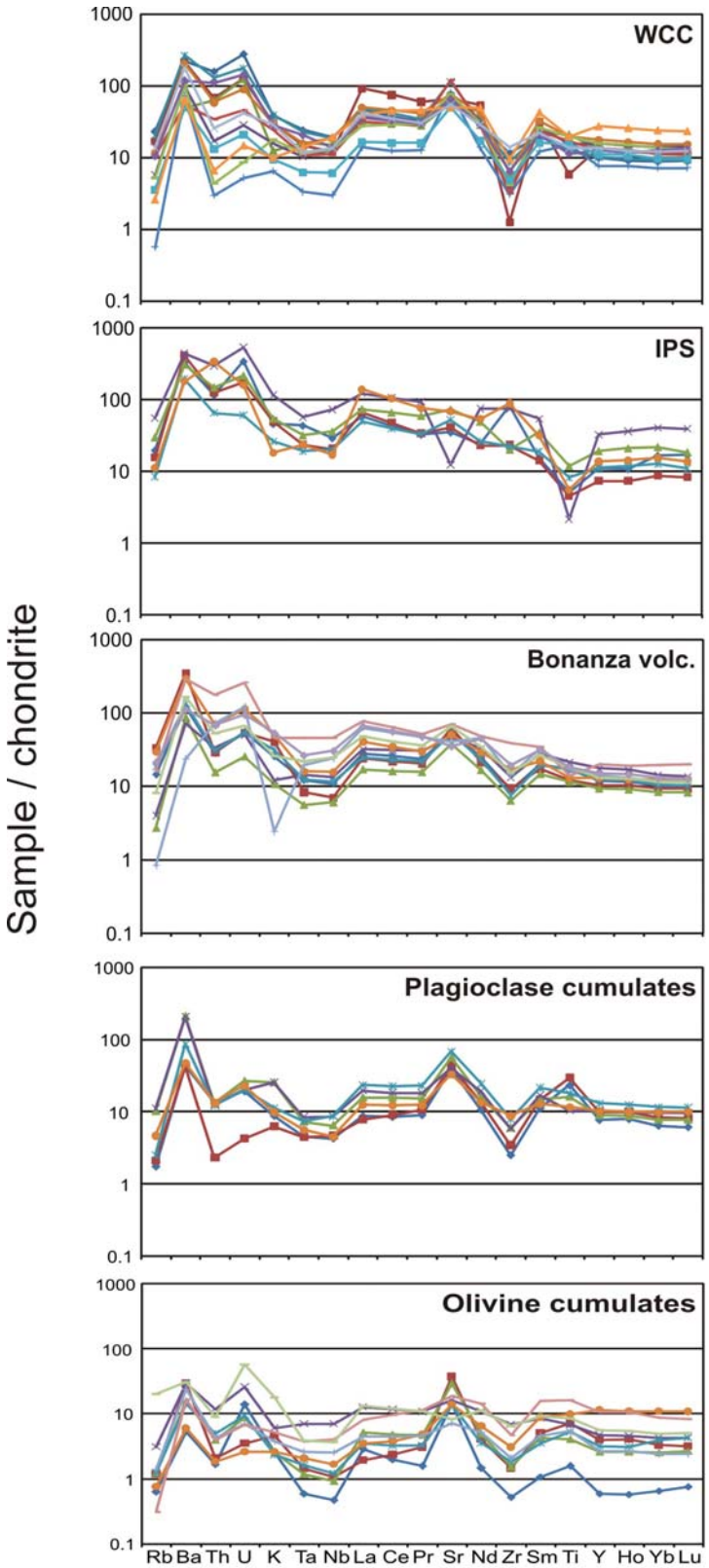

Figure 10. Chondrite-normalized trace element spider diagrams of Bonanza arc lithologies. WCC- West Coast Complex: IPS- Island Plutonic Suite

Trace Elements

All samples show chondrite-normalized negative Ta-Nb typical of an arc signature (figure 10). Negative Zr anomalies are ubiquitous, while positive Sr anomalies are nearly so (two volcanic samples and one olivine cumulate show only weak negative Sr anomalies). Positive Ti anomalies, corresponding with the presence of Fe-Ti oxides, are present in many of the cumulate samples, and mirrored by negative Ti anomalies in the volcanics and WCC rocks. Chondrite-normalized rare earth elements among all units show broadly similar, variably light rare earth enriched patterns (figure 11). A select few samples display LREE depleted patterns (JL-042, JL-101, JL-021). The cumulate rocks have nearly flat REE patterns with minimal LREE enrichment, and have lower concentrations than do the non-cumulate rocks. The distinct lack of Eu anomaly among the gabbroic cumulates is noteworthy. The WCC, IPS, and volcanic units show essentially identical patterns of LREE enrichment, with some samples having minor positive or negative Eu anomalies.

The concentrations of Ni and Cr form a well-defined array which encompasses all units and lithologies, from olivine cumulates to the IPS (figure 12 A,B). The lower Cr plagioclase-cumulates form an array with the IPS samples whose slope is significantly shallower than the slope defined by high-Cr samples (figure 12B). Two distinct groups are defined by the Nb/Zr ratio (figure 12C). All cumulate rocks plot in the low-Nb group, while the majority of the quartz-bearing WCC plot in the high-Nb group. The volcanic and IPS samples are evenly split between the two groups. The V and Sc concentrations are highest in the gabbroic cumulates, and lowest in the most evolved IPS rocks (figure 9).

Radiogenic Isotopes

Ten samples, representative of each lithology were chosen for Sr and Nd isotopic analysis. Results are listed in Table 1, and are consistent with previous isotopic work on the Bonanza arc

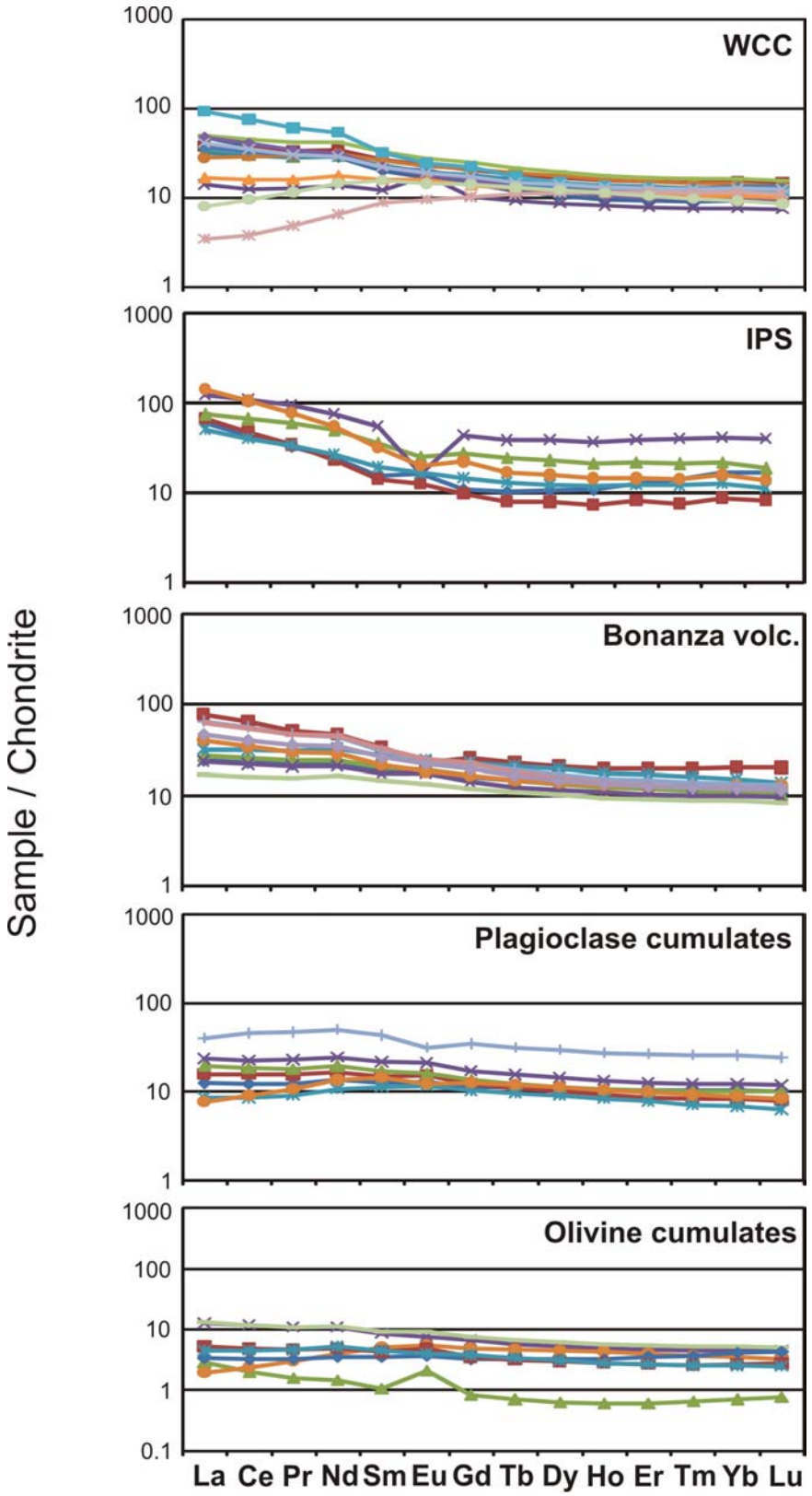

Figure 11. Chondrite-normalized rare earth element plots for Bonanza arc lithologies. WCC-West Coast Complex: IPS- Island Plutonic Suite

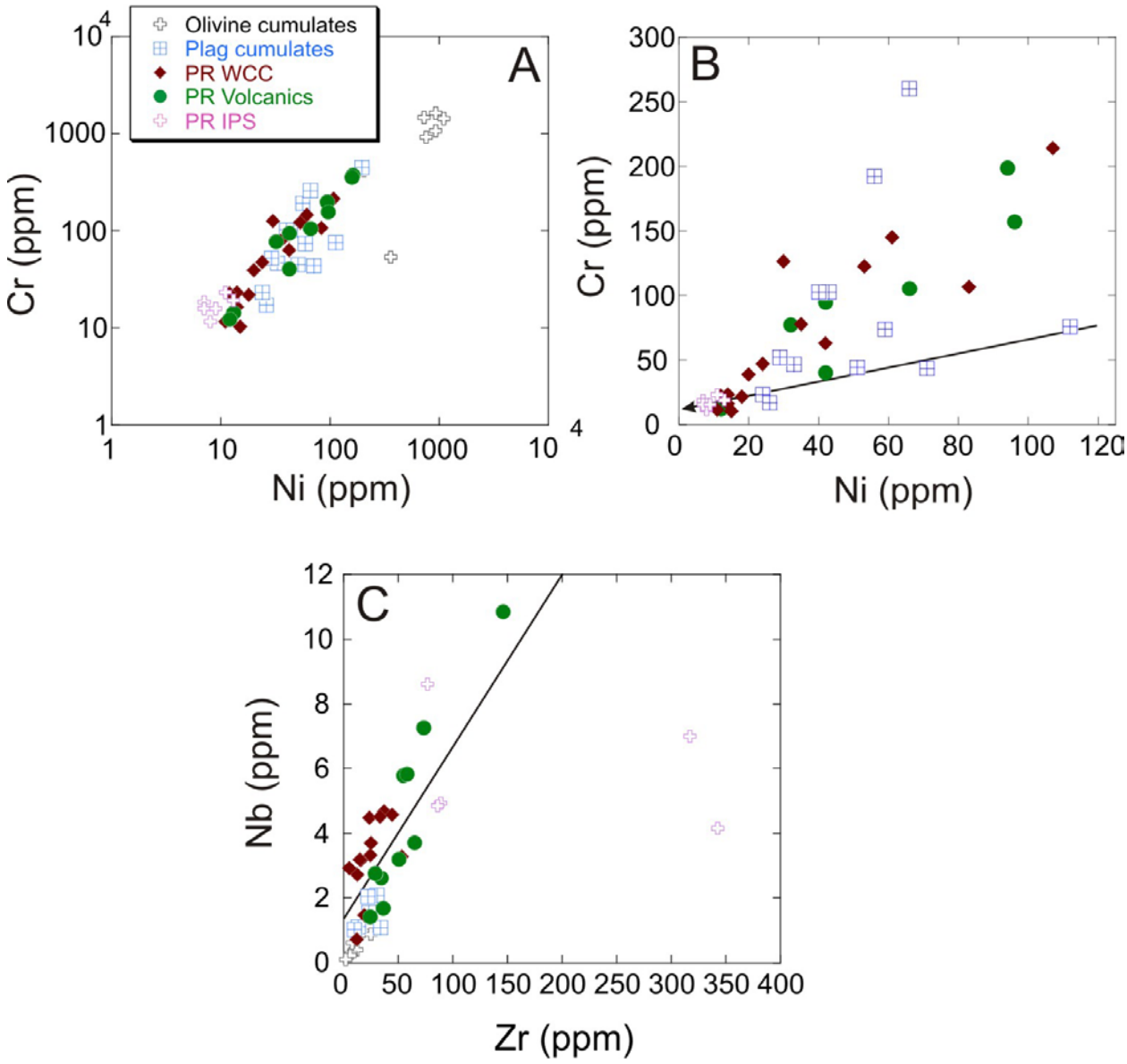

Figure 12. Trace element plots for Bonanza arc lithologies. A and B show same data set with different scales. Arrow in B delineates the low-Cr cumulate gabbro – IPS array mentioned in the tesxt. Line in C separates high Nb and low Nb groups. WCC- West Coast Complex; IPS- Island Plutonic Suite; PR- Port Renfrew samples from this study

(Andrew & Godwin, 1989; Andrew *et al*., 1991). Some samples have elevated $^{87}Sr/^{86}Sr$ ratios, notably volcanic samples JL06-092 and DC06-047. These ratios are too high to reflect interaction with seawater, or with any known radiogenic Wrangellian crust on Vancouver Island. Such elevated ratios result from either contamination with heretofore unrecognized Proterozoic crust at depth, or to a preferential enrichment in Rb over Sr at some point. All samples have positive εNd, indicating a primarily mantle-derived origin, although the ratios are permissive of some input from preexisting crust, as concluded by DeBari *et al.* (1999).

Mineral Chemistry

Analytical Methods

Samples were analyzed by a CAMECA SX50 electron microprobe at the University of British Columbia. Major and minor elements were determined at 15.03 kV acceleration voltage and a beam current of 20.1 nA for amphibole, feldspar, oxides, olivine, and pyroxene, and a beam current of 10.0 nA for mica. Standards included natural olivine (Mg, Si), diopside (Ca, Si), anorthite (Ca, Si, Al), albite (Na, Si, Al), rutile (Ti) and fayalite (Fe, Si). A number of olivine cumulates and gabbroic cumulates were selected for mineral analysis, in addition to three WCC and Bonanza volcanic samples. Mineral compositions are shown in Table 3.

Olivine

Olivine shows a bimodal composition distribution, with populations of $Fo_{74\text{-}77}$ and $Fo_{81\text{-}82}$. There is an absence of zoning, and all olivine grains in a given sample have nearly-identical Fo content. The Ni concentrations range from 200 ppm to 2400 ppm in the low Fo group, and from 1200 ppm to over 2600 ppm in the high Fo group.

Amphibole

Amphiboles in the olivine cumulates have the highest Mg# (77-83; identical to the olivine grains which they enclose), decreasing to 60-77 in the gabbroic cumulates and 30-65 in the WCC and volcanic samples. The TiO_2 concentrations are highest in the gabbroic cumulates, reaching 3.5 wt%. Cr concentrations may reach almost 7000 ppm in the olivine cumulates, and are an order of magnitude lower (<500 ppm) in the gabbroic cumulates. Amphiboles inclusions in olivine have higher octahedral Al than those which form oikocrysts in the olivine cumulates.

Clinopyroxene

Clinopyroxenes in the olivine cumulate samples contain high Mg# and Cr (80-86, > 6000 ppm), while those in the gabbroic cumulates show a greater range in Mg# (65-86) and much lower Cr (mostly <500 ppm). Zoned clinopyroxenes from a primitive dyke (JL-027) have cores which are generally high in Cr (1000-2600 ppm), and have elevated an Mg# (79-80) compared with their surrounding rims (70-75).

Orthopyroxene

Distinct orthopyroxene populations are defined by the olivine-cumulate, plagioclase-cumulate, and quartz-bearing WCC samples. Mg#s are highest in the olivine-cumulates (77-84, similar to coexisting olivines), lowest in the quartz-bearing WCC samples (56-60), and intermediate in the plagioclase-cumulates (68-72). Ni concentrations are essentially identical among all three populations.

Plagioclase

The anorthite component of plagioclase from the gabbroic cumulates varies widely, from An_{91} to An_{48}, with a population minimum at An_{85-62}. While zoning is not prevalent in the plagioclase cumulates, rare relict Na-rich cores (An_{51-53}) are found within the most Ca-rich grains. Olivine-cumulate sample JL-031 contains subhedral plagioclase of An_{56-60}. Plagioclase grains from WCC

samples range from An_{46} to An_{71}. The largest spread of compositions comes from a primitive dyke (JL-027), where plagioclase ranges from An_{31} to An_{85}.

Spinel

Spinels from the olivine cumulates fall into two populations: a magnetite-magnesioferrite-chromite solid-solution series and a spinel-hercynite-magnesioferrite-chromite series. Some samples may contain representative grains of both populations. Spinels from the gabbroic cumulates and WCC plutons are exclusively magnetite, with very little ulvospinel solid-solution (<5%), while magnetite from a mafic dyke (JL027) has 21 mol.% ulvospinel.

DISCUSSION

Amphibole and arc magma differentiation

The timing and importance of post-cumulus amphibole crystallization in arc suites remains questionable (e.g. (Conrad & Kay, 1984); (Costa *et al*., 2002); (Claeson & Meurer, 2004). The origin of large, voluminous hornblende oikocrysts within the olivine-bearing cumulates is of particular importance to the current study. The rounded anhedral shapes of cumulus olivine, orthopyroxene, and rare clinopyroxene encased in hornblende and/or phlogopite oikocrysts testify to the operation of an amphibole-producing reaction involving early-formed minerals and hydrous melt or fluids. While a model in which aqueous fluids percolating through a cumulate pile react to form amphibole may be feasible for plagioclase-bearing cumulates (see Costa *et al*. 2002), there is not a suitable source of Al in plagioclase-absent ultramafic cumulates to form large hornblende oikocrysts. Furthermore, Al is known to be highly immobile, and aqueous fluids are an unlikely source. The degree to which hornblende can influence magmatic differentiation therefore depends on whether large oikocrysts form by reaction between early cumulates and primitive basaltic magma, or conversely with more evolved melts. In the former

situation hornblende crystallization may exert a significant influence on magma compositions, whereas in the latter situation hornblende is little more than a secondary replacement phase, having little or no influence on magmatic evolution.

Conrad and Kay (1984) report the occurrence of high-Cr amphibole oikocrysts enclosing olivine, clinopyroxene and spinel within xenolith inclusions from Adak Island, Southwestern Alaska. They address the question of the timing of amphibole formation, and ultimately conclude that the high-Cr character of the amphibole oikocrysts resulted from direct crystallization from primitive basalt, rather than from the breakdown of refractory Cr-rich phases. In particular, they note a lack of Cr zoning across amphibole oikocrysts which appear to have been in reaction with Cr-rich phases, as well as the common occurrence of Cr-poor amphiboles encasing Cr-diopside and Cr-spinel (Conrad & Kay, 1984). The presence of high-Cr hornblende and associated Cr-rich spinel inclusions in cumulus olivine within the Bonanza arc section clearly shows that amphibole was indeed present early on during the crystallization sequence. There is no difference in the Cr content of amphibole included in olivine and amphibole oikocrysts, and the elevated Cr content of amphibole oikocrysts is best interpreted to reflect crystallization from a primitive mafic magma, rather than an inheritance from refractory Cr-rich phases.

The influence of hornblende crystallization on magmatic differentiation is clear in major element patterns (figure 13). The Bonanza volcanics and WCC plutons form well-defined trends whose projections intersect the locus of amphibole oikocryst compositions from the olivine-hornblendites. Neither olivine nor clinopyroxene can be significant phases in driving this trend, unless coupled with plagioclase. The WCC plutons contain neither clinopyroxene nor olivine, and so this fractionation assemblage appears unlikely. Although both the WCC plutons and Bonanza volcanics contain abundant plagioclase, including large phenocrysts in the case of the

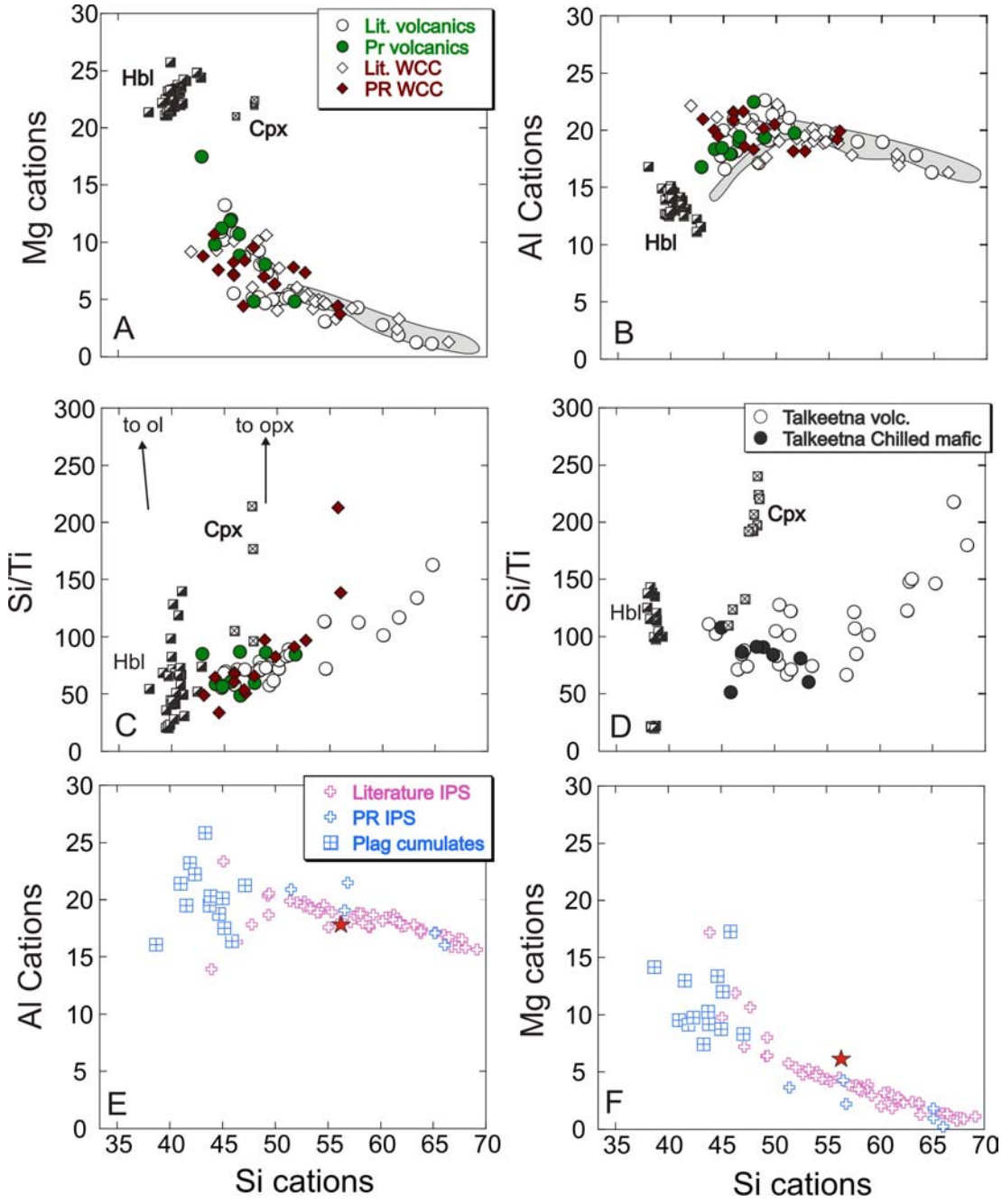

Figure 13. A,B,C). Harker diagrams illustrating the relationship between the WCC plutons, the Bonanza volcanics, and hornblende oikocrysts in ultramafic cumulates (data from current study, DeBari et al. (1999); Massey, (1992-3)). Grey areas show the trend of all of IPS samples. D) Talkeetna volcanic data (Greene et al. (2006)) for comparison. E,F) Relationship between IPS and plagioclase cumulates. Red star: bulk continental crust estimate of Rudnick and Gao (2003). WCC – Westcoast Crystalline Complex; IPS – Island Plutonic Suite; PR – Port Renfrew area samples

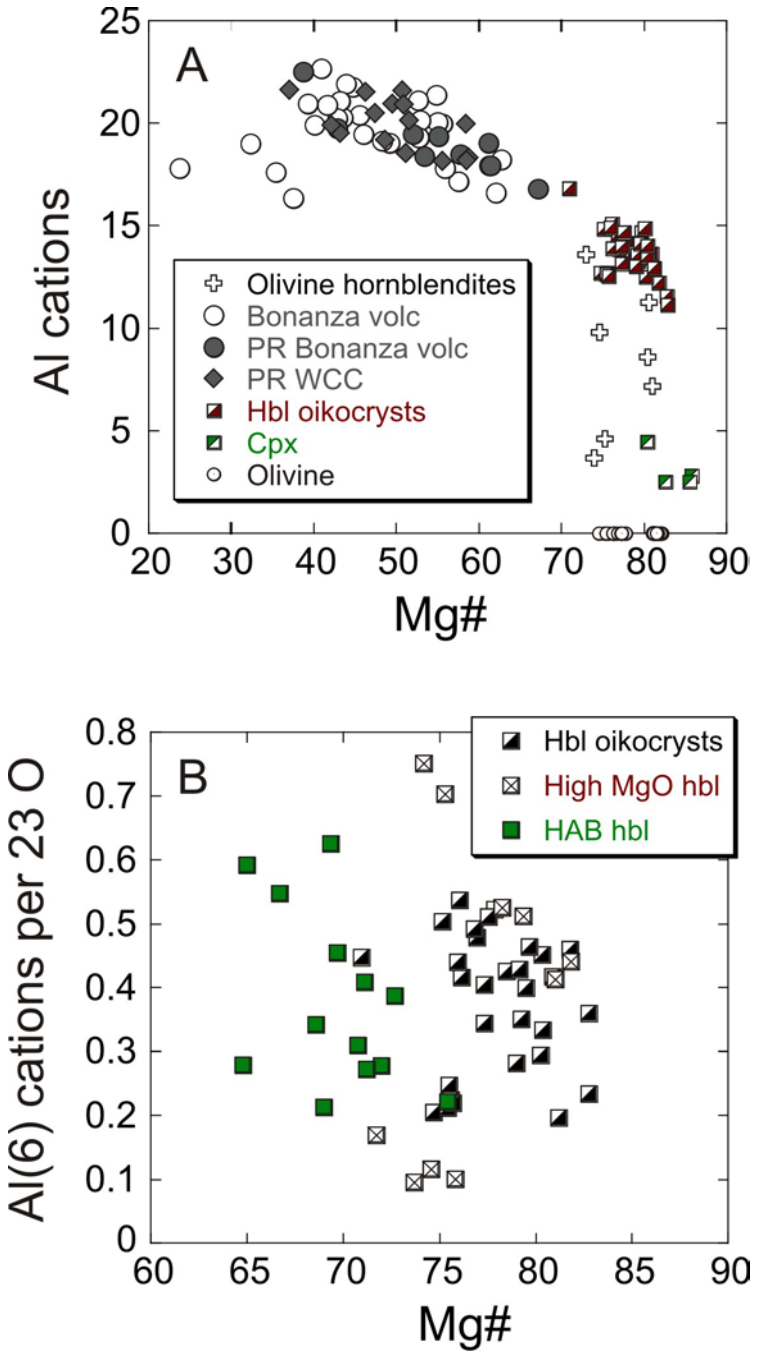

Figure 14. Mg# vs Al plots of whole rock and hornblende compositions showing relationship between hornblende oikocrysts and Bonanza array (A) and comparison of hornblende oikocrysts from olivine cumulates to experimental hornblendes from HAB and HMB compositions (B). Data from Pichavant and Macdonald (2007), Barclay and Carmichael (2004), Grove et al. (2003), Muntener et al. (2001), Hilyard et al. (2000), Sisson and Grove (1993b) HAB – high-alumina basalt; HMB – high-magnesia basalt.

volcanics, there is no indication of any significant plagioclase control among these rocks, as this would lead to a decrease in Al (figure 14a). It would appear therefore that the compositions of WCC plutons and the mafic end member (Si < 50 cations) of the Bonanza volcanic spectrum are controlled mainly by the removal of hornblende whose composition corresponds to that of the oikocrysts in the olivine-cumulates.

The poikilitic texture of the hornblende nonetheless precludes a simple fractional crystallization mechanism. Similar post-cumulus textures are reported from the Rymmen and Eriksberg Gabbros of Sweden (Claeson & Meurer, 2004). These authors interpret such textures as the result of 'imperfect fractional crystallization,' akin to the *in-situ* crystallization model of Langmuir (1989). In this light, the mafic WCC and Bonanza volcanic rocks represent escaped interstitial liquids, which are in equilibrium with hornblende, biotite, and in some cases plagioclase, these being the late-forming intercumulus phases within the olivine-hornblendites.

The Bonanza volcanics are compositionally identical to the WCC plutonics, yet unlike the latter, are devoid of amphibole and biotite, with one exception (JL-092 contains relict amphibole). The paucity of amphibole phenocrysts in mafic arc lavas is well-documented (eg. Arculus & Wills, 1980; Romick *et al*., 1992; Costa *et al*., 2002). Paradoxically, the variation of Dy/Yb ratios with differentiation indices points to widespread cryptic amphibole fractionation in arc volcanic suites (Davidson *et al*., 2007). That the mineral assemblage preserved in basic arc lavas need not reflect the processes occurring at depth has been pointed out by several workers. Rutherford and Devine (1988), for example, document the breakdown of amphibole with decreasing pressure in the Mount St. Helens dacite. Romick *et al.* (1992) suggest that magmas which contain enough H_2O to stabilize amphibole are more likely to erupt explosively, and be emplaced at the surface as pyroclastics, rather than as lava flows. Barclay and Carmichael (2004)

show that the onset of hornblende crystallization in basaltic magmas results in a greater increase in crystallinity than would occur in more felsic magmas, thereby potentially impeding the ascent and eruption of hornblende-bearing basalts. The use of volcanic phase assemblages as a window into igneous processes and differentiation pathways, therefore, ought to be treated with caution. In addition, the assumption that amphibole cannot play an important role in magmatic differentiation given its post-cumulus texture in many arc plutons needs to be reconsidered, particularly in light of the Dy/Yb ratios showing how widespread cryptic amphibole fractionation is among arc volcanic suites (Davidson *et al*., 2007).

Conditions of Bonanza Arc Differentiation

Constraints on the pressure-temperature conditions at which magmas crystallized in arc crust can provide an idea of how magmatic plumbing and crustal composition can change with depth. Unfortunately, the majority of Bonanza arc cumulate rocks have too low a variance in their mineral assemblages to utilize multi-equilibrium thermodynamic approaches such as Thermocalc (Powell & Holland, 1988). In addition, most reactions considered by Thermocalc involve amphibole, whose activity-composition relationships are poorly known, and thus introduce large uncertainties into pressure estimates. I have applied several different approaches, each having their particular shortcomings, to constrain crystallization pressures among the most primitive cumulate-textured samples.

Phase Equilibria

Constraints can be placed on the P-T-fO_2 conditions of crystallization in natural rocks by comparing phase assemblages and their order of appearance with experimental data for the same bulk compositions. Textures and chemistry of the olivine cumulates point to a reaction between olivine and basaltic melt to produce amphibole. In addition, some samples preserve inclusions of

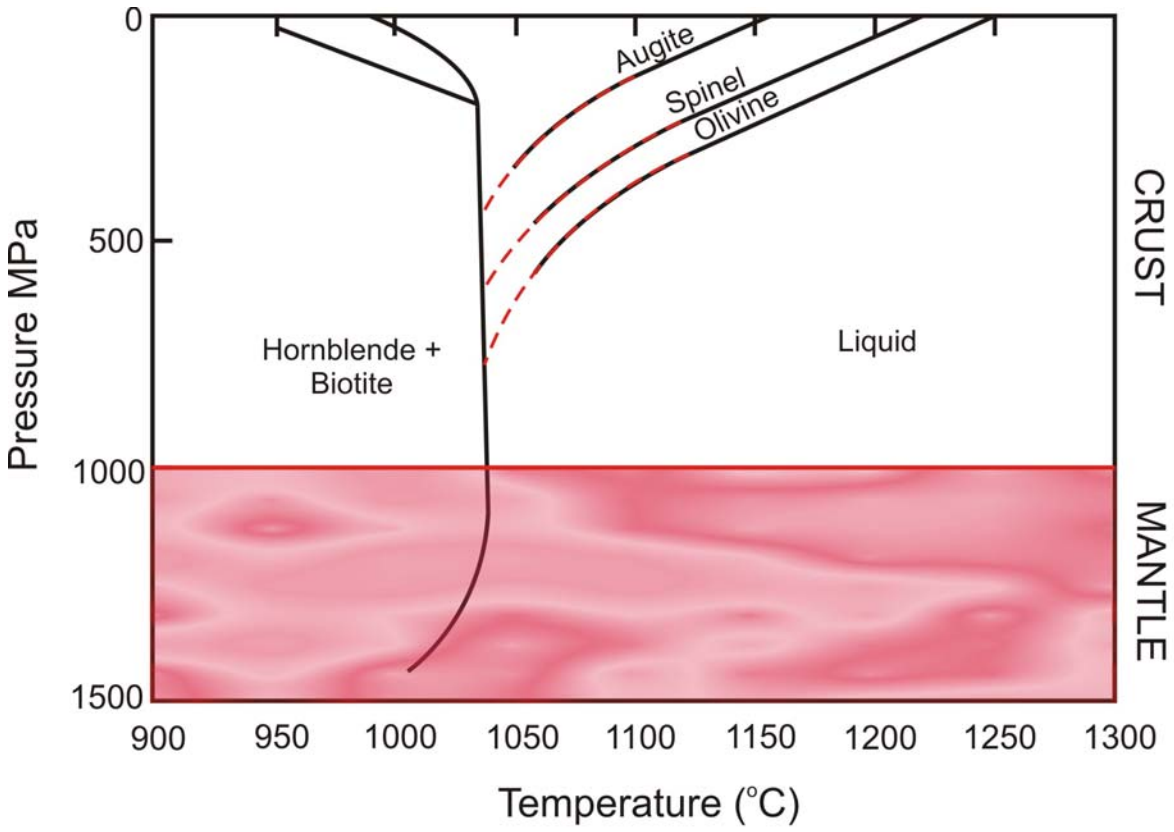

Figure 15. Phase diagram for water-saturated basalt (Mg# 65) adapted from Barclay & Carmichael (2004). Note the appearance of amphibole on the liquidus at elevated pressures.

amphibole within cumulus olivine grains, suggesting an early appearance for amphibole. The association of hornblende and olivine has been noted in arc volcanics ranging in composition from high-MgO basalt to andesite (e.g. Grove *et al*., 2003; Anderson, 1980 and references therein). Phase equilibria studies of hydrous basalts under water-saturated conditions reveal that amphibole can appear with olivine on the liquidus at pressures in excess of 700 MPa (figure 15) (Grove *et al*., 2003; Pichavant & Macdonald, 2007; Barclay & Carmichael, 2004), and at lower pressures (200-400 MPa) in high alumina basaltic and basaltic andesite (Sisson & Grove, 1993; Moore & Carmichael, 1998). Some basaltic andesite compositions, however, do not saturate with olivine under any conditions (e.g. Mercer & Johnston, 2008; Pichavant *et al*., 2002). These observations serve as broad constraints on the crystallization pressures of the olivine-cumulate rocks of 200-700 MPa.

Amphibole Chemistry

Amphibole compositions from experimental studies in basaltic compositions show a shift of Al from the tetrahedral to octahedral site with increased pressure (Adam *et al*., 2007). The compositions of amphiboles from the olivine cumulates are similar to those produced in experiments on natural high-MgO basalts at 800 – 1000 MPa pressure (figure 14b). The latter experiments show a very good correlation between octahedral Al in hornblende and pressure, which is applied as an empirical barometer for the Bonanza arc samples (figure 16a). Application to hornblende from the olivine cumulate samples produces averaged pressures of 470 to 880 MPa (averages for individual samples; see Table 4). Interestingly, amphibole inclusions in olivine give the highest pressures (> 900 MPa).

Both temperature and fO_2 can have potential effects on the empirical barometer, but can be evaluated using the extensive dataset for Pinatubo dacite (Costa *et al*., 2004). No discernible

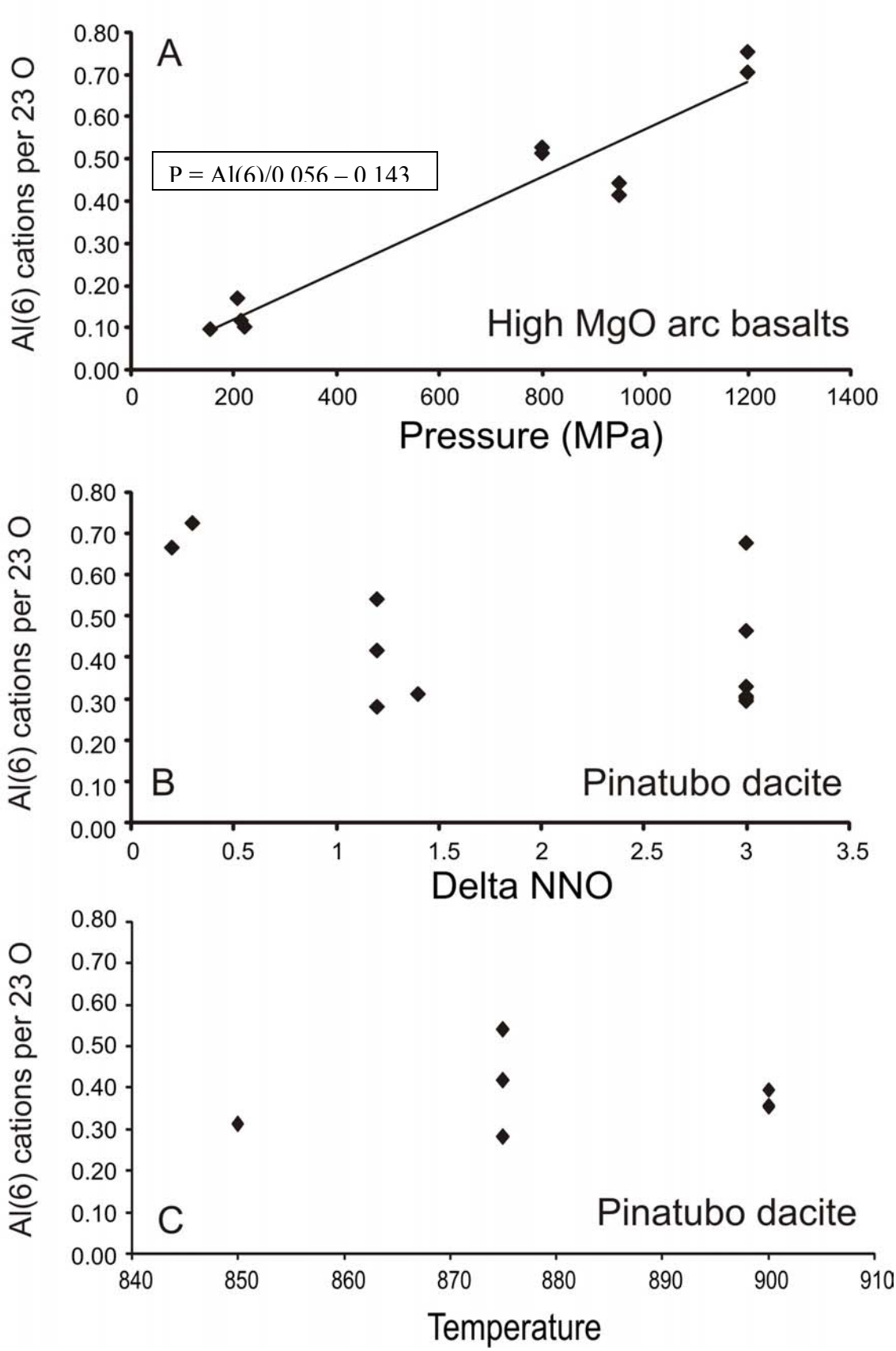
A
P = Al(6)/0.056 – 0.143
High MgO arc basalts
Al(6) cations per 23 O
Pressure (MPa)
0.00
0.10
0.20
0.30
0.40
0.50
0.60
0.70
0.80
0
200
400
600
800
1000
1200
1400
B
Pinatubo dacite
Delta NNO
0.5
1
1.5
2
2.5
3
3.5
C
Pinatubo dacite
Temperature
840
850
860
870
880
890
900
910

Figure 16. A) Correlation of octahedral Al (on basis of 23 oxygens) versus P (MPa) for amphiboles from experiments on high-MgO basalts (Data from Pichavant and Macdonald, 2007; Barclay and Carmichael, 2004; Grove et al. 2003; Muntener et al. 2001). The trend can be fit by least squares regression: Al(6) cations = 0.056*P + 0.008 (r^2 = 0.923) with pressure in MPa. B) Comparison of octahedral Al in amphibole versus fO2 at near-constant pressure (200-210 MPa) and temperature (850-875 C) in experiments on Pinatubo dacite (Costa et al. (2004)). C) Octahedral Al in amphibole versus temperature (data from Costa et al. (2004)) at near-constant pressure (200-210 MPa) and fO2 (NNO +1.2 – NNO +1.4). All experiments under water-saturated conditions.

correlation is observed between octahedral Al in amphibole and fO_2, at nearly constant pressure and temperature (200-210 MPa, 850-875 ºC) (figure 16b) or with temperature, at nearly constant pressure and fO_2 (200-210 MPa, NNO+1.2 – NNO+1.4) (figure 16c). Assuming that amphibole behaviour in dacitic bulk compositions is similar to that in basaltic systems, I conclude that temperature and fO_2 are not significant factors in the behaviour of octahedral Al in amphiboles.

Cumulate rocks with strikingly similar mineralogy and textures to the Bonanza arc cumulates are reported from the Onion Valley complex of the Sierra Nevada batholiths (Sisson *et al.* 1996). These cumulate rocks fall into two categories similar to those from the Bonanza arc: a group of olivine hornblendites, hornblendites and plagioclase hornblendites, and a group of hornblende gabbros (Sisson *et al*., 1996). Sisson and Grove (1993b) provide experimental evidence for the origins of the Sierra Nevada hornblendites and hornblende gabbro cumulates as the products of crystallization of high-alumina basalt (HAB) at 200 to 400 MPa. Olivines from the Sierra Nevada cumulates have Ni concentrations which are up to an order of magnitude lower than those from the Bonanza arc (240-420 ppm vs. 200-2500 ppm) at the same Fo content, and Ni concentrations in olivine grains from experiments on natural HAB compositions rarely exceed 1000 ppm (Sisson & Grove, 1993). This fact, and the absence of plagioclase from the majority of Bonanza arc olivine cumulates, suggests crystallization from a parental magma more primitive than HAB, although crystallization pressure and H_2O content also may be factors. I conclude, therefore, that the most primitive olivine-bearing cumulates of the Bonanza arc crystallized from a magma more primitive than HAB. For this reason, amphibole compositions from HAB experiments are not used as input into the derived empirical barometer for application to the samples.

Thermocalc

Only three of the cumulates have a sufficiently low variance to produce the independent set of reactions required by Thermocalc to provide an accurate P-T estimate. Pressure estimates vary from over 500 MPa for olivine hornblendite to 200 Mpa and under for a plagioclase cumulate and a two-pyroxene WCC gabbro (Table 4).

Trace Elements

The maximum Ce/Y ratio of mafic lavas has been shown to correspond closely with depth to the Moho beneath active island arcs (Mantle & Collins, 2008). Filtering of the database of Bonanza volcanics (for rocks having 44-53 wt.% SiO_2, >4 wt.% MgO and <4 wt.% LOI) yields a maximum depth to the Moho of approximately 32 km. This is in accord with the constraints on crystallization pressures (Table 4), which suggest maximum average pressures of 880 MPa for the olivine cumulates, corresponding roughly to 27 km depth.

The Generation of Andesite

I employ a simple graphical means to evaluate how much crystallization is required to generate the more evolved compositions of the Bonanza arc, given a parental basalt composition. Given the petrographic evidence, I assume the parental melt to the Bonanza arc suite to be in equilibrium with amphibole, and derive parental basalt composition using Fe/Mg partitioning between amphibole and basaltic melt determined by experiment. Experimentally-determined Fe/Mg exchange partition coefficients between amphibole and basaltic liquid (defined as $(Fe/Mg_{amph}) / (Fe/Mg_{liq})$) range from 0.30 to 0.38 (Pichavant & Macdonald, 2007, and references therein). Using this constraint, a range of suitable equilibrium compositions among the Bonanza volcanics is shown in figure 17. The equilibrium compositions with the highest Mg#s are very similar to those used to construct the phase diagram shown in figure 15. Because the Mg#s of coexisting amphibole and olivine in olivine hornblendites are identical, and the Fe/Mg partition

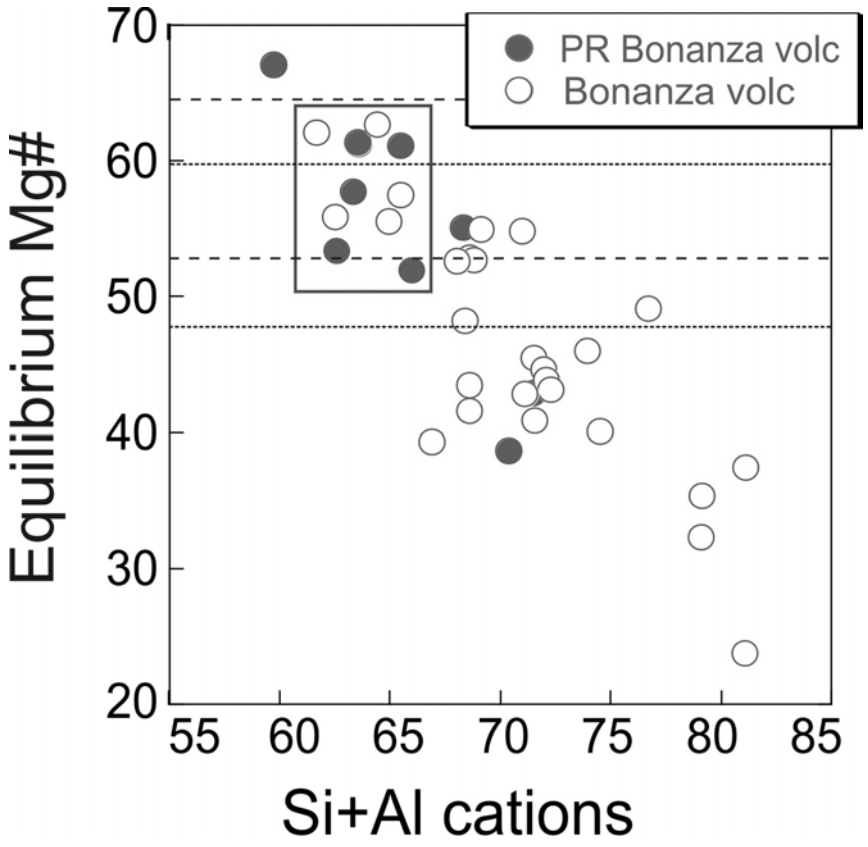

Figure 17. Permissible parental compositions based on Fe/Mg partitioning between amphibole and basalt. Long dashed lines bound the Mg# of liquids in equilibrium with amphibole oikocrysts using Kd amph/liq of 0.38. Short dashed lines bound equilibrium liquids using Kd amph/liq of 0.30. The box outlines probable parental basalt compositions among the Bonanza volcanics. PR – Port Renfrew area samples.

coefficient between olivine and basalt is similar to that between amphibole and basalt (0.3; Roeder & Emslie, 1970), similar equilibrium compositions are suggested by olivine equilibrium arguments.

Taking into account the range of possible parental magma compositions (Figure 17), the lever rule requires the removal of 30-45% hornblende to generate basaltic andesite compositions from parental basalt (Figure 18a). This corresponds to 0.43-0.82 moles of hornblende to accumulate per mole of basaltic andesite. Hornblende fractionation is thus far more economical in producing evolved liquids than a gabbroic assemblage, which requires 1.5-2 moles of cumulate per mole of basaltic andesite (Kuno, 1968; Greene *et al*., 2006). The main reason for this lies in the fact that amphibole contains less silica than gabbroic cumulates, and is therefore more effective in producing residual liquids with elevated SiO_2 (Davidson *et al*., 2007).

The basaltic andesite field of the Bonanza arc is marked by an inflection in major-element space which signals the onset of plagioclase +/- magnetite saturation (figure 13). Major and trace element plots suggest that the more intermediate to felsic compositions of the IPS and the bulk of the plagioclase cumulate samples are complementary with respect to WCC and Bonanza volcanic rocks of basaltic andesite composition (Figures 12b, 13). The presence of pyroxenes in many plagioclase cumulates poses a difficulty in establishing a straight-forward relationship between these sample populations; pyroxenes are not present in any of the IPS samples, and in only two quartz-bearing WCC samples. The removal of pyroxene-bearing cumulates therefore cannot be invoked to derive the IPS from the majority of WCC compositions. Hornblende-plagioclase cumulates, though less common, provide a suitable complement to the IPS rocks. Sisson *et al.* (1996) similarly concluded that clinopyroxene-

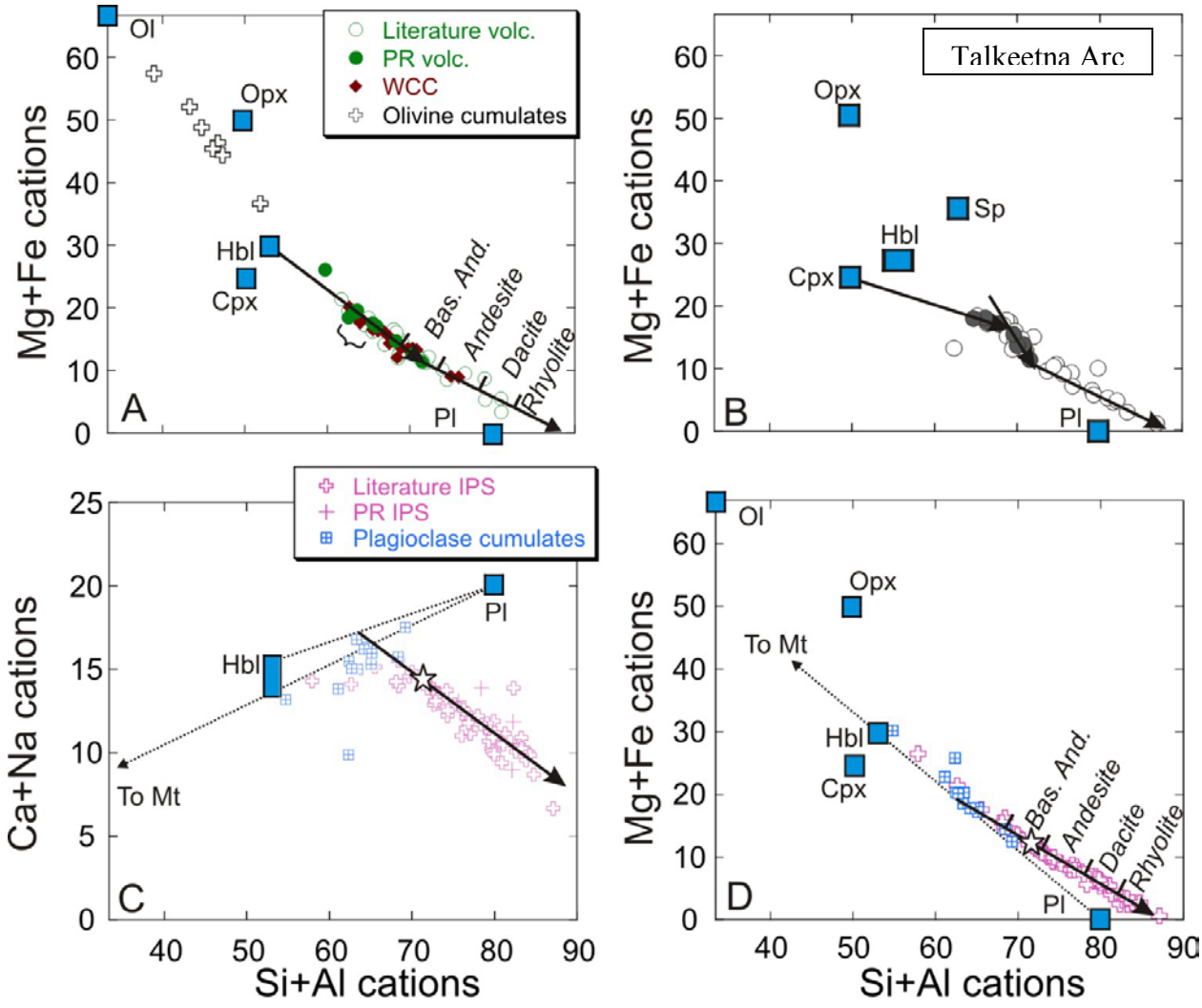

Figure 18. Major element plots illustrating the mineralogic controls on the Bonanza arc lithologies. Bracket in A indicates range of potential parental compositions (see text). B) shows Talkeetna volcanics (open circles) and chilled mafic rocks (full circles) from Greene et al. (2006) for comparison with Bonanza volcanics (A). Stars in C,D) indicate starting point of hornblende gabbro fractionation (plag-in) in the IPS. WCC – Westcoast Crystalline Complex; IPS – Island Plutonic Suite; PR – Port Renfrew area samples; Ol – olivine; Cpx – clinopyroxene; Opx – orthopyroxene; Hbl – hornblende; Sp – spinel; Pl – plagioclase; Mt - magnetite

bearing gabbroic cumulates from the Sierra Nevada batholiths must reflect the presence of distinct, possibly drier, magmas.

Experimental studies have shown that liquids in equilibrium with a phase assemblage consisting of calcic plagioclase + hornblende +/- magnetite are andesitic to dacitic in composition (Pichavant *et al*., 2002). The presence of cumulate rocks with this assemblage suggests that the generation of intermediate liquids in the Bonanza arc has been accomplished, at least in part, by crystal/liquid fractionation. The tie line connecting hornblende and plagioclase acts as an endmember towards which the plagioclase cumulates trend (Figure 18). The bulk of the plagioclase cumulates plot very near to the intersection of the hornblende-plagioclase tie line and the extension of the trend produced by the bulk of the IPS rocks. Worth noting is the virtual co-linearity of hornblende, plagioclase and magnetite on these diagrams. A few samples plot towards the magnetite end member, but magnetite is never present in plagioclase cumulates in greater proportions than 5%, and so its removal or addition has limited leverage on most major elements.

Using the point at which plagioclase appears in the fractionating assemblage as a starting composition (corresponding to the point of inflection on major element plots), andesitic compositions would be produced by the removal of 13-48% hornblende gabbro. Granitic compositions corresponding to the most evolved IPS samples would be generated by the removal of yet more hornblende gabbro, up to 65%. This implies that for every mole of andesite, there would have to be 0.15-0.92 moles of hornblende gabbro cumulate, while each mole of rhyolite would require 1.5-1.9 moles of cumulate.

DeBari *et al.* (1999) have presented abundant evidence, including field observations and trace element trends, to show that partial melting of pre-existing amphibolite has produced some of the felsic intrusions found both in the WCC and the IPS. They suggest that the range of intermediate compositions within the Bonanza Group can be modeled as mixtures of these crustally-derived melts and more primitive mantle-derived magmas. Support for this model comes from isotopic studies of the IPS and Bonanza Group volcanics showing that these units require some involvement from what would most likely have been Sicker Group crust in order to explain their lead isotopic trends (Andrew & Godwin, 1989; Andrew *et al*., 1991). Conclusions as to the degree of crustal assimilation required by Pb and Sr isotopic ratios to explain the Bonanza arc data rest on the assumption that the mantle source from which the parental Bonanza magma was removed was in fact identical to the MORB mantle source. This is not necessarily the case, given that the mantle wedge must be fluxed with fluids driven off the subducting slab, and is therefore compositionally different from MORB mantle.

It is very difficult to quantify the relative importance of crystal fractionation versus crustal melting in the generation of the more felsic compositions of the Bonanza arc, as there is supporting evidence for both processes. The argument against fractional crystallization as the mechanism by which granitoid plutons are generated traditionally relies on the observation that a vast volume of cumulate material is required (up to 50 units of cumulate per unit of dacite; Kuno, 1968). The involvement of hornblende in the fractionating assemblage, however, significantly reduces the volume of cumulate which is needed to produce evolved liquids. Given the existence of plagioclase-hornblende-magnetite cumulates which provide a suitable complement to the intermediate-felsic compositions of the arc, and which have been shown experimentally to coexist with liquids of andesitic to dacitic composition (Pichavant *et al.* 2002), it seems

reasonable to conclude that liquids as evolved as andesite, and potentially dacite, have been generated by fractionation processes in the middle crust of the Bonanza arc.

Comparison with Talkeetna arc

Aside from spatial and temporal similarities between the Talkeetna and Bonanza arcs, some important differences stand out. First and foremost is the absence of a preserved section of tectonized mantle, and of garnet-bearing cumulate rocks, in the Bonanza arc. The deeper levels of the Bonanza arc may have been displaced during the collision of the Pacific Rim terrane, but there is no geochemical support for garnet involvement in its evolution. The role for pyroxene in the Talkeetna arc (Greene *et al*. 2006), versus the olivine-hornblende assemblage of early cumulates from the Bonanza arc, suggests more hydrous conditions during differentiation of the Bonanza arc. As noted previously, there is a surprising lack of europium anomaly associated with the plagioclase cumulates of the Bonanza arc, while similar lithologies from the Talkeetna arc have quite prominent europium anomalies (Greene *et al.* 2006). Interestingly, the olivine hornblendites and gabbroic cumulates of the Sierra Nevada batholith also have small europium anomalies. I suggest that the conditions indicated by the olivine-hornblende association may occur at high fO_2. Under such elevated fO_2, europium anomalies may disappear as trivalent Eu becomes the dominant species (Carmichael & Ghiorso, 1990).

Petrologic modeling of the evolution of the Talkeetna arc has focused on anhydrous gabbroic fractionation assemblages, because these are the cumulus minerals in the deep plutonic lithologies (e.g. Greene *et al.* 2006). Greene *et al.* (2006) suggest possible fractionation of olivine+plag or plag+cpx+opx+spinel assemblages as responsible for the evolution from primitive basalt to basaltic andesite in the Talkeetna arc. The difference in fractionation pathways between the Bonanza arc and the Talkeetna arc is illustrated in Figure 16. In contrast to

the mafic end of the Bonanza arc array, which trends away from hornblende, the mafic end of the Talkeetna volcanic array trends away from clinopyroxene, and contains an inflection not seen in the Bonanza arc data (figure 18b). The petrological models of Greene *et al.* (2006) suggest that >25 wt.% pyroxenite (~70:30 cpx:opx) must have been removed from a primary melt to produce their most primitive volcanic compositions. Most of these primitive cumulates are thought to have delaminated, or to have crystallized below the Moho, due to the discrepancy between the modeled cumulate proportions and those observed in the field (DeBari & Sleep, 1991; Greene *et al.* 2006).

A similar evaluation of the proportion of cumulates preserved in the Bonanza arc section is frustrated by the poor overall exposure due to vegetation. It is therefore difficult to asses how abundant olivine hornblendite cumulates are within the WCC, although they appear to be quite minor (<5% of total WCC roadcuts). There most certainly is a missing cumulate section, as the composition of both olivine and hornblende in even the most primitive olivine hornblendites are too rich in iron to have been in equilibrium with a primary magma (Mg# ~70). Consider the relationship between the most primitive liquid compositions from the Bonanza arc, and primary island arc basalts from the literature (figure 19). Primary basalt from the island of Grenada, Lesser Antilles (Devine, 1995) can only produce the primitive Bonanza compositions documented in this study by hornblende fractionation (Mg+Fe vs. Si space, plot not shown), and requires ~70% crystallization. Primary basalt from the Aleutian arc (DeBari, 1997 and references therein) could produce primitive Bonanza compositions either by hornblende crystallization (~25%) or by olivine+/-cpx crystallization (~10%). Lastly, estimated primary basalt from the Talkeetna arc (Debari & Sleep, 1991) could produce primitive Bonanza compositions by cpx+opx (~25%) or by cpx+olivine crystallization (~40%). The composition and volume of the

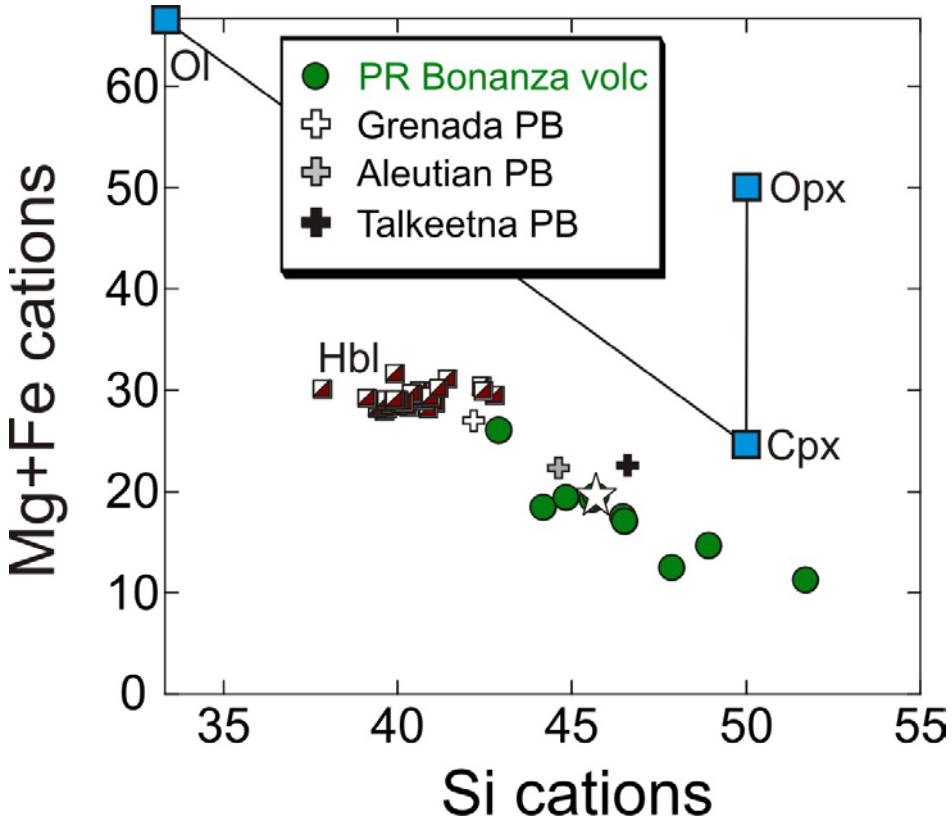

Figure 19. Relationship between Bonanza arc volcanics, primary island arc basalts from the literature, and potential fractionation assemblages. Data from Devine, (1995); DeBari and Sleep, (1991); DeBari, (1997). PR – Port Renfrew; PB – primary basalt. Star indicates most primitive Bonanza volcanic composition from the current study (JL06-050). Squares with red triangles indicate the compositions of hornblende in olivine hornblendites from this study. Ol – olivine; Opx – orthopyroxene; Cpx – clinopyroxene; Hbl - hornblende

missing Bonanza arc cumulates therefore depends on both the composition of primary basalt, as well as the nature of the extensive variables (P,T, f_{H2O}) at the time of crystallization.

Implications for the continental crust

Figure 13f shows a clear discrepancy between andesitic compositions from the Bonanza arc and the estimated compositions of bulk continental crust: the latter has higher Mg/Si than similar magmatic compositions from the Bonanza arc. Therefore, although the removal of olivine hornblendite and hornblende gabbro cumulates would drive the bulk composition of the Bonanza arc crust towards suitable silica concentrations, such a mechanism cannot account for the elevated Mg of the bulk continental crust.

Macpherson (2008) has shown that garnet+cpx fractionation can produce andesites having much higher Mg# than those produced by amphibole+plag fractionation, and that blending of these endmembers over time may produce high-Mg# andesite. Furthermore, many continental arc plutons and lavas have compositions identical to estimates of bulk continental crust (Kelemen & Hanghoj, 2003). These observations suggest that the generation of BCC requires high pressures, and therefore, thickened crust. Because most oceanic island arcs are built on thinner crust, compositions equivalent to BCC appear to be rare in the island arc environment. It seems instead that the most likely long term process generating the bulk continental crust is the accretion of island arcs to continental margins (Reymer & Schubert, 1984), subsequent tectonic thickening, and the eventual delamination of dense garnetiferous rock from the lower crust, producing a high-Mg# andesite bulk composition (see Lee *et al.* 2007).

CONCLUSIONS

The results of this study show the following:

1. The removal of amphibole from the most primitive Bonanza arc non-cumulate compositions controls the compositions of the WCC plutons and Bonanza volcanics until the onset of plagioclase crystallization. Amphibole is removed by the intercumulus crystallization of large oikocrysts, in a process similar to the in-situ fractionation of Langmuir (1989), and the imperfect fractional crystallization of Cleason and Meurer (2002). Consequently, intercumulus phases can exert significant influence on the differentiation of arc suites, and should not be ignored during petrological modeling.

2. Empirical amphibole barometry indicates crystallization pressures for primitive magmas of the Bonanza arc of 470-800 MPa, near water-saturated conditions, in good agreement with phase equilibrium constraints based on the presence of amphibole and phlogopite inclusions in olivine.

3. Phenocryst assemblages in volcanic rocks do not necessarily reflect the processes which govern their compositions. Re-equilibration in shallow magma chambers, as well as the loss of volatiles during ascent, may cause significant changes in mineralogy. Examination of only the volcanics would not have led to the appreciation of the role of amphibole in the Bonanza arc. This underscores the importance of the 'plutonic window' in evaluating arc processes.

4. The crystallization of primary arc basalt to yield the liquids in equilibrium with the most primitive olivine hornblendites has left no record in the Bonanza arc section. Cumulates whose volume and composition depend on the composition of primary basalt, as well as the nature of extensive variables during crystallization, would likely have been formed as the ascending primary magma stalled at the mantle-crust boundary. Because the Bonanza

arc section does not contain any in-situ lower crust or mantle, the fate of these cumulates is unknown.

5. Garnet saturation may be crucial in generating the high Mg# andesites which are thought to be the magmatic analogue of bulk continental crust. Arc suites which differentiate at pressures below the garnet stability field (like the Bonanza arc) are unable to produce the distinct Mg/Si ratio of bulk continental crust. Island arc terranes likely retain their basaltic bulk composition until accretion, whereupon tectonic thickening causes the formation of garnet and eventual delamination of dense garnetiferous (eclogitic) rock, leaving a remainder of andesitic bulk continental crust.

Acknowledgements – Sincere thanks to G. Pearson, P. Heatherington and T. Mawson of Port Renfrew for their hospitality and for sharing their geologic and logistic information. Analytical assistance with EMP and ICPMS analyses was provided by M. Raudsepp and J. Spence, respectively. This study was supported by grants from NSERC of Canada, Geoscience BC and Emeralds Fields Resources to Dante Canil.

Chapter 3

SUMMARY

This thesis sheds light on a number of problematic aspects of arc petrology, the first of which is the role of amphibole during igneous differentiation. Experimental work shows that hornblende can appear on the liquidus in high-MgO arc basalts at or near water-saturated conditions, and mid-crustal pressures. Experiments also show that once hornblende and olivine +/- clinopyroxene appear together, olivine and clinopyroxene quickly react with the liquid to form more hornblende. Olivine hornblendite cumulates have textures which document the operation of both of these processes: hornblende inclusions in olivine, and the inclusion of anhedral olivine and rare clinopyroxene in hornblende oikocrysts. There is no combination of olivine, clinopyroxene, and/or orthopyroxene which can account for the trend of the Bonanza array. Olivine and plagioclase fractionating together could explain the trend, but such an assemblage is not evidenced by the rocks; plagioclase is rare in primitive cumulates, and olivine is entirely absent from non-cumulate plutonic lithologies. Instead, the composition of hornblende oikocrysts from olivine hornblendites provides a perfect complement to the Bonanza liquid array. The post-cumulus nature of the hornblende, often cited as reason to preclude its involvement in fractionation models, suggests a liquid rather than crystal fractionation process. The correspondence of mineralogy in the WCC plutons and the post-cumulus phases in the olivine hornblendites is further evidence in support of this view: the WCC plutons represent escaped interstitial liquid which is in equilibrium with amphibole, biotite, and plagioclase.

A corollary to this conclusion is that differentiation models which use phenocryst assemblages and/or cumulus minerals alone as constraints run the risk of ignoring the roles of important phases such as amphibole. The cryptic role for amphibole as required by Dy/Yb in arc

lavas worldwide implies that in-situ style amphibole fractionation as observed in the Bonanza arc may be a common process in arc suites.

Significantly different conclusions as to fractionation pathways have been reached for the Bonanza arc and the Talkeetna arc. Petrologic modeling suggests that pyroxene-rich cumulates form the complement to primitive Talkeetna arc basalt, while this thesis shows that hornblende-rich cumulates complement primitive Bonanza arc basalt. This difference is likely due to either more hydrous conditions in the Bonanza setting, which stabilize olivine (and hornblende) over pyroxene, or to greater crystallization pressure in the Talkeetna setting, which stabilizes pyroxene over olivine, or some combination of these factors.

Although DeBari *et al.* (1999) do not propose any detailed petrologic models for the evolution of the Bonanza arc, they did suggest that much of the intermediate compositions of the WCC could be modeled as mixtures of mafic arc magmas and partial melts of amphibolite country rock, based on trace element patterns and field observations of migmatite textures. While no textures indicative of partial melting were observed (or recognized) as part of this study, it is important to point out that both this study and DeBari *et al.* (1999) suggest an important role for amphibole in the evolution of the Bonanza arc.

Another important conclusion of this thesis is that there is no magmatic equivalent to the composition of bulk continental crust (BCC) in the Bonanza array. No amount of delamination of the known lithologies will drive the bulk arc composition to match BCC. The generation of high-Mg# andesite, the magmatic analogue of BCC, seems to require the fractionation of garnet from basalt. This is only possible at high pressures, and is therefore unlikely to occur in most island arcs, as these tend to be built on relatively thin crust. Instead, garnet fractionation,

delamination, and the processing of basalt into high-Mg# andesite are likely to proceed mainly along thicker continental arcs.

FUTURE WORK

One avenue of future work entails the search for the lower crust of the Bonanza arc section. The Wark diorite and Colquitz Gneiss units which underlie much of Victoria proper appear to be part of the WCC, displaced by sinistral motion along the San Juan Fault. If this is the case, then cumulates of a more primitive nature which could shed light on the early differentiation of primary basalt may be present near Victoria.

Another avenue of future work would be more detailed analyses of mineral compositions from the WCC plutons and the olivine hornblendites. If these rocks are indeed related as per my conclusions, then there should be a systematic relationship between the hornblende, plagioclase and biotite in the WCC samples and those in the olivine hornblendites. For example, if the WCC plutons represent the escaped interstitial liquids from the olivine hornblendites, then there should be no compositional gap between the compositions of intercumulus phases and the most primitive, true liquid compositions in the WCC.

Lastly, the apparent correlation between octahedral Al and pressure in experimental hornblende from high-MgO basalts requires much more work before truly robust application to barometry is possible. Given the rarity of hornblende phenocrysts in natural arc basalts, such a barometer would be far more useful in plutonic applications.

References

Adam, J., Oberti, R., Camara, F. & Green, T. H. (2007). An electron microprobe, LAM-ICP-MS and single-crystal X-ray structure refinement study of the effects of pressure, melt-H2O concentration and fO2 on experimentally produced basaltic amphiboles. *European Journal of Mineralogy*, **19**, 641-655.

Allen, J. C. & Boettcher, A. L. (1983). The stability of amphibole in adesite and basalt at high pressures. *American Mineralogist*, **68**, 307-314.

Anderson, A. T. J. (1980). Significance of hornblende in calc-alkaline andesites and basalts. *American Mineralogist*, **65**, 837-851.

Andrew, A., Armstrong, R. L. & Runkle, D. (1991). Neodymium-strontium-lead isotopic study of Vancouver Island igneous rocks. *Canadian Journal of Earth Science*, **28**, 1744-1752.

Andrew, A. & Godwin, C. I. (1989). Lead- and strontium-isotope geochemistry of Paleozoic Sicker Group and Jurassic Bonanza Group volcanic rocks and Island Intrusions, Vancouver Island, British Columbia. *Canadian Journal of Earth Science*, **26**, 894-907.

Annen, C., Blundy, J. D. & Sparks, R. S. J. (2006). The genesis of intermediate and silicic magmas in deep crustal hot zones. *Journal of Petrology*, **47**(3), 505-539.

Arculus, R. J. (1981). Island arc magmatism in relation to the evolution of the crust and mantle. *Tectonophysics*, **75**, 113-133.

Arculus, R. J. (1999). Origins of the Continental Crust. *Journal & Proceedings of the Royal Society of New South Wales*, **132**, 83-110.

Arculus, R. J. & Wills, K. J. A. (1980). The petrology of plutonic blocks and inclusions from the Lesser Antilles island arc. *Journal of Petrology*, **21**(4), 743-799.

Barclay, J. & Carmichael, I. S. E. (2004). A hornblende basalt from Western Mexico: water-saturated phase relations constrain a pressure-temperature window of eruptability. *Journal of Petrology*, **45**(3), 485-506.

Behn, M. D. & Kelemen, P. B. (2006). Stability of arc lower crust: insights from the Talkeetna arc section, south central Alaska, and the seismic structure of modern arcs. *Journal of Geophysical Research*, **111**, in print.

Beswick, A. E. & Soucie, G. (1978). A correction procedure for metasomatism in an Archean greenstone belt. *Precambrian Research*, **6**, 235-248.

Bowen, N. L. (1928). *The evolution of the igneous rocks*. Dover Publciations Inc., New York.

Burns, L. (1985). The Border Ranges ultramafic and mafic complex, south-central Alaska: cumulate fractionates of island arc volcanics. *Can. J. Earth Sci.*, **22**, 1020-1038.

Carmichael, I. S. E. (1991). The redox states of basic and silicic magmas: a reflection of their source regions? *Contrib. Mineral. Petrol.*, **106**, 129-141.

Carmichael, I. S. E. & Ghiorso, M. S. (1990). Controls on oxidation-reduction relations in magmas. *Rev. Mineralogy, Min. Soc. America, Washington, D.C*, **24**, 191-212.

Cawthorn, R. G., Curran, E. B. & Arculus, R. J. (1973). A petrogenetic model for the origin of the calc-alkaline suite of Grenada, Lesser Antilles. *Journal of Petrology*, **14**, 327-337.

Cawthorn, R. G. & O'Hara, M. J. (1976). Amphibole fractionation in calc-alkaline magma genesis. *American Journal of Science*, **276**, 309-329.

Claeson, D. T. & Meurer, W. P. (2004). Fractional crystallization of hydrous basaltic "arc-type" magmas and the formation of amphibole-bearing gabbroic cumulates. *Contributions to Mineralogy and Petrology*, **147**, 288-304.

Clift, P. D., Pavlis, T., DeBari, S. M., Draut, A. E., Rioux, M. & Kelemen, P. B. (2005). Subduction erosion of the Jurassic Talkeetna-Bonanza arc and the Mesozoic accretionary tectonics of western North America. *Geology*, **33**, 881-884.

Conrad, W. K. & Kay, R. W. (1984). Ultramafic and mafic inclusions from Adak Island: crystallization history, and implications for the nature of primary magmas and crustal evolution in the Aleutian Arc. *Journal of Petrology*, **25**, 88-125.

Costa, F., Dungan, M. A. & Singer, B. S. (2002). Hornblende- and phlogopite-bearing gabbroic xenoliths from Volcan San Pedro (36S), Chilean Andes: evidence for melt and fluid migration and reactions in subduction-related plutons. *Journal of Petrology*, **43**(2), 219-241.

Costa, F., Scaillet, B. & Pichavant, M. (2004). Petrological and experimental constraints on the pre-eruption conditions of Holocene dacite from Volcan San Pedro (36S, Chilean Andes) and the importance of sulphur in silicic subduction-related magmas. *Journal of Petrology*, **45**(4), 855-881.

Creaser, R. A., Grutter, H. S., Carlson, J. & Crawfor, B. (2004). Macrocrystal phlogopite Rb-Sr dates for the Ekati property kimberlites: evidence for multiple intrusive episodes during Paleocene and Eocene time. *Lithos*, **76**, 399-414.

Davidson, J., Turner, S., Handley, H., Macpherson, C. & Dosseto, A. (2007). Amphibole "sponge" in arc crust? *Geology*, **35**(9), 787-790.

DeBari, S. M. (1997). Evolution of magmas in continental and oceanic arcs; the role of the lower crust. *The Canadian Mineralogist*, **35**(2), 501-519.

DeBari, S. M., Anderson, R. G. & Mortensen, J. K. (1999). Correlation among lower to upper crustal components in an island arc: the Jurassic Bonanza arc, Vancouver Island, Canada. *Can. J. Earth Sci.*, **36**, 1371-1413.

DeBari, S. M. & Coleman, R. G. (1989). Examination of the deep levels of an island arc: evidence from the Tonsina ultramafic-mafic assemblage, Tonsina, Alaska. *J. Geophys. Res.*, **94**, 4373-4391.

DeBari, S. M. & Sleep, N. H. (1991). High-Mg, low-Al bulk composition of the talkeetna island arc, Alaska: Implications for primary magmas and the nature of arc crust. *Geol. Soc. Amer. Bull.*, **103**, 37-47.

Devine, J. D. (1995). Petrogenesis of the basalt-andesite-dacite association of Grenada, Lesser Antilles island arc, revisited. *Journal of Volcanology and Geothermal Research*, **69**, 1-33.

Eggins, S. M., Woodhead, J. D., Kinsley, L. P. J., Mortimer, G. E., Sylvester, P., McCulloch, M. T., Hergt, J. M. & Handler, M. R. (1997). A simple method for the precise determination of > 40 trace elements in geological samples by ICPMS using enriched isotope internal standardisation. *Chemical Geology*, **134**, 311-326.

Eichelberger, J. C., Izbekov, P. E. & Browne, B. L. (2006). Bulk chemical trends at arc volcanoes are not liquid lines of descent. *Lithos*, **87**, 135-154.

England, T.J.E., Calon, T.J. (1991). The Cowichan fold and thrust system, Vancouver Island, southwestern British Columbia. *Geological Society of America Bulletin,* **103,** 336-362.

Francis, D. (1986). The pyroxene paradox in MORB glasses - a signature of picritic parental magmas? *Nature*, **319**, 586-589.

Gill, J. (1981). *Orogenic andesites and plate Tectonics*. Springer, Berlin.

Greene, A. R., DeBari, S. M., Kelemen, P. B., Blusztajn, J. & Clift, P. D. (2006). A detailed geochemical study of island arc crust: the Talkeetna arc section, South-Central Alaska. *Journal of Petrology*, **47**(6), 1051-1093.

Grove, T. L., Elkins-Tanton, L. T., Parman, S. W., Chatterjee, N., Muntener, O. & Gaetani, G. A. (2003). Fractional crystallization and mantle-melting controls on calc-alkaline differentiation trends. *Contributions to Mineralogy and Petrology*, **145**, 515-533.

Grove, T. L. & Kinzler, R. J. (1986). Petrogenesis of andesites. *Annual Review of Earth and Planetary Sciences*, **14**, 417-454.

Hacker, B. R., Mehl, L., Kelemen, P. B., Rioux, M., Behn, M. D. & Luffi, P. (2008). Reconstruction of the Talkeetna intraoceanic arc of Alaska through thermobarometry. *Journal of Geophysical Research*, **113**.

Hawkesworth, C. J. & Kemp, A. I. S. (2006). The differentiation and rates of generation of the continental crust. *Chemical Geology*, **226**, 134-143.

Holloway, J. R. & Burnham, C. W. (1972). Melting relations of basalt with equilibrium pressure less than total pressure. *Journal of Petrology*, **13**, 1-29.

Huppert, H. E. & Sparks, S. J. (1988). The generation of granitic magmas by intrusion of basalt into continental crust. *Journal of Petrology*, **29**, 599-624.

Isachsen, C. E. (1987). Geology, geochemistry, and cooling history of the Westcoast Crystalline Complex and related rocks, Meares Island and vicinity, Vancouver Island, British Columbia. *Canadian Journal of Earth Sciences*, **24**, 2047-2064.

Jagoutz, O., Muntener, O., J.-P., B., Ulmer, P. & Jagoutz, E. (2006). Lower continental crust formation through focused flow in km-scale melt conduits: the zoned ultramafic bodies of the Chilas Complex in the Kohistan island arc (NW Pakistan). *Earth and Planetary Science Letters*, **242**, 320-342.

Johnston, S. T. (2008). The Cordilleran ribbon continent of North America. *Annu. Rev. Earth Planet. Sci.*, **36**, 495-530.

Jones, D. L., Silberling, N. J. & Hillhouse, J. (1977). Wrangellia - a displaced terrane in northwestern North America. *Canadian Journal of Earth Sciences*, **14**, 2565-2577.

Kelemen, P. B. & Hanghoj, K. (2003). One view of the geochemistry of subduction-related magmatic arcs, with an emphasis on primitive andesite and lower crust. *The Crust, Treatise in Geochemistry*, **3**, 593-659.

Kuno, H. (1968). Origin of andesite and its bearing on the island arc structure. *Bull. volcanol.*, **32**, 141-176.

Langmuir, C. H., 1989. Geochemical consequences of *in situ* crystallization. *Nature*, **340**, 199-205.

Lee, C.-T. A., Morton, D. M., Kistler, R. W. & Baird, A. K. (2007). Petrology and tectonics of Phanerozoic continent formation: from island arcs to accretion and continental arc magmatism. *Earth and Planetary Science Letters*, **263**, 370-387.

Macpherson, C. G. (2008). Lithosphere erosion and crustal growth in subduction zones: insights from initiation of the nascent East Philippine arc. *Geology*, **36**(4), 311-314.

Mantle, G. W. & Collins, W. J. (2008). Quantifying crustal thickness variations in evolving orogens: correlation between arc basalt composition and Moho depth. *Geology*, **36**(1), 87-90.

Massey, N. W. D. & Friday, S. J. (1987). Geology of the Cowichan Lake area, Vancouver Island (92C/16). *Geological Fieldwork 1987*, **Paper 2003-1**, 223-229.

Massey, N.W.D. (1995). Geology and mineral resources of the Cowichan Lake area (92C/16). **Paper 1992-3,** 112 p.

Mercer, C. N. & Johnston, A. D. (2008). Experimental studies of the P-T-H2O near-liquidus phase relations of basaltic andesite from North Sister Volcano, High Oregon Cascades: constraints on lower-crustal mineral assemblages. *Contributions to Mineralogy and Petrology*, **155**, 571-592.

Moore, G. & Carmichael, I. S. E. (1998). The hydrous phase equilibria (to 3 kbar) of an andesite and basaltic andesite from western Mexico: constraints on the water content and conditions of phenocryst growth. *Contributions to Mineralogy and Petrology*, **130**, 304-319.

Muller, J. E., Cameron, B. E. B. & Northcote, K. E. (1981). Geology and mineral deposits of Nootka Sound map-area, Vancouver Island, British Columbia. *Geological Survey of Canada*, **Paper 80-16**.

Nixon, G. T., Hammack, J. L., Hamilton, J. V. & Jennings, H. (1993). Preliminary geology of the Mahatta Creek Area, northern Vancouver Island (92L/5). *Geological Fieldwork 1992*, **Paper 1993-1**, 17-35.

Nixon, G. T., Hammack, J. L., Payie, G. J., Snyder, L. D., Archibald, D. A. & Barron, D. J. (1995). Quatsino-San Josef map area, northern Vancouver Island: Geological overview (92L/12W, 1021/8, 9). *Geological Fieldwork 1994*, **Paper 1995-1**, 9-21.

Nixon, G. T. & Orr, A. J. (2007). Recent revisions to the Early Mesozoic stratigraphy of Northern Vancouver Island (NTS 102I; 092L) and metallogenic implications, British Columbia. In: *Geological Fieldwork 2006*, pp. 163-177, BC Ministry of Energy, Mines and Petroleum Resources.

Pichavant, M. & Macdonald, R. (2007). Crystallization of primitive basaltic magmas at crustal pressures and genesis of the calc-alkaline igneous suite: experimental evidence from St Vincent, Lesser Antilles arc. *Contributions to Mineralogy and Petrology*, **154**, 535-558.

Pichavant, M., Martel, C., Bourdier, J.-L. & Scaillet, B. (2002). Physical conditions, structure, and dynamics of a zoned magma chamber: Mount Pelee (Martinique, Lesser Antilles Arc). *Journal of Geophysical Research*, **107**(B5).

Powell, R. & Holland, T. J. B. (1988). An internally consistent database with uncertainties and correlations: 3. applications to geobarometry, worked examples and a computer program. *J. metamorphic Geol.*, **6**, 173-204.

Prouteau, G. & Scaillet, B. (2003). Experimental constraints on the origin of the 1991 Pinatubo dacite. *Journal of Petrology*, **44**(12), 2203-2241.

Rapp, R. P. & Watson, E. B. (1995). Dehydration melting of metabasalt at 8-32 kbar: implications for continental growth and crust-mantle recycling. *Journal of Petrology*, **36**(4), 891-931.

Reymer, A. & Schubert, G. (1984). Phanerozoic addition rates to the continental crust. *Tectonics*, **3**, 63-77.

Roeder, P. L. & Emslie, R. F. (1970). Olivine-liquid equilibrium. *Contributions to Mineralogy and Petrology*, **29**, 275-289.

Romick, J. D., Kay, S. M. & Kay, R. W. (1992). The influence of amphibole fractionation on the evolution of calc-alkaline andesite and dacite tephra from the Central Aleutians, Alaska. *Contributions to Mineralogy and Petrology*, **112**, 101-118.

Rudnick, R. L. (1995). Making continental crust. *Nature*, **378**, 571-578.

Rudnick, R. L. & Gao, S. (2003). Composition of the continental crust. *The Crust, Treatise in Geochemistry*, **3**, 1-64.

Rutherford, M. J. & Devine, J.,(1988). The May 18, 1980, eruption of Mount St. Helens 3. Stability and chemistry of amphibole in the magma chamber. *Journal of Geophysical Research*, **93**(B10), 11949-11959.

Schmidberger, S. S., Heaman, L. M., Simonetti, A., Creaser, R. A. & Whitefor, S. (2007). Lu-Hf, in situ Sr and Pb isotope and trace element systematics for mantle eclogites from the Diavik diamond mine: Evidence for Paleoproterozoic subduction beneath the Slave Craton, Canada. *Earth and Planetary Science Letters*, **254**, 55-68.

Sisson, T. W. & Grove, T. L. (1993). Experimental investigations of the role of H2O in calc-alkaline differentiation and subduction zone magmatism. *Contributions to Mineralogy and Petrology*, **113**, 143-166.

Sisson, T. W., Grove, T. L. & Coleman, D. S. (1996). Hornblende gabbro sill complex at Onion Valley, California, and a mixing origin for the Sierra Nevada batholith. *Contributions to Mineralogy and Petrology*, **126**, 81-108.

Ulmer, P. (2001). Partial melting in the mantle wedge - the role of H2O in the genesis of mantle-derived 'arc-related' magmas. *Physics of the Earth and Planetary Interiors*, **127**, 215-232.

Unterschutz, J. L. E., Creaser, R. A., Erdmer, P., Thompson, R. I. & Daughtry, K. L. (2002). North American margin origin of Quesnel terrance strata in the southern Canadian Cordillera: Inferences from geochemical and Nd isotopic characteristics of Triassic metasedimentary rocks. *Geological Society of America Bulletin*, **114**, 462-475.

Yoder, H. S. & Tilley, C. E. (1962). Origin of basalt magmas: experimental study of natural and synthetic rock systems. *Journal of Petrology*, **3**, 342-532.

Appendix A

Table 1 – Whole rock analyses

Sample	JL06-001	JL06-003	JL06-006	JL06-010	JL06-013	JL06-014	JL06-017	JL06-019	JL06-020	JL06-022	JL06-025	JL06-044
Rock Type	WCC	WCC	WCC	WCC	WCC	WCC	WCC	WCC	WCC	WCC	WCC	WCC
Map Unit	10	10	10	10	10	10	10	10	10	10	10	10
UTM Zone	403673	403699	403629	412720	404212	405063	392804	393874	393392	392435	415781	391400
UTM E	5389127	5389566	5387463	5387075	5390800	5386424	5388843	5387227	5385237	5386793	5385266	5386446
Major elements (oxides wt %)												
SiO2	55.75	59.57	49.82	48.56	55.15	46.74	49.57	50.67	48.76	48.24	58.57	45.15
TiO2	0.76	0.37	1.31	0.96	0.81	1.84	1.23	1.02	0.94	1.06	0.56	1.22
Al2O3	16.29	17.41	16.70	19.28	16.49	17.39	19.43	16.45	19.46	18.63	17.66	18.65
Fe2O3t	8.28	6.57	11.37	11.63	7.90	13.93	10.67	9.44	9.94	11.11	7.13	12.53
FeOt												
MnO	0.15	0.21	0.17	0.22	0.12	0.22	0.21	0.17	0.17	0.18	0.18	0.19
MgO	5.23	3.14	5.99	5.05	5.61	5.35	3.16	6.79	5.16	5.80	2.62	6.20
CaO	7.53	5.04	10.56	9.42	6.98	9.85	8.97	8.23	10.97	6.71	6.67	10.28
Na2O	2.86	4.68	2.95	3.02	3.76	3.35	4.01	3.36	3.18	4.14	3.16	2.96
K2O	1.77	1.41	0.58	0.73	1.82	0.26	1.37	1.71	0.30	1.11	1.43	0.82
P2O5	0.20	0.40	0.17	0.28	0.21	0.50	0.41	0.20	0.13	0.27	0.23	0.21
LOI	1.62	1.34	0.99	1.46	1.53	0.47	1.58	2.01	1.69	3.29	1.68	1.67
Total	**100.47**	**100.14**	**100.62**	**100.61**	**100.39**	**99.42**	**100.60**	**98.04**	**100.72**	**100.53**	**98.22**	**99.89**
Trace elements (ppm) -XRF												
Lab	McGill	McGill	McGill	McGill	McGill	McGill	McGill	McGill	McGill	McGill	McGill	McGill
Cr2O3	179	57	114	32	212	92	17	313	185	15	33	24
Ni	53	20	35	18	61	42	11	107	30	15	12	14
V	189	82	330	232	208	334	274	180	308	254	105	350
Ga	14	16	15	18	14	19	18	13	17	15	15	16
Nb	4	3	3	2	3	2	4	2	1	2	4	2
Pb	1	0	0	0	<d/l	<d/l	0	1	<d/l	<d/l	2	0
Rb	52	38	9	15	50	4	22	43	3	27	31	12
Sr	423	502	429	502	833	494	482	314	593	871	414	492
Th	7	6	5	4	8	<d/l	6	0	4	6	0	4
U	3	3	3	2	4	2	2	2	2	4	2	2
Y	15	20	19	25	16	26	27	24	13	20	20	25
Zr	82	109	52	72	87	27	79	91	24	66	92	62

Sample	JL06-001	JL06-003	JL06-006	JL06-010	JL06-013	JL06-014	JL06-017	JL06-019	JL06-020	JL06-022	JL06-025	JL06-044
Trace elements (ppm) - ICPMS												
Lab	**UVic**	**UVic**	**UVic**	**UVic**	**UVic**	**UVic**	**UVic**	**UVic**	**UVic**	**UVic**	**UVic**	**UVic**
Sc	23.3	5.5	41.3	27.0	24.0	31.5	31.2	28.1	40.3			
V	194	74	361	240	205	283	323	265	359			
Co	24.4	11.2	33.1	26.0	22.9	20.8	26.1	21.8	33.5			
Ni	40.4	11.4	27.4	9.6	45.9	4.4	19.0	7.7	6.6			
Cu	66	10	210	48	5	90	8	28	56			
Rb	54.3	39.5	8.2	13.3	47.6	26.5	1.3	24.5	11.9			
Sr	439	479	422	508	835	555	589	886	561			
Y	15.7	21.7	21.5	25.1	16.3	28.1	12.1	20.1	25.1			
Zr	44	5	25	15	33	23	12	12	16			
Nb	4.6	2.9	3.7	3.2	4.5	4.5	0.7	2.7	3.2			
Ba	552	523	123	244	651	498	176	133	251			
Hf	1.42	0.26	1.26	0.80	1.19	1.13	0.48	0.56	0.91			
Ta	0.33	0.20	0.22	0.14	0.31	0.22	0.05	0.15	0.16			
Th	4.64	1.99	1.87	0.50	3.83	1.73	0.09	1.00	0.13			
U	2.09	0.94	0.93	0.21	1.32	0.67	0.04	0.34	0.06			
Rare Earth Elements (ppm) - ICPMS												
La	11.3	22.2	7.6	9.0	11.4	11.9	3.3	7.7	6.7			
Ce	23.6	46.6	18.4	22.1	25.4	28.1	7.8	18.5	18.1			
Pr	2.9	5.7	2.6	3.2	3.2	3.9	1.2	2.7	2.8			
Nd	13.2	24.7	13.2	15.9	14.4	19.3	6.4	13.5	14.2			
Sm	3.0	4.8	3.4	4.0	3.3	4.9	1.8	3.5	3.9			
Eu	0.95	1.37	1.11	1.31	1.04	1.58	0.99	1.09	1.29			
Gd	2.9	4.5	3.6	4.1	3.2	5.0	2.0	3.5	4.2			
Tb	0.44	0.63	0.59	0.66	0.48	0.78	0.34	0.56	0.69			
Dy	2.6	3.6	3.6	4.1	2.8	4.8	2.2	3.5	4.3			
Ho	0.53	0.74	0.75	0.86	0.57	0.96	0.45	0.71	0.88			
Er	1.50	2.07	2.14	2.43	1.60	2.72	1.27	2.00	2.46			
Tm	0.23	0.30	0.32	0.37	0.24	0.41	0.19	0.30	0.36			
Yb	1.51	1.92	2.06	2.45	1.59	2.66	1.23	2.00	2.33			
Lu	0.23	0.28	0.30	0.36	0.23	0.39	0.18	0.29	0.33			

Sample	JL06-066	JL06-103	JL06-108	DC06-047	DC06-048	JL06-027	JL06-038	JL06-050	JL06-053	JL06-061	JL06-090	JL06-092
Rock Type												
Map Unit	WCC	WCC	WCC	Bon. Volc.	Bon. Volc.	Bon. Volc.	Bon. Volc.	Bon. Volc.	Bon. Volc.	Bon. Volc.	Bon. Volc.	Bon. Volc.
UTM Zone	10	10	10	10	10	10	10	10	10	10	10	10
UTM E	372623	393105	411744			408959	415057	385254	385589	387233	396953	396437
UTM N	5395509	5386920	5388666			5392773	5390142	5391473	5398648	5418628	5416048	5415837
Major elements (oxides wt %)												
SiO2	51.76	46.68	52.08	48.28	48.70	44.53	48.97	48.79	51.29	45.53	53.52	46.07
TiO2	0.71	0.96	0.84	1.05	0.74	0.70	1.32	1.06	0.79	1.03	0.84	1.08
Al2O3	18.12	17.96	18.16	16.13	16.93	14.81	17.39	16.25	17.24	16.08	17.35	16.14
Fe2O3t	9.30	10.72	9.83	10.65	9.66	12.01	11.65	10.96	9.35	11.98	9.06	11.43
FeOt												
MnO	0.19	0.18	0.18	0.22	0.23	0.19	0.18	0.21	0.19	0.18	0.18	0.19
MgO	4.98	7.60	4.47	8.42	7.55	12.19	6.27	8.62	5.70	6.82	3.38	7.76
CaO	8.76	11.49	7.21	9.89	9.68	10.21	9.20	9.15	5.75	10.34	6.21	8.41
Na2O	3.43	2.45	3.36	2.54	2.15	1.24	3.08	2.64	4.06	3.64	3.89	3.10
K2O	1.29	0.44	1.33	1.17	1.84	0.48	0.55	1.45	2.25	0.11	2.03	1.15
P2O5	0.11	0.15	0.23	0.23	0.17	0.15	0.22	0.23	0.21	0.44	0.27	0.26
LOI	1.34	1.43	2.36	1.24	2.24	3.57	1.80	1.12	3.42	4.36	3.55	4.77
Total	**99.99**	**100.07**	**100.05**	**99.87**	**99.92**	**100.10**	**100.65**	**100.53**	**100.25**	**100.53**	**100.28**	**100.38**
Trace elements (ppm) -XRF												
Lab	**McGill**	**McGill**	**McGill**	**McGill**	**McGill**	**McGill**	**McGill**	**McGill**	**McGill**	**McGill**	**McGill**	**McGill**
Cr2O3	69	156	34	520	291	230	154	546	59	139	21	113
Ni	24	83	14	158	94	96	66	162	42	42	13	32
V	230	261	226	253	217	228	243	253	208	304	172	321
Ga	16	14	17	14	13	12	15	15	14	15	17	16
Nb	2	1	3	2	1	1	2	2	3	5	10	4
Pb	0	0	0	<d/l	<d/l	0	<d/l	0	3	3	1	0
Rb	29	8	33	36	74	7	9	41	65	3	42	19
Sr	565	315	393	395	426	267	303	361	348	267	564	453
Th	7	3	4	4	4	4	3	3	4	5	9	4
U	3	1	2	2	2	1	2	2	2	2	4	2
Y	16	16	20	19	15	14	25	19	19	20	33	20
Zr	58	47	70	65	51	32	95	64	78	61	179	69

Sample	JL06-066	JL06-103	JL06-108	DC06-047	DC06-048	JL06-027	JL06-038	JL06-050	JL06-053	JL06-061	JL06-090	JL06-092
Trace elements (ppm) - ICPMS												
Lab	**UVic**	**UVic**	**UVic**	**UVic**	**UVic**	**UVic**	**UVic**	**UVic**	**UVic**	**UVic**	**UVic**	**UVic**
Sc	29.1	38.2	27.6	28.9	38.0	47.3	30.4	35.3	28.6	42.4	22.9	41.4
V	261	277	237	253	227	246	240	268	213	320	169	322
Co	22.6	41.0	23.9	31.7	40.8	53.6	38.3	32.3	27.2	37.4	18.0	36.5
Ni	15.2	63.6	7.6	120.9	69.9	78.9	47.2	127.3	29.8	29.5	4.6	22.7
Cu	34	86	21	69	79	76	60	71	61	53	46	41
Rb	24.3	8.3	32.1	33.2	77.4	6.3	9.3	42.5	68.1	1.9	36.6	18.4
Sr	482	372	400	394	454	275	337	385	364	296	505	476
Y	20.1	17.9	21.3	18.6	16.2	14.5	27.5	19.5	20.3	21.8	31.1	20.4
Zr	25	19	53	34	36	24	50	29	65	55	146	58
Nb	3.3	1.5	3.3	2.6	1.7	1.4	3.2	2.8	3.7	5.8	10.9	5.8
Ba	292	125	437	293	845	210	172	325	709	57	704	399
Hf	1.21	0.85	1.50	1.06	1.10	0.83	1.60	0.95	1.95	1.62	4.05	1.78
Ta	0.28	0.09	0.16	0.16	0.11	0.08	0.19	0.17	0.22	0.27	0.62	0.29
Th	3.26	0.39	0.75	0.83	0.84	0.45	0.98	0.89	2.02	2.08	5.08	1.52
U	1.08	0.16	0.31	0.41	0.40	0.19	0.38	0.40	0.84	0.90	1.94	0.49
Rare Earth Elements (ppm) - ICPMS												
La	8.6	4.0	9.8	6.6	5.7	4.0	7.6	5.8	9.7	14.8	18.4	11.2
Ce	20.3	10.0	21.6	15.8	13.5	9.8	19.3	14.1	21.1	33.1	39.4	25.1
Pr	2.8	1.5	2.8	2.2	1.9	1.4	2.8	2.1	2.8	4.3	4.8	3.3
Nd	13.2	8.0	13.5	11.3	9.7	7.6	14.8	10.6	13.2	20.7	21.7	15.8
Sm	3.2	2.4	3.3	3.0	2.6	2.2	4.1	2.9	3.2	4.8	5.1	3.9
Eu	1.16	0.90	1.09	1.08	0.99	0.76	1.39	1.07	1.04	1.42	1.30	1.26
Gd	3.2	2.8	3.4	3.3	2.8	2.4	4.6	3.2	3.3	4.5	5.1	3.9
Tb	0.52	0.47	0.54	0.53	0.45	0.39	0.76	0.53	0.54	0.65	0.82	0.60
Dy	3.3	3.0	3.5	3.3	2.9	2.5	4.8	3.3	3.4	3.8	5.2	3.7
Ho	0.68	0.63	0.72	0.68	0.59	0.52	0.97	0.69	0.71	0.75	1.08	0.73
Er	2.03	1.79	2.05	1.89	1.67	1.46	2.69	1.93	2.05	2.06	3.18	2.04
Tm	0.32	0.26	0.31	0.28	0.25	0.22	0.40	0.28	0.31	0.30	0.49	0.30
Yb	2.19	1.69	2.06	1.78	1.61	1.42	2.44	1.79	2.10	1.95	3.27	1.93
Lu	0.34	0.25	0.31	0.25	0.24	0.21	0.34	0.26	0.32	0.29	0.50	0.28

Sample	JL06-093	JL06-052	JL06-059	JL06-060	JL06-074	JL06-077	JL06-089	JL06-002	JL06-040	JL06-041	JL06-054	JL06-076
Rock Type												
Map Unit	Bon. Volc.	?? Volc.*	?? Volc.	?? Volc.	?? Volc.	?? Volc.	?? Volc.	IPS	IPS	IPS	IPS	IPS
UTM Zone	10	10	10	10	10	10	10	10	10	10	10	10
UTM E	400758	384961	385977	386784	417448	423043	392974	403707	418621	398191	385589	421738
UTM N	5414266	5395873	5416780	5418171	5405242	5384583	5410037	5389526	5392761	5393513	5398648	5387048
Major elements (oxides wt %)												
SiO2	48.15	52.03	48.08	49.59	47.41	62.88	47.33	70.12	69.00	54.30	70.70	59.96
TiO2	1.07	2.60	1.90	0.75	2.30	0.93	1.84	0.40	0.34	0.92	0.19	0.61
Al2O3	19.21	14.51	13.84	19.25	13.84	14.72	13.88	15.63	15.34	18.69	14.57	17.13
Fe2O3t	10.46	14.57	14.83	8.03	15.62	7.84	14.00	2.78	3.21	8.36	2.86	6.82
FeOt												
MnO	0.17	0.22	0.25	0.15	0.21	0.15	0.23	0.06	0.09	0.19	0.08	0.15
MgO	3.28	2.87	6.57	3.34	5.87	3.38	6.76	0.71	1.29	2.58	0.16	3.04
CaO	4.97	7.18	9.79	10.16	9.57	2.18	9.60	2.33	3.09	6.90	0.87	6.55
Na2O	3.97	3.10	3.12	5.03	4.10	4.26	3.36	5.30	4.05	3.75	4.47	3.54
K2O	2.31	1.25	0.37	0.12	0.31	1.31	0.58	2.14	2.26	2.47	5.38	1.20
P2O5	0.31	0.94	0.17	0.36	0.21	0.25	0.18	0.08	0.10	0.31	0.03	0.17
LOI	6.51	1.05	0.77	3.88	0.49	2.75	2.20	0.76	1.18	1.97	0.94	1.30
Total	**100.41**	**100.32**	**99.71**	**100.65**	**99.94**	**100.65**	**99.98**	**100.31**	**99.95**	**100.44**	**100.25**	**100.47**
Trace elements (ppm) -XRF												
Lab	**McGill**	**McGill**	**McGill**	**McGill**	**McGill**	**McGill**	**McGill**	**McGill**	**McGill**	**McGill**	**McGill**	**McGill**
Cr2O3	18	57	136	20	149	15	328	27	17	28	23	34
Ni	12	29	87	10	77	8	106	7	8	13	7	11
V	280	349	360	173	412	125	354	27	56	181	<d/l	152
Ga	18	19	17	21	21	14	16	14	12	15	17	14
Nb	7	12	7	6	11	5	8	4	4	6	13	3
Pb	4	2	<d/l	3	0	2	<d/l	2	2	5	7	0
Rb	51	53	6	3	5	43	13	45	36	62	129	21
Sr	259	352	457	299	256	317	548	245	304	447	84	371
Th	4	9	5	5	4	4	5	4	7	7	9	5
U	2	4	2	2	1	2	3	4	2	3	4	2
Y	23	60	26	19	32	30	25	17	12	32	51	16
Zr	78	294	108	90	138	141	108	274	97	80	274	71

Sample	JL06-093	JL06-052	JL06-059	JL06-060	JL06-074	JL06-077	JL06-089	JL06-002	JL06-040	JL06-041	JL06-054	JL06-076
Trace elements (ppm) - ICPMS												
Lab	**UVic**	**UVic**	**UVic**	**UVic**	**UVic**	**UVic**	**UVic**	**USask**	**USask**	**USask**	**USask**	**USask**
Sc	26.6	35.4	40.9	17.0	3.6	17.6	44.8	8.4	13.8	26.8	10.9	25.5
V	278	355	391	174	43	114	379	26	64	183	2	163
Co	23.2	29.5	46.3	16.5	3.9	13.8	45.3	3.2	6.4	14.4	0.9	16.1
Ni	5.0	19.7	67.2	4.3	5.6	3.3	84.9	1.9	1.2	2.9	0.5	4.8
Cu	18	89	175	26	3	6	206	4	5	21	12	23
Rb	48.9	53.1	4.1	2.1	0.3	44.1	12.7	45.5	35.7	68.6	128.2	19.6
Sr	253	352	461	299	24	329	637	255	297	526	90	377
Y	23.3	64.8	27.3	18.2	3.2	30.7	29.5	17.3	11.6	30.2	51.4	17.8
Zr	73	278	25	73	5	132	109	317	89	77	286	86
Nb	7.3	13.7	10.2	6.8	1.3	5.9	10.9	7.0	4.9	8.6	17.6	4.9
Ba	269	258	165	28	8	315	218	798	994	742	1080	466
Hf	1.93	6.94	1.20	2.01	0.22	3.41	3.10	7.85	2.47	2.36	7.52	2.27
Ta	0.36	0.79	0.65	0.33	0.08	0.36	0.68	0.59	0.32	0.43	0.78	0.26
Th	1.96	5.87	0.70	2.62	0.08	2.34	0.84	3.38	3.68	4.30	8.70	1.91
U	0.70	2.85	0.17	0.91	0.02	0.99	0.27	2.55	1.32	1.60	3.99	0.45
Rare Earth Elements (ppm) - ICPMS												
La	15.6	29.1	8.0	16.9	0.9	13.0	8.0	13.9	15.8	17.5	29.2	11.9
Ce	34.4	77.8	20.1	36.1	2.5	30.3	21.2	26.1	29.1	40.4	65.6	24.3
Pr	4.4	10.6	2.9	4.4	0.4	4.2	3.1	3.0	3.2	5.5	8.7	3.1
Nd	20.5	46.1	14.8	19.3	1.8	20.5	16.0	11.0	10.6	22.6	34.3	12.0
Sm	4.6	11.0	4.2	4.1	0.5	5.2	4.5	2.3	2.1	5.2	8.1	2.8
Eu	1.39	2.53	1.47	1.18	0.18	1.52	1.50	0.92	0.71	1.43	0.92	0.93
Gd	4.5	11.0	4.8	3.7	0.6	5.3	5.1	2.2	2.0	5.4	8.7	2.9
Tb	0.68	1.71	0.79	0.54	0.10	0.87	0.85	0.38	0.29	0.87	1.38	0.47
Dy	4.1	10.5	5.0	3.3	0.6	5.4	5.3	2.6	1.9	5.6	9.5	3.0
Ho	0.83	2.14	0.99	0.65	0.12	1.12	1.05	0.59	0.40	1.15	1.98	0.65
Er	2.34	6.01	2.67	1.85	0.32	3.26	2.92	2.01	1.30	3.45	6.15	1.97
Tm	0.34	0.90	0.39	0.29	0.05	0.50	0.42	0.35	0.19	0.52	0.98	0.30
Yb	2.19	5.87	2.40	1.96	0.28	3.26	2.68	2.70	1.40	3.51	6.55	2.05
Lu	0.32	0.86	0.34	0.30	0.04	0.48	0.39	0.42	0.20	0.46	0.97	0.28

Sample	JL06-107	JL06-008	JL06-009	JL06-011	JL06-015	JL06-023	JL06-024	JL06-045	JL06-067	JL06-068	JL06-069	JL06-100
Rock Type												
Map Unit	IPS	Plag. Cum.	Plag. Cum.	Plag. Cum.	Plag. Cum.	Plag. Cum.	Plag. Cum.	Plag. Cum.	Plag. Cum.	Plag. Cum.	Plag. Cum.	Plag. Cum.
UTM Zone	10	10	10	10	10	10	10	10	10	10	10	10
UTM E	412336	412556	412720	412334	405084	392332	414195	389013	371930	371538	371183	409315
UTM N	5386098	5385656	5387075	5386105	5385889	5387705	5386734	5385584	5394121	5393252	5390137	5390155
Major elements (oxides wt %)												
SiO2	60.21	43.52	43.03	40.04	46.12	46.13	44.88	49.93	43.76	48.71	48.00	47.51
TiO2	0.40	1.06	1.44	1.80	0.46	1.03	1.00	0.59	1.00	0.65	1.17	1.12
Al2O3	19.29	20.43	19.05	14.11	23.35	17.45	19.99	19.11	17.43	14.76	15.78	18.03
Fe2O3t	5.57	11.91	15.00	21.88	7.04	11.36	11.22	8.53	13.58	11.79	11.33	11.79
FeOt												
MnO	0.08	0.20	0.19	0.27	0.13	0.20	0.19	0.16	0.21	0.25	0.28	0.21
MgO	1.56	6.38	6.72	9.84	5.30	7.27	6.96	5.93	9.17	12.32	8.57	6.19
CaO	6.44	11.03	12.36	11.05	14.51	12.50	12.81	9.97	10.78	6.62	9.96	10.36
Na2O	4.01	2.10	1.56	0.94	1.59	2.22	1.85	3.10	1.56	1.75	2.75	2.97
K2O	0.84	0.58	0.40	0.28	0.35	0.41	0.25	0.71	1.16	1.17	0.87	0.52
P2O5	0.30	0.22	0.07	0.06	0.06	0.19	0.19	0.09	0.09	0.13	0.12	0.18
LOI	1.71	2.40	0.89	0.77	1.35	1.36	0.89	1.94	1.72	2.52	1.33	1.56
Total	**100.41**	**97.43**	**100.71**	**101.05**	**98.91**	**98.76**	**99.34**	**98.12**	**100.46**	**100.68**	**98.83**	**100.45**
Trace elements (ppm) -XRF												
Lab	**McGill**	**McGill**	**McGill**	**McGill**	**McGill**	**McGill**	**McGill**	**McGill**	**McGill**	**McGill**	**McGill**	**McGill**
Cr2O3	23	68	34	25	380	281	150	150	65	111	64	76
Ni	9	33	24	26	66	56	43	40	51	112	71	29
V	76	330	544	721	171	302	318	211	388	152	247	341
Ga	15	18	17	16	15	16	16	17	14	12	18	17
Nb	2	3	2	1	0	2	2	1	1	2	5	2
Pb	1	<d/l	<d/l	<d/l	<d/l	<d/l	<d/l	<d/l	<d/l	0	<d/l	<d/l
Rb	27	11	7	6	9	7	4	9	23	26	14	6
Sr	481	451	402	320	543	355	488	496	376	293	388	446
Th	11	<d/l	4	3	<d/l	<d/l	<d/l	<d/l	4	2	<d/l	4
U	3	2	2	2	2	1	2	2	2	1	1	2
Y	20	29	17	16	7	24	20	11	14	16	43	20
Zr	240	48	24	20	27	38	37	35	35	36	75	40

Sample	JL06-107	JL06-008	JL06-009	JL06-011	JL06-015	JL06-023	JL06-024	JL06-045	JL06-067	JL06-068	JL06-069	JL06-100
Trace elements (ppm) - ICPMS												
Lab	**USask**		**UVic**	**UVic**					**UVic**	**UVic**		**UVic**
Sc	20.9		35.9	62.0					43.1	23.2		43.8
V	80		421	749					396	134		341
Co	12.1		30.6	66.1					52.9	54.6		33.0
Ni	4.3		7.4	14.5					35.7	89.3		18.3
Cu	52		103	211					109	32		61
Rb	26.1		4.0	4.9					23.4	25.5		5.8
Sr	499		287	317					413	296		499
Y	21.8		12.2	15.7					14.1	16.4		20.6
Zr	343		10	13					23	22		30
Nb	4.2		1.0	1.1					1.6	2.1		2.1
Ba	441		105	103					510	503		213
Hf	7.17		0.44	0.59					0.89	0.92		1.06
Ta	0.32		0.06	0.06					0.10	0.12		0.10
Th	9.89		0.39	0.07					0.39	0.37		0.35
U	1.20		0.14	0.03					0.20	0.15		0.15
Rare Earth Elements (ppm) - ICPMS												
La	33.4		2.1	1.9					3.8	4.7		5.6
Ce	64.0		5.2	5.6					9.7	11.4		14.0
Pr	7.1		0.8	1.0					1.5	1.7		2.1
Nd	24.8		4.9	6.2					7.6	8.9		11.3
Sm	4.7		1.7	2.2					2.2	2.5		3.2
Eu	1.11		0.66	0.70					0.86	0.92		1.19
Gd	4.4		2.1	2.6					2.5	2.7		3.4
Tb	0.60		0.35	0.43					0.39	0.45		0.56
Dy	3.9		2.3	2.8					2.5	2.8		3.6
Ho	0.79		0.46	0.57					0.50	0.58		0.73
Er	2.29		1.26	1.60					1.38	1.65		2.05
Tm	0.35		0.18	0.23					0.21	0.25		0.31
Yb	2.52		1.10	1.44					1.33	1.66		1.99
Lu	0.34		0.16	0.21					0.20	0.25		0.29

Sample	JL06-104	JL06-105	JL06-005	JL06-021	JL06-029	JL06-030	JL06-031	JL06-043	JL06-106	JL06-042	JL06-101
Rock Type											
Map Unit	Plag. Cum.	Plag. Cum.	Ol. Cum.	Ol. Cum.	Ol. Cum.	Ol. Cum.	Ol. Cum.	Ol. Cum.	Ol. Cum.	Hblite	Hblite
UTM Zone	10	10	10	10	10	10	10	10	10	10	10
UTM E	393105	393135	403501	390494	405110	404511	404319	391021	404168	406520	390187
UTM N	5386920	5386903	5388596	5386212	5385995	5387000	5386734	5386186	5389078	5390645	5388291
Major elements (oxides wt %)											
SiO2	46.31	46.91	38.16	40.34	41.32	41.31	42.26	36.78	41.64	43.49	44.10
TiO2	1.23	0.72	0.10	0.44	0.26	0.45	0.34	0.34	0.55	0.61	1.01
Al2O3	18.20	16.71	10.29	12.14	9.16	6.68	4.26	3.25	8.09	11.95	10.05
Fe2O3t	11.96	9.50	12.85	13.86	16.54	13.52	18.70	20.71	13.12	12.48	12.78
FeOt											
MnO	0.21	0.15	0.18	0.18	0.24	0.19	0.29	0.30	0.25	0.20	0.20
MgO	6.51	9.44	26.97	18.88	24.48	29.14	28.68	29.67	27.17	17.46	16.33
CaO	11.02	10.79	5.40	9.34	6.75	4.00	3.12	2.15	5.05	8.59	12.26
Na2O	2.75	2.17	0.52	0.66	0.58	0.79	0.38	0.34	1.02	1.06	1.19
K2O	0.46	0.45	0.12	0.21	0.12	0.29	0.11	0.17	0.87	0.12	0.24
P2O5	0.26	0.12	0.02	0.02	0.04	0.12	0.02	0.05	0.12	0.06	0.06
LOI	0.91	3.16	6.14	4.62	1.58	3.77	2.96	7.04	2.24	4.68	1.89
Total	**99.83**	**100.19**	**100.97**	**100.75**	**101.20**	**100.46**	**101.36**	**100.81**	**100.27**	**100.81**	**100.24**
Trace elements (ppm) -XRF											
Lab	**McGill**	**McGill**	**McGill**	**McGill**	**McGill**	**McGill**	**McGill**	**McGill**	**McGill**	**McGill**	**McGill**
Cr2O3	108	656	2145	609	1347	2095	2372	78	1569	1190	1289
Ni	59	196	726	205	758	1103	932	358	928	645	284
V	305	173	45	152	96	96	113	102	112	199	310
Ga	16	12	4	6	6	6	3	2	7	9	8
Nb	4	1	0	0	0	2	1	1	1	0	1
Pb	<d/l	0	1	<d/l	1	1	0	2	1	1	1
Rb	6	11	2	3	4	8	3	4	45	2	1
Sr	330	233	95	254	191	115	99	57	67	87	129
Th	3	2	1	3	2	2	2	1	1	1	3
U	2	1	1	1	1	1	1	0	1	1	1
Y	40	15	1	6	4	7	5	4	8	15	15
Zr	50	47	4	12	10	32	10	10	31	24	24

Sample	JL06-104	JL06-105	JL06-005	JL06-021	JL06-029	JL06-030	JL06-031	JL06-043	JL06-106	JL06-042	JL06-101
Trace elements (ppm) - ICPMS											
Lab	**UVic**	**UVic**	**UVic**	**UVic**	**UVic**	**UVic**	**UVic**	**UVic**	**UVic**	**UVic**	**UVic**
Sc	41.9	35.4	7.5	40.1	21.8	14.7	17.0	16.8	17.9	38.6	68.7
V	319	171	37	167	102	97	113	82	113	206	328
Co	38.1	43.5	105.4	97.0	100.9	105.8	120.3	139.0	100.1	78.1	62.1
Ni	47.9	156.4	591.0	171.6	630.4	926.3	785.4	276.4	784.0	548.3	221.3
Cu	67	87	2	17	14	34	8	58	17	70	100
Rb	6.0	10.7	1.5	2.8	2.9	7.2	2.9	3.2	46.6	1.8	0.7
Sr	373	243	105	271	212	119	101	53	60	102	136
Y	43.5	16.3	0.9	6.2	4.1	7.5	5.0	4.2	8.9	18.2	16.7
Zr	37	34	2	6	6	26	7	8	25	12	18
Nb	4.7	1.1	0.1	0.3	0.2	1.7	0.3	0.6	0.9	0.4	1.0
Ba	159	115	13	71	39	72	35	58	74	14	41
Hf	1.67	1.07	0.07	0.26	0.21	0.75	0.26	0.29	0.74	0.55	0.83
Ta	0.19	0.08	0.01	0.02	0.02	0.10	0.02	0.04	0.05	0.03	0.05
Th	0.19	0.39	0.05	0.06	0.12	0.34	0.14	0.12	0.26	0.05	0.12
U	0.11	0.17	0.10	0.03	0.07	0.19	0.07	0.05	0.42	0.02	0.05
Rare Earth Elements (ppm) - ICPMS											
La	9.6	3.0	0.7	0.5	1.2	3.0	0.8	1.1	3.1	0.8	1.9
Ce	27.9	7.6	1.2	1.5	3.0	7.3	2.0	2.8	7.4	2.3	5.9
Pr	4.4	1.2	0.1	0.3	0.4	1.0	0.3	0.4	1.0	0.5	1.1
Nd	23.1	6.2	0.7	1.9	2.3	5.0	1.6	2.4	5.1	3.0	6.6
Sm	6.4	1.9	0.2	0.8	0.6	1.3	0.5	0.7	1.4	1.3	2.4
Eu	1.78	0.74	0.12	0.31	0.27	0.44	0.21	0.23	0.53	0.54	0.82
Gd	6.9	2.3	0.2	1.0	0.7	1.3	0.6	0.8	1.5	2.0	2.8
Tb	1.15	0.41	0.03	0.17	0.12	0.21	0.12	0.12	0.24	0.40	0.47
Dy	7.4	2.7	0.2	1.1	0.7	1.3	0.8	0.8	1.5	2.8	3.0
Ho	1.51	0.58	0.03	0.24	0.15	0.27	0.18	0.16	0.32	0.63	0.62
Er	4.29	1.67	0.10	0.65	0.43	0.75	0.56	0.43	0.89	1.87	1.70
Tm	0.64	0.25	0.02	0.09	0.06	0.11	0.09	0.06	0.13	0.28	0.24
Yb	4.14	1.68	0.11	0.57	0.44	0.73	0.67	0.41	0.86	1.87	1.50
Lu	0.60	0.25	0.02	0.08	0.07	0.11	0.11	0.06	0.13	0.27	0.21

Sample	JL06-006	JL06-044	DC06-047	JL06-092	JL06-040	JL06-054	JL06-011	JL06-068	JL06-021	JL06-030
Isotopic ratios -	**UAlberta**	**UAlberta**	**UAlberta**	**UAlberta**	**UAlberta**	**UAlberta**	**UAlberta**	**UAlberta**	**UAlberta**	**UAlberta**
87Sr/86Sr	0.70433	0.70400	0.71372	0.70821	0.70474	0.73698	0.70470	0.70437	0.70574	0.70684
143Nd/144Nd	0.512884	0.512865	0.512905	0.512731	0.512780	0.512782	0.512924	0.512880	0.512988	0.512889

* Samples labelled ??Volc. May not be related to the Bonanza arc, but are included in the table for the sake of completeness. They have been left out of all plots and diagrams.

WCC - Westcoast Crystalline Complex
Bon Volc - Bonanza volcanics
IPS - Island Plutonic Suite
Plag Cum. - plagioclase cumulate
Ol. Cum. - olivine cumulate
Hblite - hornblendite

Standard	BCR-1		AGV-1		MRG-1	
	*Avg. value**	*Accuracy***	*Avg. value*	*Accuracy*	*Avg. value*	*Accuracy*
Trace elements (ppm) - ICPMS						
Lab	**Uvic**		**Uvic**		**Uvic**	
Sc	34.0 (4)	96%	12.31 (2)	99%	53.7 (5)	98%
V	405 (7)	99%	105 (12)	87%	533 (9)	99%
Co	33.96 (2)	92%	13.86 (6)	91%	84 (4)	97%
Ni	11.0 (2)	84%	13.5 (3)	84%	164 (1)	85%
Cu	22 (1)	86%	59.3 (6)	99%	142 (1)	95%
Rb	47.6 (9)	99%	69 (1)	98%	7.3 (1)	86%
Sr	333 (7)	99%	658 (9)	99%	273 (1)	97%
Y	37.4 (3)	98%	20.1 (6)	99%	13.3 (4)	95%
Zr	178 (7)	94%	240 (33)	94%	98 (10)	91%
Nb	12.7 (4)	91%	14.6 (3)	98%	21.40 (3)	93%
Ba	658 (76)	97%	1240 (120)	98%	43 (1)	71%
Hf	4.860 (4)	98%	5.19 (3)	98%	3.62 (2)	96%
Ta	0.805 (2)	99%	0.888 (1)	99%	0.84 (3)	95%
Th	6.1 (1)	97%	6.6 (1)	98%	0.765 (1)	82%
U	1.72 (1)	98%	1.982 (4)	97%	0.250 (1)	96%
Rare Earth Elements (ppm) - ICPMS						
La	25 (3)	99%	38.6 (8)	98%	8.9 (1)	91%
Ce	52.1 (7)	97%	73 (5)	92%	25.7 (1)	99%
Pr	6.45 (5)	95%	8.4 (1)	90%	3.7 (1)	92%
Nd	28.8 (2)	99%	34 (2)	97%	19.1 (3)	99%
Sm	6.6 (2)	99%	6.1 (2)	97%	4.6 (1)	97%
Eu	1.93 (1)	99%	1.70 (2)	96%	1.42 (1)	98%
Gd	6.5 (3)	97%	5.13 (5)	97%	4.1 (1)	98%
Tb	1.00 (7)	95%	0.67 (1)	95%	0.56 (4)	91%
Dy	6.1 (4)	96%	3.6 (2)	99%	2.9 (2)	99%
Ho	1.22 (7)	97%	0.68 (3)	98%	0.50 (3)	99%
Er	3.46 (7)	95%	1.87 (2)	91%	1.17 (1)	95%
Tm	0.51 (2)	90%	0.266 (4)	78%	0.145 (2)	76%
Yb	3.2 (2)	96%	1.70 (9)	99%	0.83 (6)	73%
Lu	0.483 (2)	95%	0.254 (1)	94%	0.110 (1)	92%

*Numbers in parentheses indicate 2-σ error on smallest reported digit
**ICPMS calibrations based on published values from Govindaraju, 1994; accuracy is relative to these values

Govindaraju, K. 1994 compilation of working values and sample description for 383 geostandards. 1994. Geostandards Newsletter 18, pp. 1-158

BCR-1 – basalt standard; AGV-1 – andesite standard; MRG-1 – gabbro standard

Table 2 - Petrography

Sample ID	Primary Phases (vol.%)	Accessory	Alteration
JL06-001	Plag (55); Amph (32); Bt (3) Qtz (10)		Sericite + epidote after plag, epidote after amph
JL06-003	Feldspar (75); Qtz (10); Bt (9); Amph (5); Fe-Ti ox (1)	zr, ap	minor sericite after plag, rare chl after bt
JL06-006	Amph (45); Plag (48); Qtz (5); Fe-Ti ox (2)	tnt, bt; kspar	Sericite + epidote after plag, chl after bt
JL06-010	Amph (40); Plag (50); Bt (5); Qtz (2); Fe-Ti ox (3)	ap	chl after bt; sericite after plag
JL06-013	Amph (37); Plag (52); Qtz (7); Bt (3); Fe-Ti ox (1)	ap, tnt	chl after bt, amph; sericite+ep after plag
JL06-014	Amph (35); Feld (55); Qtz (3); Fe-Ti ox (7)	ap, relict cpx (?)	
JL06-019	Amph (40); Plag (55); Qtz (2); Bt (3)	tnt, ap, Fe-Ti ox	chl+/-prehn after bt, sericite after plag; prehn+cc in veins
JL06-020	Plag (60); Opx (20); Cpx (12); Amph (4); Fe-Ti oxides (2); Bt (2)		clay (?) after plag
JL06-022			
JL06-025	Amph (9); Bt (6); Feld (65); Qtz (20)	ap, Fe-Ti ox	plag cores altered to prehn; chl after bt
JL06-044	Amph (54); Feld (40); Qtz (4); Fe-Ti ox (2)	bt	chl after bt; sericite+clay after plag
JL06-066	Plag (61); Amph (30); Bt (5); Qtz (3); Fe-Ti ox (1)	relict Cpx	sericite after plag; chl after bt
JL06-027	Relict Ol; Cpx; Plag; Sp/Fe-Ti ox		pervasive talc after ol; intersertal groundmass chl, cc
JL06-038	Plag; Cpx; Fe-Ti ox		chl+act filling amygdules; act after cpx
JL06-050			
JL06-053	Plag; Cpx; Fe-Ti ox; Relict ol/amph	ap	intersertal groundmass chl; chl+cc after ol/amph; ep after plag
JL06-061	Plag; Cpx; Fe-Ti ox	relict ol (?)	chl+ep+cc filling voids; sauss after plag; qtz+prehn filling fractures in cpx
JL06-090	Plag; Cpx; Relict amph?; Fe-Ti ox	ap	chl+cc after amph?; cc after cpx; sericite after plag; intergranular chl
JL06-092	Plag; Amph; Cpx; Fe-Ti ox		sericite after plag; patches of cc+chl in groundmass
JL06-093	Plag; relict Ol; Fe-Ti ox		sericite+cc after plag; pervasive serp+mgt after ol; groundmass chl+cc+silica(?)
JL06-008	Amph (40); Plag (56); Bt (3); Fe-Ti ox (1)	relict cpx (?), ap	chl after bt; chl +/- act veins, minor cc, ep
JL06-009	Plag (52); Amph (40); Cpx (5); Fe-Ti ox (3)	bt	chl+ep after bt; minor sericite after plag
JL06-011	Amph (60); Opx (20); Plag (12); Cpx (3); Fe-Ti ox (5)		prehn, chl veins
JL06-015	Amph (18); Plag (80); Fe-Ti ox (2)	ap	sericite+/-prehn after plag, prehn veins
JL06-023	Plag (55); Amph (37); Cpx (5); Fe-Ti ox (3)	ap	sericite+/-prehn after plag, cc+act(?) veins
JL06-024	Plag (50); Amph (45); Cpx (3); Fe-Ti ox (2)	ap	rare patches of ep, prehn in plag
JL06-045	Plag (72); Relict Amph? (25); Bt (2); Fe-Ti ox (1)	qtz?	pervasive act after hbl (?); sericite after plag; chl after bt
JL06-067	Plag (30); Amph (64); Cpx (3); Fe-Ti ox (1); Bt (2)	tnt	chl+ep after bt; sericite after plag; patches of chl, ep
JL06-068	Opx (10); Amph (38); Bt (2); Plag (50)		sericite after plag; ; fine bt/amph after opx
JL06-069	Amph (65); Plag (35)	bt, ap, Fe-Ti ox	sericite after plag
JL06-100	Plag (65); Amph (29 - 10 primary); Cpx (5); Opx (1)	relict bt	interstitial green act; sericite after plag; chl+ep after bt; prehn? veins
JL-06-105			

Sample ID	Texture
JL06-001	Porphyritic (blocky plag <5mm); clots of subhedral amph, rarely prismatic (<4mm); inclusions of bt, mgt in prismatic amph
JL06-003	Subhedral granoblastic; coarse grained; qtz interstitial to euhedral feld
JL06-006	Subhedral granoblastic; coarse grained; bt+plag inclusions in amph
JL06-010	granoblastic; prismatic embayed amph with inclusions of plag, Fe-Ti, bt
JL06-013	Porphyritic, blocky plag (<2.5mm); embayed prismatic amph (<4mm); inclusions of Fe-Ti, amph in plag; inclusions of bt, Fe-Ti in amph
JL06-014	Anhedral granoblastic; medium grained; interstitial Fe-Ti
JL06-019	Subhedral granoblastic; medium grained
JL06-020	Subhedral granoblastic; coarse grained; late amph rimming px; cpx inclusions in opx
JL06-022	
JL06-025	Euhedral-subhedral amph; subhedral plag w/ later growth @ rim; inclusions of Fe-Ti, plag, bt in amph
JL06-044	Subhedral inequigranular; prismatic amph (<4mm) containing inclusions of Fe-Ti, bt
JL06-066	Subhedral granoblastic; interstitial&subhedral amph; relict cpx cores rarely noted in amph; plag+Fe-Ti inclusions in amph
JL06-027	Porphyritic; clusters of coarse (<3mm) plag+ol+cpx+sp/Fe-Ti; some cpx phenos likely pseudomorphs, show relict amph island in optical continuity
JL06-038	seriate plag; subophitic-ophitic cpx; amygdaloidal
JL06-050	
JL06-053	Porphyritic; blocky plag (<4.5mm); euhedral cpx phenos; intergranular groundmass cpx, Fe-Ti; hiatal plag
JL06-061	Porphyritic (blocky plag <2mm, euhedral cpx <6mm); seriate plag; zoned, badly fractured cpx w/ inclusions of relict ol(?); oxidized groundmass
JL06-090	Porphyritic, well-crystallized; seriate plag; Fe-Ti inclusions in cpx
JL06-092	Porphyritic; euhedral fractured cpx phenos; rounded amph phenos; seriate plag; well-zoned cpx; evidence of mixing - different oxidation in groundmasses
JL06-093	Porphyritic; blocky seriate plag (<2mm); clusters of subhedral relict ol (<2mm)
JL06-008	Euhedral accumulated plag; subhedral amph; plag, mgt inclusions in amph
JL06-009	Heteradcumulate; poikilitic amph; euhedral plag; relict cpx, opx replaced by amph; mgt+amph inclusions in plag
JL06-011	Heteradcumulate; poikilitic amph; subhedral opx, cpx, Fe-Ti, plag; cpx, amph, mgt inclusions in opx; plag inclusions in Fe-Ti
JL06-015	Accumulation of euhedral plag; interstitial 'veins' of igneous amph; filter pressing?
JL06-023	Inequigranular; subhedral accumulated plag, euhedral amph+cpx; Fe-Ti ox, plag, cpx inclusions in amph; cpx, amph inclusions in plag
JL06-024	Heteradcumulate; euhedral accumulated plag; poikilitic amph; relict cpx; inclusions of Fe-Ti, amph in plag
JL06-045	Subhedral equigranular; accumulated plag;
JL06-067	Heteradcumulate; euhedral plag; poikilitic amph; relict anhedral cpx replaced by amph; inclusions of amph, bt in plag
JL06-068	Heteradcumulate; poikilitic amph; anhedral relict opx, cpx; subhedral-anhedral plag
JL06-069	Euhedral amph; rare relict cpx cores in amph; plag, bt inclusions in amph
JL06-100	Poikilitic amph; relict ragged cpx, opx; subhedral accumulated plag
JL-06-105	

Sample ID	Primary Phases (vol.%)	Accessory	Alteration
JL06-005	Ol (27); Amph (65); Opx (3); Sp (5)		serp+act after ol; diss. green spinel
JL06-021	Ol (12); Plag (20); Amph (62); Cpx (3); Opx (3)	sp/Fe-Ti ox	serp+idd+/-cc after ol; pervasive sauss after plag
JL06-030	Ol (13); Amph (73); Opx (8); Cpx (3); Bt (3)		serp after ol; patches of fibrous act (?)
JL06-031	Ol (21); Amph (20); Opx (45); Plag (10); Bt (3); Sp/Fe-Ti ox (1)		serp after ol; clay + prehn alteration of plag
JL06-043	Ol (45); Amph (54); Sp/Fe-Ti ox (1)	bt, opx	
JL-06-106			
JL06-002	Feldspar (70); Qtz (25); Bt (3); Fe-Ti ox (2)	zr, ap	minor sericite after plag, chl after bt
JL06-040	Amph (3); Bt (5); Qtz (25); Plag (54); Kspar (12); Fe-Ti ox (1)	tnt	chl+ep after bt; chl after amph; sericite+ep after plag cores
JL06-041	Amph (15); Plag (63); Kspar (10); Qtz (7); Bt (5)	tnt, ap, Fe-Ti ox	chl+ep+prehn+/-pump(?) after bt; sericite+ep after plag; few prehn+ep veins
JL06-054	Feld (80); Qtz (18); Relict amph/bt (2)	Fe-Ti ox, ap	pervasive chl+cc after amph/bt, and plag
JL06-076	Amph (10); Bt (3); Plag (50); Kspar (24); Qtz (12); Fe-Ti ox (1)	ap	sericite after plag; ep+chl after bt
JL-06-107			
JL06-042			
JL06-052			
JL06-101			
JL-06-104			
JL-06-108			

Sample ID	Texture
JL06-005	Heteradcumulate; poikilitic amph; anhedral ol, opx; coarse grained; sp inclusions in ol
JL06-021	Heteradcumulate; anhedral ol, cpx, opx, plag(?); poikilitic amph; opx rimming ol in places; inclusions of opx, amph, sp/Fe-Ti in ol
JL06-030	Heteradcumulate; subhedral ol, opx; anhedral resorbed cpx; poikilitic amph, bt, opx; ol+amph inclusions in opx; amph inclusions in ol
JL06-031	Heteradcumulate; anhedral ol; poikilitic amph, opx; interstitial plag; ol replaced by amph and/or opx; sp/Fe-Ti inclusions in ol
JL06-043	
JL-06-106	
JL06-002	Subhedral granoblastic; coarse grained
JL06-040	Subhedral inequigranular; euhedral blocky plag (<5mm); interstitial kspar, qtz; euhedral amph w/ plag, Fe-Ti inclusions
JL06-041	Subhedral granoblastic; coarse grained; euhedral plag, amph
JL06-054	Anhedral granoblastic; coarse grained; graphic texture; interstitial relict Fe-Mg silicates
JL06-076	granoblastic; subhedral amph, plag, bt; interstitial kspar, qtz; well-zoned plag
JL-06-107	
JL06-042	
JL06-052	
JL06-101	
JL-06-104	
JL-06-108	

ol - olivine	zr - zircon
cpx - clinopyroxene	ap - apatite
opx - orthopyroxene	cc - calcite
plag - plagioclase	chl - chlorite
amph - amphibole	ep - epidote
sp - spinel	serp - serpentine
qtz - quartz	prehn - prehnite
feld - feldspar	pump - pumpellyite
bt - biotite	idd - iddingsite
kspar - K feldspar	sauss - saussurite
ox - oxide	act - actinolite

Table 3 – Mineral Chemistry

Amphibole Analyses

Ferric iron recalculation: Schumacher, J.C. Canadian Mineralogist Vol. 35, pp. 238-246 (1997)

Amphibole classification scheme: Morimoto, N., Canadian Mineralogist Vol. 27, pp.143-156 (1989)

Sample ID	**005-1**	**005-2**	**005-3**	**005-4**	**21-1**	**21-3**
Rock Type	Ol. Hblite	Ol. Hblite	Ol. Hblite	Ol. Hblite	Ol. Hblite	Ol. Hblite
Map Unit	WCC	WCC	WCC	WCC	WCC	WCC
Oxide wt. %						
SiO_2	46.122	45.620	44.681	43.266	40.098	43.198
TiO_2	0.827	1.157	0.163	0.785	0.972	0.693
Al_2O_3	10.602	10.189	12.052	12.303	15.153	13.877
FeO(T)	6.579	6.657	9.150	7.071	11.135	8.855
MnO	0.102	0.114	0.158	0.102	0.251	0.107
MgO	17.686	17.906	17.473	16.752	15.219	15.753
CaO	12.240	12.281	10.915	11.699	10.499	12.002
Na_2O	1.444	1.307	1.601	1.622	1.811	2.036
K_2O	0.276	0.350	0.186	0.457	0.180	0.092
Cr_2O_3	0.476	0.686	0.009	0.708	0.204	0.158
F	0.048	0.011	0.000	0.000	0.000	0.105
Cl	0.520	0.281	0.291	0.401	0.013	0.002
Total	**96.353**	**96.267**	**96.387**	**94.764**	**95.523**	**96.770**
Species name	Mg-hbl	Mg-hbl	Tscherm.	Tscherm.	Tscherm.	Tscherm.

Sample ID	**21-4**	**21-5**	**21-6**	**21-7**	**21-8**	**030-1**
Rock Type	Ol. Hblite	Ol. Hblite	Ol. Hblite	Ol. Hblite	Ol. Hblite	Ol. Hblite
Map Unit	WCC	WCC	WCC	WCC	WCC	WCC
Oxide wt. %						
SiO_2	44.379	43.372	43.153	43.856	43.576	43.094
TiO_2	1.182	1.381	0.797	0.865	0.844	0.866
Al_2O_3	12.728	13.320	13.605	12.910	12.779	13.534
FeO(T)	8.619	8.513	9.203	8.056	8.992	7.709
MnO	0.124	0.120	0.054	0.124	0.146	0.149
MgO	16.101	15.781	15.569	15.865	16.070	16.922
CaO	11.758	11.934	12.308	12.232	12.184	11.435
Na_2O	1.848	1.852	1.869	1.818	1.838	2.296
K_2O	0.199	0.247	0.261	0.207	0.502	0.151
Cr_2O_3	0.133	0.103	0.090	0.297	0.126	0.327
F	0.095	0.069	0.047	0.112	0.079	0.026
Cl	0.036	0.011	0.031	0.013	0.016	0.183
Total	**97.071**	**96.623**	**96.911**	**96.229**	**97.056**	**96.484**
Species name	Tscherm.	Tscherm.	Tscherm.	Tscherm.	Tscherm.	Tscherm.

Amphibole Analyses cont'd

Sample ID	**030-2**	**030-3**	**030-4**	**030-5**	**030-6**	**030-7**	**030-8**
Rock Type	Ol. Hblite	Ol. Hblite	Ol. Hblite	Ol. Hblite	Ol. Hblite	Ol. Hblite	Ol. Hblite
Map Unit	WCC	WCC	WCC	WCC	WCC	WCC	WCC
Oxide wt. %							
SiO_2	43.509	44.301	43.375	43.178	43.049	42.506	43.201
TiO_2	1.284	1.886	1.118	2.012	1.388	1.269	0.582
Al_2O_3	13.080	11.440	11.885	12.350	11.840	12.659	13.688
FeO(T)	7.826	7.706	8.034	7.305	7.711	7.269	7.551
MnO	0.149	0.117	0.175	0.180	0.134	0.158	0.151
MgO	16.975	17.520	16.912	16.729	18.647	16.666	16.941
CaO	11.493	10.646	11.484	11.307	10.485	11.195	11.429
Na_2O	2.267	1.899	1.966	2.148	1.849	2.132	2.230
K_2O	0.182	0.248	0.249	0.192	0.268	0.210	0.153
Cr_2O_3	0.416	0.472	0.883	0.664	0.440	0.500	0.087
F	0.049	0.071	0.009	0.028	0.011	0.048	0.100
Cl	0.125	0.172	0.156	0.178	0.145	0.108	0.149
Total	**97.181**	**96.236**	**96.079**	**96.064**	**95.811**	**94.564**	**96.013**
Species name	Tscherm.	Tscherm.	Tscherm.	Tscherm.	Tscherm.	Tscherm.	Tscherm.

Sample ID	**6031-1**	**6031-2**	**6031-3**	**6031-4**	**6031-5**	**6031-6**	**043-1**
Rock Type	Ol. Hblite	Ol. Hblite	Ol. Hblite	Ol. Hblite	Ol. Hblite	Ol. Hblite	Ol. Hblite
Map Unit	WCC	WCC	WCC	WCC	WCC	WCC	WCC
Oxide wt. %							
SiO_2	42.478	42.451	42.141	42.290	42.607	46.611	42.323
TiO_2	2.608	2.733	2.673	2.543	2.394	0.062	1.550
Al_2O_3	11.572	11.540	11.537	11.476	11.395	11.420	12.715
FeO(T)	8.830	8.854	9.186	9.009	8.953	7.297	8.488
MnO	0.112	0.081	0.122	0.083	0.071	0.165	0.138
MgO	15.223	15.361	15.183	15.480	15.610	18.343	16.216
CaO	11.937	11.646	11.669	11.434	11.661	11.319	11.623
Na_2O	2.202	2.093	2.201	2.135	2.123	2.039	2.248
K_2O	1.148	1.113	1.122	1.255	1.072	0.128	0.480
Cr_2O_3	0.642	0.736	0.777	0.660	0.631	0.000	0.017
F	0.112	0.155	0.139	0.133	0.218	0.000	0.099
Cl	0.183	0.149	0.152	0.163	0.135	0.052	0.032
Total	**96.751**	**96.609**	**96.610**	**96.365**	**96.517**	**97.384**	**95.798**
Species name	Tscherm.	Tscherm.	Tscherm.	Tscherm.	Tscherm.	Mg-hbl.	Tscherm.

Sample ID	**043-2**	**106-1**	**106-2**	**106-3**	**106-4**	**106-5**	**011-1**
Rock Type	Ol. Hblite	Ol. Hblite	Ol. Hblite	Ol. Hblite	Ol. Hblite	Ol. Hblite	Plag. Cum.
Map Unit	WCC	WCC	WCC	WCC	WCC	WCC	WCC
Oxide wt. %							
SiO_2	41.833	43.302	43.780	44.125	44.247	44.589	47.402
TiO_2	0.808	0.446	0.489	0.875	1.010	0.423	1.124
Al_2O_3	13.548	13.450	12.162	12.588	12.497	12.430	8.139

Amphibole Analyses cont'd

Sample ID	**043-2**	**106-1**	**106-2**	**106-3**	**106-4**	**106-5**	**011-1**
FeO(T)	9.025	8.402	8.039	8.196	7.930	7.545	9.824
MnO	0.160	0.192	0.189	0.145	0.196	0.164	0.213
MgO	15.957	16.238	17.200	16.744	16.843	17.231	16.808
CaO	11.225	11.683	11.292	11.512	11.615	11.427	11.833
Na_2O	2.303	2.181	1.966	2.048	2.044	2.199	1.245
K_2O	0.465	0.203	0.151	0.226	0.195	0.176	0.247
Cr_2O_3	0.043	0.175	0.932	0.394	0.152	0.615	0.015
F	0.034	0.043	0.050	0.000	0.019	0.052	0.161
Cl	0.083	0.860	0.492	0.347	0.198	0.321	0.005
Total	**95.366**	**96.271**	**96.199**	**96.853**	**96.729**	**96.798**	**96.848**
Species name	Tscherm.	Tscherm.	Tscherm.	Tscherm.	Tscherm.	Tscherm.	Mg-Hbl.

Sample ID	**011-2**	**011-3**	**011-4**	**011-5**	**067-1**	**067-2**	**067-3**
Rock Type	Plag. Cum.	Plag. Cum.	Plag. Cum.	Plag. Cum.	Plag. Cum.	Plag. Cum.	Plag. Cum.
Map Unit	WCC	WCC	WCC	WCC	WCC	WCC	WCC
Oxide wt. %							
SiO_2	43.404	42.621	43.105	47.387	43.629	45.645	45.254
TiO_2	2.002	2.511	2.297	1.449	1.396	1.497	1.681
Al_2O_3	10.322	10.721	10.424	7.617	11.129	8.841	9.906
FeO(T)	12.983	12.035	12.191	10.240	13.085	11.777	9.698
MnO	0.240	0.229	0.248	0.257	0.224	0.322	0.211
MgO	14.505	14.224	14.443	16.307	14.074	14.874	15.863
CaO	11.078	11.328	11.291	12.010	11.367	11.944	12.197
Na_2O	1.628	1.868	1.803	1.134	1.685	1.234	1.510
K_2O	0.348	0.443	0.382	0.256	0.580	0.443	0.420
Cr_2O_3	0.023	0.000	0.008	0.057	0.010	0.000	0.028
F	0.099	0.102	0.062	0.151	0.042	0.064	0.137
Cl	0.058	0.046	0.019	0.042	0.090	0.086	0.069
Total	**96.533**	**95.980**	**96.192**	**96.714**	**97.178**	**96.577**	**96.768**
Species name	Tscherm.	Tscherm.	Tscherm.	Mg-Hbl.	Tscherm.	Mg-Hbl.	Mg-Hbl.

Sample ID	**011-2**	**011-3**	**011-4**	**011-5**	**067-1**	**067-2**	**067-3**
Rock Type	Plag. Cum.	Plag. Cum.	Plag. Cum.	Plag. Cum.	Plag. Cum.	Plag. Cum.	Plag. Cum.
Map Unit	WCC	WCC	WCC	WCC	WCC	WCC	WCC
Oxide wt. %							
SiO_2	43.404	42.621	43.105	47.387	43.629	45.645	45.254
TiO_2	2.002	2.511	2.297	1.449	1.396	1.497	1.681
Al_2O_3	10.322	10.721	10.424	7.617	11.129	8.841	9.906
FeO(T)	12.983	12.035	12.191	10.240	13.085	11.777	9.698
MnO	0.240	0.229	0.248	0.257	0.224	0.322	0.211
MgO	14.505	14.224	14.443	16.307	14.074	14.874	15.863
CaO	11.078	11.328	11.291	12.010	11.367	11.944	12.197
Na_2O	1.628	1.868	1.803	1.134	1.685	1.234	1.510
K_2O	0.348	0.443	0.382	0.256	0.580	0.443	0.420
Cr_2O_3	0.023	0.000	0.008	0.057	0.010	0.000	0.028

Amphibole Analyses cont'd

Sample ID	**011-2**	**011-3**	**011-4**	**011-5**	**067-1**	**067-2**	**067-3**
F	0.099	0.102	0.062	0.151	0.042	0.064	0.137
Cl	0.058	0.046	0.019	0.042	0.090	0.086	0.069
Total	**96.533**	**95.980**	**96.192**	**96.714**	**97.178**	**96.577**	**96.768**
Species name	Tscherm.	Tscherm.	Tscherm.	Mg-Hbl.	Tscherm.	Mg-Hbl.	Mg-Hbl.

Sample ID	**067-4**	**067-5**	**067-6**	**067-7**	**68-1**	**68-2**	**68-3**
Rock Type	Plag. Cum.	Plag. Cum.	Plag. Cum.	Plag. Cum.	Plag. Cum.	Plag. Cum.	Plag. Cum.
Map Unit	WCC	WCC	WCC	WCC	WCC	WCC	WCC
Oxide wt. %							
SiO_2	45.530	42.681	57.043	42.070	42.998	49.075	49.715
TiO_2	1.626	1.507	0.029	2.337	2.171	0.801	0.642
Al_2O_3	9.148	11.071	0.817	12.043	11.408	7.017	6.123
FeO(T)	8.743	14.934	3.698	10.498	13.088	11.950	11.202
MnO	0.166	0.310	0.158	0.230	0.189	0.272	0.249
MgO	16.620	12.501	23.125	14.551	13.443	17.627	17.137
CaO	12.590	11.512	12.632	12.271	11.334	9.403	10.952
Na_2O	1.402	1.646	0.152	1.810	1.762	1.051	0.874
K_2O	0.319	0.568	0.061	0.501	0.549	0.233	0.265
Cr_2O_3	0.000	0.025	0.028	0.000	0.006	0.000	0.023
F	0.169	0.052	0.058	0.043	0.067	0.000	0.115
Cl	0.065	0.148	0.030	0.073	0.055	0.033	0.053
Total	**96.145**	**96.755**	**97.743**	**96.309**	**96.948**	**97.428**	**97.182**
Species name	Mg-Hbl.	Tscherm.	Tremolite	Tscherm.	Tscherm.	Mg-Hbl.	Mg-Hbl.

Sample ID	**68-4**	**68-5**	**68-6**	**6100-1**	**6100-2**	**6100-3**	**6100-4**
Rock Type	Plag. Cum.	Plag. Cum.	Plag. Cum.	Plag. Cum.	Plag. Cum.	Plag. Cum.	Plag. Cum.
Map Unit	WCC	WCC	WCC	WCC	WCC	WCC	WCC
Oxide wt. %							
SiO_2	55.267	43.685	42.884	41.708	41.796	42.169	41.585
TiO_2	0.080	1.709	1.987	3.150	3.312	3.295	3.571
Al_2O_3	1.044	10.559	11.631	10.521	10.518	10.250	10.779
FeO(T)	16.563	13.345	13.499	16.392	15.969	15.907	16.144
MnO	0.540	0.262	0.177	0.291	0.271	0.263	0.269
MgO	22.541	14.236	13.739	11.142	10.923	11.231	10.926
CaO	1.026	10.481	11.147	10.824	11.111	11.302	10.862
Na_2O	0.126	1.421	1.620	2.026	1.645	1.749	1.726
K_2O	0.017	0.474	0.731	0.943	1.016	0.997	1.078
Cr_2O_3	0.043	0.043	0.025	0.004	0.000	0.039	0.057
F	0.024	0.041	0.062	0.046	0.062	0.077	0.240
Cl	0.006	0.069	0.048	0.085	0.106	0.089	0.114
Total	**97.246**	**96.216**	**97.440**	**97.002**	**96.562**	**97.202**	**96.998**
Species name	Anthoph.	Tscherm.	Tscherm.	Tscherm.	Tscherm.	Tscherm.	Tscherm.

Amphibole Analyses cont'd

Sample ID	**6100-5**	**6100-6**	**6100-7**	**6100-8**	**105-1**	**516-1**	**516-2**
Rock Type	Plag. Cum.	Plag. Cum.	Plag. Cum.	Plag. Cum.	Plag. Cum.	Qtz. WCC	Qtz. WCC
Map Unit	WCC	WCC	WCC	WCC	WCC	WCC	WCC
Oxide wt. %							
SiO_2	42.048	41.831	41.981	41.579	42.417	45.465	45.441
TiO_2	3.047	3.325	2.867	3.410	2.515	1.496	1.621
Al_2O_3	10.461	11.077	10.047	10.853	11.473	9.038	8.909
FeO(T)	16.961	16.460	17.582	15.549	13.527	15.722	15.831
MnO	0.204	0.261	0.265	0.265	0.185	0.245	0.209
MgO	10.757	10.709	10.526	11.172	12.726	12.828	12.233
CaO	10.923	10.869	10.821	11.102	11.016	10.992	11.138
Na_2O	1.832	1.902	1.658	1.880	1.859	1.359	1.352
K_2O	0.995	0.844	1.011	1.200	0.468	0.480	0.459
Cr_2O_3	0.000	0.000	0.037	0.000	0.037	0.000	0.000
F	0.101	0.005	0.061	0.000	0.000	0.000	0.005
Cl	0.126	0.078	0.122	0.138	0.050	0.015	0.013
Total	**97.228**	**97.278**	**96.794**	**97.008**	**96.223**	**97.625**	**97.193**
Species name	Tscherm.	Tscherm.	Tscherm.	Tscherm.	Tscherm.	Mg-Hbl.	Mg-Hbl.

Sample ID	**516-3**	**516-4**	**020-1**	**6066-1**	**6066-2**	**6066-3**	**6066-4**
Rock Type	Qtz. WCC	Qtz. WCC	Qtz. WCC	Qtz. WCC	Qtz. WCC	Qtz. WCC	Qtz. WCC
Map Unit	WCC	WCC	WCC	WCC	WCC	WCC	WCC
Oxide wt. %							
SiO_2	46.141	43.373	45.347	46.568	44.891	46.540	47.554
TiO_2	1.421	2.067	1.340	1.116	1.585	1.281	1.085
Al_2O_3	8.901	10.679	8.761	7.319	8.610	7.332	6.771
FeO(T)	14.347	13.195	13.680	14.513	15.799	15.018	13.415
MnO	0.215	0.188	0.086	0.473	0.418	0.481	0.503
MgO	13.297	13.619	13.668	13.693	12.217	13.011	14.414
CaO	11.500	11.055	11.848	11.655	11.601	11.860	11.522
Na_2O	1.114	1.622	1.063	1.084	1.178	0.949	1.069
K_2O	0.498	0.551	0.795	0.792	0.860	0.819	0.538
Cr_2O_3	0.035	0.000	0.044	0.000	0.002	0.029	0.015
F	0.000	0.124	0.069	0.180	0.158	0.036	0.052
Cl	0.017	0.087	0.104	0.129	0.193	0.155	0.123
Total	**97.469**	**96.349**	**96.632**	**97.213**	**97.161**	**97.318**	**96.884**
Species name	Mg-Hbl.	Tscherm.	Mg-Hbl.	Mg-Hbl.	Mg-Hbl.	Mg-Hbl.	Mg-Hbl.

Sample ID	**6027-2**	**6027-3**	**6027-4**	**6027-5**
Rock Type	Basalt dyke	Basalt dyke	Basalt dyke	Basalt dyke
Map Unit	Bon. Volc.	Bon. Volc.	Bon. Volc.	Bon. Volc.
Oxide wt. %				
SiO_2	36.225	46.731	38.321	38.931
TiO_2	0.377	1.308	2.064	1.628
Al_2O_3	20.652	7.137	15.734	15.103

Amphibole Analyses cont'd

Sample ID	**6027-2**	**6027-3**	**6027-4**	**6027-5**
FeO(T)	19.806	13.800	17.597	16.152
MnO	0.510	0.165	0.254	0.243
MgO	4.889	14.050	8.765	10.421
CaO	12.007	12.037	11.867	11.676
Na_2O	1.758	1.315	2.145	2.359
K_2O	0.602	0.648	0.416	0.474
Cr_2O_3	0.026	0.066	0.000	0.049
F	0.000	0.021	0.100	0.251
Cl	0.143	0.234	0.036	0.050
Total	**96.851**	**97.256**	**97.163**	**97.035**
Species name	Fe-Tscherm.	Mg-Hbl.	Tscherm.	Tscherm.

Ilmenite Analyses

Sample ID	**005-2**	**030-5**	**030-6**	**043-1**	**011-2**	**011-3**	**011-5**
Rock Type	Ol. Hblite	Ol. Hblite	Ol. Hblite	Ol. Hblite	Plag cum.	Plag cum.	Plag cum.
Map Unit	WCC	WCC	WCC	WCC	WCC	WCC	WCC
Oxide wt. %							
SiO_2	0.049	0.034	1.122	0.008	0.027	0.022	0.006
TiO_2	50.187	51.008	51.389	51.868	50.207	52.811	50.695
Al_2O_3	0.000	0.000	0.000	0.000	0.000	0.000	0.000
FeO(T)	44.314	43.418	40.167	43.982	46.005	42.910	45.738
MnO	3.742	1.320	1.884	1.155	3.052	4.231	3.336
MgO	0.911	3.926	5.021	3.103	0.087	0.057	0.065
CaO	0.066	0.011	0.048	0.000	0.021	0.012	0.037
Cr_2O_3	0.164	0.229	0.127	0.006	0.025	0.006	0.000
NiO	0.022	0.019	0.035	0.029	0.008	0.000	0.030
Total	**99.453**	**99.964**	**99.793**	**100.150**	**99.431**	**100.049**	**99.908**

Sample ID	**011-7**	**067-2**	**067-4**	**067-6**	**105-1**	**516-2**	**516-4**
Rock Type	Plag cum.	Plag cum.	Plag cum.	Plag cum.	Plag cum.	Qtz. WCC	Qtz. WCC
Map Unit	WCC	WCC	WCC	WCC	WCC	WCC	WCC
Oxide wt. %							
SiO_2	0.016	0.011	0.046	0.000	0.051	1.242	0.049
TiO_2	50.422	47.738	60.020	46.750	46.780	48.896	48.365
Al_2O_3	0.000	0.000	0.000	0.000	0.000	0.180	0.000
FeO(T)	47.739	33.670	30.792	43.509	49.111	46.536	48.402
MnO	2.341	16.611	7.952	6.921	1.242	1.612	1.447
MgO	0.086	0.380	0.122	1.996	0.126	0.087	0.424
CaO	0.000	0.004	0.040	0.008	0.016	1.195	0.023
Cr_2O_3	0.000	0.011	0.023	0.058	0.037	0.026	0.037
NiO	0.041	0.044	0.000	0.000	0.003	0.013	0.000
Total	**100.645**	**98.469**	**98.995**	**99.242**	**97.365**	**99.787**	**98.747**

Sample ID	**516-5**	**020-1**	**020-3**	**020-5**
Rock Type	Qtz. WCC	Qtz. WCC	Qtz. WCC	Qtz. WCC
Map Unit	WCC	WCC	WCC	WCC
Oxide wt. %				
SiO_2	0.000	0.187	0.018	0.354
TiO_2	47.863	48.124	47.892	46.967
Al_2O_3	0.000	0.000	0.000	0.000
FeO(T)	48.382	49.523	49.816	49.731
MnO	1.226	1.102	0.968	1.315
MgO	0.730	0.275	0.517	0.540
CaO	0.000	0.169	0.012	0.005
Cr_2O_3	0.000	0.036	0.011	0.017
NiO	0.000	0.000	0.033	0.000
Total	**98.201**	**99.415**	**99.268**	**98.930**

Mica Analyses

Sample ID	**030-2**	**030-3**	**031-1**	**031-2**	**6031-1**	**6031-2**	**043-1**
Rock Type	Ol. Hblite	Ol. Hblite	Ol. Hblite	Ol. Hblite	Ol. Hblite	Ol. Hblite	Ol. Hblite
Map Unit	WCC	WCC	WCC	WCC	WCC	WCC	WCC
Oxide wt. %							
SiO_2	38.937	38.692	38.933	38.172	38.086	39.248	38.983
TiO_2	0.261	0.557	2.325	2.278	2.057	1.354	0.711
Al_2O_3	17.421	16.982	16.250	16.567	15.813	15.832	16.536
FeO(T)	5.247	4.900	7.794	8.010	7.010	5.719	7.048
MnO	0.068	0.078	0.039	0.056	0.007	0.007	0.095
MgO	23.501	22.782	21.001	20.707	21.214	22.666	22.088
CaO	0.229	0.562	0.019	0.040	0.000	0.000	0.004
Na_2O	1.531	1.616	1.521	1.324	1.536	1.527	1.094
K_2O	6.480	6.853	7.578	7.461	7.392	7.825	8.036
BaO	0.130	0.217	0.363	0.430	0.355	0.094	0.262
Li_2O	0.000	0.000	0.000	0.000	0.000	0.000	0.000
Cr_2O_3	0.109	0.135	0.407	0.355	0.521	0.401	0.000
F	0.008	0.046	0.149	0.095	0.123	0.370	0.090
Cl	0.000	0.000	0.000	0.000	0.026	0.180	0.000
Total	**93.912**	**93.373**	**96.231**	**95.400**	**93.991**	**94.671**	**94.856**

Sample ID	**043-2**	**106-1**	**106-2**	**106-3**	**106-5**	**68-1**	**68-2**
Rock Type	Ol. Hblite	Ol. Hblite	Ol. Hblite	Ol. Hblite	Ol. Hblite	Plag. Cum.	Plag. Cum.
Map Unit	WCC	WCC	WCC	WCC	WCC	WCC	WCC
Oxide wt. %							
SiO_2	34.700	39.723	39.690	40.075	39.924	36.610	37.248
TiO_2	0.284	0.505	0.697	0.631	0.806	3.333	3.415
Al_2O_3	16.984	16.504	16.965	16.676	17.098	14.937	14.954
FeO(T)	7.337	5.600	5.610	5.560	5.491	13.731	13.209
MnO	0.893	0.041	0.022	0.032	0.000	0.010	0.101
MgO	24.985	23.329	22.586	23.066	22.544	16.782	16.392
CaO	0.427	0.041	0.062	0.013	0.012	0.121	0.000
Na_2O	0.535	1.226	1.570	1.583	1.504	0.423	0.633
K_2O	2.525	7.114	7.181	7.046	7.567	7.267	8.330
BaO	0.133	0.061	0.067	0.016	0.153	0.549	0.548
Li_2O	0.000	0.000	0.000	0.000	0.000	0.000	0.000
Cr_2O_3	0.000	0.036	0.214	0.156	0.159	0.000	0.037
F	0.088	0.000	0.128	0.000	0.000	0.007	0.139
Cl	0.000	0.000	0.000	0.000	0.000	0.088	0.111
Total	**88.802**	**94.181**	**94.665**	**94.854**	**95.256**	**93.763**	**94.868**

Mica Analyses cont'd

Sample ID	**68-3**	**68-4**	**6066-1**	**6066-2**
Rock Type	Plag. Cum.	Plag. Cum.	Qtz. WCC	Qtz. WCC
Map Unit	WCC	WCC	WCC	WCC
Oxide wt. %				
SiO_2	36.677	37.521	35.491	34.572
TiO_2	2.826	3.149	4.359	4.472
Al_2O_3	15.239	14.900	14.114	14.133
FeO(T)	13.332	13.583	18.866	18.615
MnO	0.115	0.088	0.354	0.371
MgO	17.013	16.647	12.066	12.616
CaO	0.096	0.120	0.225	0.521
Na_2O	0.474	0.441	0.123	0.084
K_2O	7.611	8.016	8.720	7.209
BaO	0.439	0.384	0.241	0.131
Li_2O	0.000	0.000	0.000	0.000
Cr_2O_3	0.029	0.000	0.000	0.029
F	0.119	0.165	0.221	0.150
Cl	0.134	0.127	0.223	0.204
Total	**93.851**	**94.847**	**94.560**	**92.750**

Olivine Analyses

Sample ID	**005-1**	**005-2**	**005-3**	**005-4**	**21-5**	**21-3**	**21-1**
Rock Type	Ol. Hblite	Ol. Hblite	Ol. Hblite	Ol. Hblite	Ol. Hblite	Ol. Hblite	Ol. Hblite
Map Unit	WCC	WCC	WCC	WCC	WCC	WCC	WCC
Oxide wt. %							
SiO_2	38.949	39.020	39.508	39.385	37.906	38.084	38.301
TiO_2	0.004	0.007	0.031	0.049	0.000	0.000	0.008
Al_2O_3	0.000	0.002	0.000	0.004	0.012	0.012	0.006
FeO	17.725	17.648	17.563	17.268	23.145	23.562	22.679
MnO	0.280	0.305	0.260	0.280	0.387	0.405	0.371
MgO	42.686	42.818	43.181	42.803	39.291	38.647	39.496
CaO	0.011	0.002	0.000	0.028	0.026	0.021	0.000
Na_2O	0.010	0.000	0.011	0.015	0.001	0.000	0.000
Cr_2O_3	0.000	0.014	0.000	0.027	0.022	0.000	0.024
NiO	0.149	0.134	0.161	0.120	0.020	0.092	0.106
Total	**99.813**	**99.950**	**100.715**	**99.978**	**100.811**	**100.823**	**100.989**
Species name	**Chrysolite**	**Chrysolite**	**Chrysolite**	**Chrysolite**	**Chrysolite**	**Chrysolite**	**Chrysolite**
Endmembers mol. %							
Fo	80.85	80.95	81.20	81.27	74.82	74.16	75.33
Fa	18.83	18.72	18.53	18.39	24.73	25.37	24.27
Tph	0.30	0.33	0.28	0.30	0.42	0.44	0.40
Ca-Ol	0.02	0.00	0.00	0.04	0.04	0.03	0.00

Sample ID	**030-3**	**030-4**	**030-5**	**030-7**	**030-8**	**6031-1**	**6031-4**
Rock Type	Ol. Hblite	Ol. Hblite	Ol. Hblite	Ol. Hblite	Ol. Hblite	Ol. Hblite	Ol. Hblite
Map Unit	WCC	WCC	WCC	WCC	WCC	WCC	WCC
Oxide wt. %							
SiO_2	39.115	38.522	38.901	38.802	38.726	38.183	38.561
TiO_2	0.022	0.041	0.013	0.005	0.052	0.031	0.004
Al_2O_3	0.000	0.007	0.011	0.008	0.000	0.000	0.000
FeO	16.939	16.957	17.125	16.770	16.731	22.998	22.079
MnO	0.271	0.279	0.262	0.214	0.252	0.315	0.342
MgO	43.290	43.100	42.815	43.035	43.133	39.647	39.728
CaO	0.000	0.000	0.006	0.002	0.011	0.007	0.021
Na_2O	0.000	0.008	0.000	0.000	0.024	0.023	0.016
Cr_2O_3	0.033	0.022	0.018	0.016	0.004	0.000	0.042
NiO	0.216	0.211	0.188	0.134	0.177	0.164	0.195
Total	**99.887**	**99.146**	**99.339**	**98.985**	**99.111**	**101.369**	**100.987**
Species name	**Chrysolite**	**Chrysolite**	**Chrysolite**	**Chrysolite**	**Chrysolite**	**Chrysolite**	**Chrysolite**
Endmembers mol. %							
Fo	81.76	81.67	81.44	81.87	81.89	75.18	75.93
Fa	17.95	18.03	18.27	17.90	17.82	24.47	23.67
Tph	0.29	0.30	0.28	0.23	0.27	0.34	0.37
Ca-Ol	0.00	0.00	0.01	0.00	0.02	0.01	0.03

Olivine Analyses cont'd

Sample ID	**031-4**	**031-5**	**031-6**	**031-10**	**043-2**	**043-3**	**043-5**
Rock Type	Ol. Hblite	Ol. Hblite	Ol. Hblite	Ol. Hblite	Ol. Hblite	Ol. Hblite	Ol. Hblite
Map Unit	WCC	WCC	WCC	WCC	WCC	WCC	WCC
Oxide wt. %							
SiO_2	38.000	38.280	38.577	38.283	38.185	37.878	42.867
TiO_2	0.000	0.014	0.000	0.006	0.010	0.000	1.584
Al_2O_3	0.003	0.000	0.007	0.000	0.000	0.000	13.230
FeO	20.494	21.556	21.352	21.827	20.929	20.866	8.416
MnO	0.314	0.377	0.354	0.404	0.356	0.356	0.145
MgO	40.021	39.147	39.579	39.161	39.703	39.716	15.834
CaO	0.010	0.009	0.000	0.004	0.006	0.023	11.612
Na_2O	0.000	0.000	0.021	0.006	0.016	0.040	2.031
Cr_2O_3	0.049	0.000	0.000	0.002	0.000	0.026	0.006
NiO	0.149	0.219	0.205	0.241	0.081	0.122	0.039
Total	**99.039**	**99.601**	**100.094**	**99.933**	**99.287**	**99.026**	**95.764**
Species name	**Chrysolite**	**Chrysolite**	**Chrysolite**	**Chrysolite**	**Chrysolite**	**Chrysolite**	**Hyalosiderite**
Endmembers mol. %							
Fo	77.40	76.07	76.47	75.84	76.87	76.91	54.63
Fa	22.24	23.50	23.14	23.71	22.73	22.67	16.29
Tph	0.35	0.42	0.39	0.44	0.39	0.39	0.28
Ca-Ol	0.01	0.01	0.00	0.01	0.01	0.03	28.79

Sample ID	**031-3**	**043-7**	**043-6**	**106-1**	**106-2**	**106-3**	**106-5**
Rock Type	Ol. Hblite	Ol. Hblite	Ol. Hblite	Ol. Hblite	Ol. Hblite	Ol. Hblite	Ol. Hblite
Map Unit	WCC	WCC	WCC	WCC	WCC	WCC	WCC
Oxide wt. %							
SiO_2	38.220	38.040	38.394	38.965	39.021	38.978	38.971
TiO_2	0.024	0.030	0.000	0.039	0.000	0.000	0.015
Al_2O_3	0.000	0.009	0.009	0.016	0.013	0.000	0.005
FeO	21.373	20.394	20.743	17.425	17.604	17.597	17.562
MnO	0.379	0.355	0.386	0.339	0.358	0.395	0.352
MgO	39.105	40.038	39.592	41.961	42.112	42.246	42.518
CaO	0.026	0.011	0.000	0.034	0.030	0.008	0.011
Na_2O	0.007	0.014	0.000	0.019	0.018	0.046	0.000
Cr_2O_3	0.000	0.012	0.000	0.016	0.016	0.000	0.004
NiO	0.214	0.054	0.049	0.154	0.266	0.144	0.170
Total	**99.347**	**98.957**	**99.174**	**98.968**	**99.439**	**99.414**	**99.606**
Species name	**Chrysolite**	**Chrysolite**	**Chrysolite**	**Chrysolite**	**Chrysolite**	**Chrysolite**	**Chrysolite**
Endmembers mol. %							
Fo	76.18	77.46	76.95	80.77	80.65	80.70	80.87
Fa	23.36	22.13	22.62	18.82	18.91	18.86	18.74
Tph	0.42	0.39	0.43	0.37	0.39	0.43	0.38
Ca-Ol	0.04	0.02	0.00	0.05	0.04	0.01	0.01

Olivine Analyses cont'd

Sample ID	**106-6**	**106-7**	**106-9**
t	Ol. Hblite WCC	Ol. Hblite WCC	Ol. Hblite WCC
Oxide wt. %			
SiO_2	39.048	39.409	39.229
TiO_2	0.000	0.014	0.014
Al_2O_3	0.004	0.000	0.002
FeO	17.103	17.215	17.573
MnO	0.362	0.374	0.352
MgO	42.723	42.581	42.533
CaO	0.003	0.004	0.017
Na_2O	0.035	0.011	0.000
Cr_2O_3	0.002	0.006	0.004
NiO	0.210	0.250	0.210
Total	**99.490**	**99.863**	**99.934**
Species name	**Chrysolite**	**Chrysolite**	**Chrysolite**
Endmembers mol. %			
Fo	81.34	81.18	80.86
Fa	18.27	18.41	18.74
Tph	0.39	0.41	0.38
Ca-Ol	0.00	0.00	0.02

Felspar Analyses

Sample ID	**031-1**	**031-2**	**031-3**	**011-1**	**011-2**	**011-3**	**011-4**	**011-5**
Rock Type	Ol. Hblite.	Ol. Hblite.	Ol. Hblite.	Plag. Cum.	Plag. Cum.	Plag. Cum.	Plag. Cum.	Plag. Cum.
Map Unit	WCC	WCC	WCC	WCC	WCC	WCC	WCC	WCC
Oxide wt. %								
SiO_2	53.326	53.142	53.695	45.781	45.154	46.407	45.916	46.385
TiO_2	0.000	0.000	0.000	0.000	0.000	0.000	0.000	0.000
Al_2O_3	29.873	30.166	29.485	34.447	34.945	34.010	34.631	34.162
Fe_2O_3	0.000	0.000	0.000	0.000	0.000	0.000	0.000	0.000
FeO	0.121	0.166	0.061	0.450	0.183	0.466	0.434	0.553
MnO	0.000	0.000	0.000	0.019	0.004	0.009	0.008	0.000
MgO	0.003	0.000	0.024	0.011	0.010	0.019	0.007	0.018
CaO	12.159	12.320	11.390	18.113	18.141	17.435	17.920	17.674
Na_2O	4.646	4.442	4.932	1.336	1.111	1.703	1.474	1.656
K_2O	0.034	0.034	0.017	0.036	0.027	0.033	0.013	0.040
BaO	0.000	0.000	0.000	0.000	0.000	0.000	0.000	0.000
Total	**0.000**	**0.000**	**0.000**	**100.191**	**99.575**	**100.082**	**100.403**	**0.000**
Endmembers mol. %								
An	59.01	60.39	56.01	88.04	89.88	84.82	86.98	85.31
Ab	40.80	39.41	43.89	11.75	9.96	14.99	12.95	14.46
Or	0.20	0.20	0.10	0.21	0.16	0.19	0.08	0.23

Sample ID	**011-6**	**011-7**	**011-8**	**067-1**	**067-2**	**067-3**	**067-4**	**067-5**
Rock Type	Plag. Cum.	Plag. Cum.	Plag. Cum.	Plag. Cum.	Plag. Cum.	Plag. Cum.	Plag. Cum.	Plag. Cum.
Map Unit	WCC	WCC	WCC	WCC	WCC	WCC	WCC	WCC
Oxide wt. %								
SiO_2	45.709	54.730	46.018	45.792	45.015	45.138	54.899	45.682
TiO_2	0.000	0.000	0.000	0.000	0.000	0.000	0.000	0.000
Al_2O_3	34.423	28.490	34.337	34.635	35.147	35.111	28.262	34.436
Fe_2O_3	0.000	0.000	0.000	0.000	0.000	0.000	0.000	0.000
FeO	0.362	0.341	0.325	0.424	0.357	0.343	0.245	0.412
MnO	0.015	0.000	0.016	0.000	0.013	0.011	0.000	0.007
MgO	0.018	0.031	0.008	0.000	0.003	0.003	0.005	0.018
CaO	18.038	10.963	17.645	17.888	18.322	18.008	10.573	17.552
Na_2O	1.371	5.272	1.442	1.373	0.924	1.046	5.384	1.332
K_2O	0.000	0.139	0.018	0.030	0.025	0.212	0.134	0.008
BaO	0.000	0.000	0.000	0.000	0.000	0.000	0.000	0.000
Total	**0.000**	**0.000**	**0.000**	**0.000**	**0.000**	**0.000**	**0.000**	**0.000**
Endmembers mol. %								
An	87.91	53.04	87.03	87.65	91.50	89.36	51.64	87.89
Ab	12.09	46.16	12.87	12.18	8.35	9.39	47.58	12.07
Or	0.00	0.80	0.11	0.18	0.15	1.25	0.78	0.05

Sample ID	067-6	067-7	067-8	68-1	68-2	68-3	68-4	68-5
Rock Type	Plag. Cum.	Plag. Cum.	Plag. Cum.	Plag. Cum.	Plag. Cum.	Plag. Cum.	Plag. Cum.	Plag. Cum.
Map Unit	WCC	WCC	WCC	WCC	WCC	WCC	WCC	WCC
Oxide wt. %								
SiO_2	45.918	45.082	44.967	54.840	53.205	55.540	52.037	55.640
TiO_2	0.000	0.000	0.000	0.000	0.000	0.000	0.000	0.000
Al_2O_3	34.319	34.613	35.215	28.924	29.287	28.039	30.093	28.149
Fe_2O_3	0.000	0.000	0.000	0.000	0.000	0.000	0.000	0.000
FeO	0.386	0.398	0.314	0.211	0.173	0.249	0.295	0.164
MnO	0.012	0.007	0.008	0.023	0.000	0.055	0.000	0.000
MgO	0.009	0.009	0.030	0.015	0.007	0.007	0.182	0.006
CaO	17.390	18.306	18.348	11.313	11.993	9.517	12.208	10.436
Na_2O	1.441	1.061	1.001	4.911	4.610	5.225	3.819	5.386
K_2O	0.010	0.026	0.052	0.078	0.041	0.654	0.536	0.086
BaO	0.000	0.000	0.000	0.000	0.000	0.056	0.039	0.025
Total	**0.000**	**0.000**	**0.000**	**100.313**	**99.315**	**99.342**	**99.208**	**99.891**
Endmembers mol. %								
An	86.91	90.37	90.74	55.75	58.84	48.19	61.79	51.45
Ab	13.03	9.47	8.96	43.79	40.92	47.87	34.98	48.05
Or	0.06	0.15	0.30	0.46	0.24	3.94	3.23	0.51

Sample ID	6100-1	6100-2	6100-3	6100-4	105-1	105-2	105-3	516-1
Rock Type	Plag. Cum.	Plag. Cum.	Plag. Cum.	Plag. Cum.	Plag. Cum.	Plag. Cum.	Plag. Cum.	Qtz. WCC
Map Unit	WCC	WCC	WCC	WCC	WCC	WCC	WCC	WCC
Oxide wt. %								
SiO_2	54.642	55.641	56.091	56.140	54.152	56.143	57.681	53.090
TiO_2	0.000	0.000	0.000	0.000	0.000	0.000	0.000	0.000
Al_2O_3	28.593	27.647	27.298	27.570	26.886	27.515	24.512	29.703
Fe_2O_3	0.000	0.000	0.000	0.000	0.000	0.000	0.000	0.000
FeO	0.239	0.295	0.252	0.562	0.307	0.024	0.040	0.163
MnO	0.000	0.000	0.026	0.054	0.007	0.005	0.000	0.020
MgO	0.001	0.006	0.021	0.014	0.366	0.012	0.041	0.004
CaO	10.989	10.565	9.216	9.543	10.252	9.723	8.231	12.445
Na_2O	5.143	5.177	5.642	5.402	5.448	5.845	6.997	4.437
K_2O	0.102	0.174	0.360	0.624	0.071	0.109	0.099	0.119
BaO	0.016	0.021	0.052	0.102	0.009	0.000	0.011	0.055
Total	**99.725**	**99.527**	**98.958**	**100.010**	**97.498**	**99.376**	**97.611**	**100.034**
Endmembers mol. %								
An	53.82	52.46	46.42	47.57	50.76	47.59	39.18	60.37
Ab	45.58	46.51	51.42	48.73	48.82	51.77	60.26	38.95
Or	0.59	1.03	2.16	3.70	0.42	0.64	0.56	0.68

Sample ID	516-2	516-3	020-1	020-2	6066-1	6066-2	6066-3	6027-1
Rock Type	Qtz. WCC	Qtz. WCC	Qtz. WCC	Qtz. WCC	Qtz. WCC	Qtz. WCC	Qtz. WCC	Bas. Dyke
Map Unit	WCC	WCC	WCC	WCC	WCC	WCC	WCC	Bon. Volc.
Oxide wt. %								
SiO_2	50.985	52.059	53.137	53.436	54.613	56.648	56.406	48.136
TiO_2	0.000	0.000	0.000	0.000	0.000	0.000	0.000	0.000
Al_2O_3	31.488	30.225	29.486	29.441	28.267	27.559	27.437	32.177
Fe_2O_3	0.000	0.000	0.000	0.000	0.000	0.000	0.000	0.000
FeO	0.507	0.220	0.269	0.219	0.231	0.193	0.161	0.686
MnO	0.014	0.007	0.003	0.009	0.000	0.016	0.011	0.017
MgO	0.011	0.000	0.040	0.000	0.008	0.000	0.010	0.091
CaO	14.220	12.743	11.218	12.056	10.743	9.514	9.433	15.818
Na_2O	3.182	3.973	4.652	4.492	5.111	5.696	5.783	2.389
K_2O	0.042	0.110	0.282	0.265	0.244	0.226	0.377	0.066
BaO	0.084	0.000	0.000	0.000	0.019	0.000	0.006	0.016
Total	**100.533**	**99.337**	**99.086**	**99.917**	**99.235**	**99.852**	**99.622**	**99.396**
Endmembers mol. %								
An	71.00	63.51	56.17	58.81	52.97	47.35	46.36	78.23
Ab	28.75	35.83	42.15	39.65	45.60	51.30	51.44	21.38
Or	0.25	0.65	1.68	1.54	1.43	1.34	2.20	0.39

Sample ID	6027-2	6027-3	6027-4	6027-5	6027-6
Rock Type	Bas. Dyke	Bas. Dyke	Bas. Dyke	Bas. Dyke	Bas. Dyke
Map Unit	Bon. Volc.	Bon. Volc.	Bon. Volc.	Bon. Volc.	Bon. Volc.
Oxide wt. %					
SiO_2	47.000	58.141	59.906	46.381	54.027
TiO_2	0.000	0.000	0.000	0.000	0.000
Al_2O_3	33.054	25.605	24.144	33.343	29.097
Fe_2O_3	0.000	0.000	0.000	0.000	0.000
FeO	0.917	0.432	1.257	0.821	0.723
MnO	0.004	0.021	0.029	0.000	0.000
MgO	0.169	0.019	0.832	0.108	0.367
CaO	16.410	7.989	6.198	17.313	8.862
Na_2O	1.681	6.444	7.312	1.624	4.060
K_2O	0.631	0.290	0.215	0.090	2.290
BaO	0.069	0.037	0.001	0.000	0.076
Total	**99.935**	**98.976**	**99.894**	**99.681**	**99.502**
Endmembers mol. %					
An	81.23	39.95	31.49	85.03	46.80
Ab	15.05	58.32	67.21	14.44	38.80
Or	3.72	1.73	1.30	0.53	14.40

Pyroxene Analyses

Morimoto classification scheme: Morimoto, N., Canadian Mineralogist Vol. 27, pp.143-156 (1989)

DHZ classification scheme: Deer, Howie & Zussman, 'An Introduction to the Rock Forming Minerals' pp.99,112 (1976 ed.)

Sample ID	**21-2**	**21-4**	**21-6**	**21-7**	**21-8**	**030-1**	**030-2**	**030-6**	**030-9**	**030-11**
Rock Type	Ol. Hblite	Ol. Hblite	Ol. Hblite	Ol. Hblite	Ol. Hblite	Ol. Hblite	Ol. Hblite	Ol. Hblite	Ol. Hblite	Ol. Hblite
Map Unit	WCC	WCC	WCC	WCC	WCC	WCC	WCC	WCC	WCC	WCC
Oxide wt. %										
SiO_2	49.501	52.145	51.792	53.708	54.659	55.426	55.289	55.511	54.116	54.306
TiO_2	0.624	0.323	0.388	0.083	0.019	0.126	0.111	0.060	0.075	0.144
Al_2O_3	4.086	2.346	2.593	2.077	1.561	1.191	1.413	1.076	1.131	1.293
FeO	6.544	4.877	4.688	14.038	14.923	11.072	11.097	10.704	10.621	11.169
MnO	0.136	0.149	0.087	0.361	0.392	0.284	0.213	0.286	0.325	0.218
MgO	14.986	16.061	15.798	28.503	28.679	31.425	30.874	30.936	30.943	30.988
CaO	22.521	24.053	23.827	1.097	0.410	0.364	0.375	0.589	0.653	0.337
Na_2O	0.215	0.135	0.155	0.000	0.003	0.000	0.017	0.000	0.000	0.012
Cr_2O_3	0.610	0.201	0.159	0.078	0.037	0.105	0.122	0.029	0.180	0.090
NiO	0.000	0.039	0.068	0.019	0.000	0.020	0.029	0.022	0.046	0.049
Total	**99.222**	**100.329**	**99.554**	**99.963**	**100.683**	**100.014**	**99.540**	**99.213**	**98.091**	**98.607**
Morimoto Class.	**Diopside**	**Diopside**	**Diopside**	**Enstatite**	**Enstatite**	**Enstatite**	**Enstatite**	**Enstatite**	**Enstatite**	**Enstatite**
DHZ Class.	**Diopside**	**Diopside**	**Diopside**	**Bronzite**	**Bronzite**	**Bronzite**	**Bronzite**	**Bronzite**	**Bronzite**	**Bronzite**
Endmember mol. %										
Ca-Mg-Fe	98.33	99.00	98.84	100.00	99.98	100.00	99.88	100.00	100.00	99.91
Jd	0.05	0.01	0.02	0.00	0.00	0.00	0.00	0.00	0.00	0.00
Aeg	1.62	0.99	1.13	0.00	0.02	0.00	0.12	0.00	0.00	0.09
En	45.57	46.30	45.86	79.50	78.69	84.77	83.52	83.40	85.64	85.32
Fs	5.21	3.85	4.43	18.30	20.50	14.53	15.75	15.46	13.06	14.02
Wo	49.22	49.84	49.71	2.20	0.81	0.71	0.73	1.14	1.30	0.67

Pyroxene Analyses cont'd

Sample ID	**031-1**	**031-2**	**031-7**	**031-9**	**031-11**	**031-12**	**6031-3**	**6031-2**	**043-1**	**106-8**
Rock Type	Ol. Hblite	Ol. Hblite	Ol. Hblite	Ol. Hblite	Ol. Hblite	Ol. Hblite	Ol. Hblite	Ol. Hblite	Ol. Hblite	Ol. Hblite
Map Unit	WCC	WCC	WCC	WCC	WCC	WCC	WCC	WCC	WCC	WCC
Oxide wt. %										
SiO_2	54.834	55.155	54.705	55.085	52.117	54.909	54.080	55.134	53.389	55.173
TiO_2	0.283	0.160	0.330	0.283	0.718	0.273	0.180	0.135	0.010	0.041
Al_2O_3	1.129	0.804	1.269	1.184	2.352	1.107	1.345	1.109	3.172	1.900
FeO	12.870	13.140	13.030	13.425	6.124	12.742	13.942	14.037	13.790	11.772
MnO	0.347	0.335	0.345	0.334	0.215	0.306	0.364	0.386	0.369	0.411
MgO	29.185	29.385	29.031	28.838	16.219	28.750	29.052	29.493	28.054	30.741
CaO	0.988	0.380	0.904	0.663	21.837	1.625	1.042	0.441	0.465	0.088
Na_2O	0.017	0.012	0.005	0.013	0.324	0.005	0.006	0.000	0.001	0.016
Cr_2O_3	0.076	0.090	0.082	0.092	0.299	0.113	0.121	0.123	0.000	0.235
NiO	0.045	0.003	0.034	0.031	0.048	0.045	0.000	0.000	0.029	0.048
Total	**99.775**	**99.464**	**99.734**	**99.947**	**100.252**	**99.876**	**100.132**	**100.859**	**99.277**	**100.424**
Morimoto Class.	**Enstatite**	**Enstatite**	**Enstatite**	**Enstatite**	**Diopside**	**Enstatite**	**Enstatite**	**Enstatite**	**Enstatite**	**Enstatite**
DHZ Class.	**Bronzite**	**Bronzite**	**Bronzite**	**Bronzite**	**Diopside**	**Bronzite**	**Bronzite**	**Bronzite**	**Bronzite**	**Bronzite**
Endmember mol. %										
Ca-Mg-Fe	99.88	99.91	99.97	99.91	97.60	99.97	99.96	100.00	99.99	99.89
Jd	0.00	0.00	0.00	0.00	0.11	0.00	0.00	0.00	0.00	0.00
Aeg	0.12	0.09	0.03	0.09	2.29	0.03	0.04	0.00	0.01	0.11
En	79.61	79.73	79.24	78.27	47.24	78.21	80.38	80.07	78.82	83.69
Fs	18.45	19.53	18.99	20.44	7.05	18.62	17.55	19.07	20.24	16.13
Wo	1.94	0.74	1.77	1.29	45.71	3.18	2.07	0.86	0.94	0.17

Pyroxene Analyses cont'd

Sample ID	**011-1**	**011-2**	**011-3**	**011-4**	**011-5**	**011-6**	**011-7**	**011-8**	**011-9**	**067-1**
Rock Type	Plag. Cum.	Plag. Cum.	Plag. Cum.	Plag. Cum.	Plag. Cum.	Plag. Cum.	Plag. Cum.	Plag. Cum.	Plag. Cum.	Plag. Cum.
Map Unit	WCC	WCC	WCC	WCC	WCC	WCC	WCC	WCC	WCC	WCC
Oxide wt. %										
SiO_2	51.411	53.323	51.250	52.991	53.012	51.971	53.162	53.095	52.806	51.603
TiO_2	0.437	0.216	0.312	0.214	0.179	0.359	0.199	0.183	0.194	0.226
Al_2O_3	2.305	1.402	1.840	1.319	1.253	1.954	1.331	1.059	1.254	2.022
FeO	8.297	18.172	7.278	18.126	18.335	7.359	17.248	18.321	18.310	5.682
MnO	0.425	0.713	0.328	0.643	0.688	0.363	0.628	0.649	0.654	0.319
MgO	14.775	24.748	14.874	24.646	24.413	14.648	25.323	24.414	24.678	15.479
CaO	21.342	0.858	21.979	0.967	0.899	22.468	1.055	0.898	0.882	23.418
Na_2O	0.211	0.007	0.259	0.019	0.036	0.271	0.000	0.007	0.004	0.291
Cr_2O_3	0.011	0.000	0.000	0.033	0.006	0.013	0.000	0.000	0.000	0.019
NiO	0.000	0.026	0.101	0.017	0.000	0.036	0.000	0.000	0.061	0.022
Total	**99.212**	**99.465**	**98.221**	**98.975**	**98.821**	**99.442**	**98.945**	**98.625**	**98.843**	**99.082**
Morimoto Class.	**Diopside**	**Enstatite**	**Diopside**	**Enstatite**	**Enstatite**	**Diopside**	**Enstatite**	**Enstatite**	**Enstatite**	**Diopside**
DHZ Class.	**Salite**	**Bronzite**	**Diopside**	**Bronzite**	**Hypersthene**	**Diopside**	**Bronzite**	**Hypersthene**	**Hypersthene**	**Diopside**
Endmember mol. %										
Ca-Mg-Fe	98.41	99.95	98.03	99.86	99.73	97.97	100.00	99.95	99.97	97.81
Jd	0.05	0.00	0.05	0.00	0.00	0.08	0.00	0.00	0.00	0.04
Aeg	1.54	0.05	1.92	0.14	0.26	1.95	0.00	0.05	0.03	2.15
En	43.56	69.83	44.24	69.95	69.42	42.94	71.52	69.12	70.30	45.82
Fs	11.22	28.43	8.78	28.07	28.74	9.72	26.33	29.05	27.90	4.35
Wo	45.22	1.74	46.98	1.97	1.84	47.34	2.14	1.83	1.81	49.83

Pyroxene Analyses cont'd

Sample ID	**011-1**	**011-2**	**011-3**	**011-4**	**011-5**	**011-6**	**011-7**	**011-8**	**011-9**	**067-1**
Rock Type	Plag. Cum.	Plag. Cum.	Plag. Cum.	Plag. Cum.	Plag. Cum.	Plag. Cum.	Plag. Cum.	Plag. Cum.	Plag. Cum.	Plag. Cum.
Map Unit	WCC	WCC	WCC	WCC	WCC	WCC	WCC	WCC	WCC	WCC
Oxide wt. %										
SiO_2	51.411	53.323	51.250	52.991	53.012	51.971	53.162	53.095	52.806	51.603
TiO_2	0.437	0.216	0.312	0.214	0.179	0.359	0.199	0.183	0.194	0.226
Al_2O_3	2.305	1.402	1.840	1.319	1.253	1.954	1.331	1.059	1.254	2.022
FeO	8.297	18.172	7.278	18.126	18.335	7.359	17.248	18.321	18.310	5.682
MnO	0.425	0.713	0.328	0.643	0.688	0.363	0.628	0.649	0.654	0.319
MgO	14.775	24.748	14.874	24.646	24.413	14.648	25.323	24.414	24.678	15.479
CaO	21.342	0.858	21.979	0.967	0.899	22.468	1.055	0.898	0.882	23.418
Na_2O	0.211	0.007	0.259	0.019	0.036	0.271	0.000	0.007	0.004	0.291
Cr_2O_3	0.011	0.000	0.000	0.033	0.006	0.013	0.000	0.000	0.000	0.019
NiO	0.000	0.026	0.101	0.017	0.000	0.036	0.000	0.000	0.061	0.022
Total	**99.212**	**99.465**	**98.221**	**98.975**	**98.821**	**99.442**	**98.945**	**98.625**	**98.843**	**99.082**
Morimoto Class.	**Diopside**	**Enstatite**	**Diopside**	**Enstatite**	**Enstatite**	**Diopside**	**Enstatite**	**Enstatite**	**Enstatite**	**Diopside**
DHZ Class.	**Salite**	**Bronzite**	**Diopside**	**Bronzite**	**Hypersthene**	**Diopside**	**Bronzite**	**Hypersthene**	**Hypersthene**	**Diopside**
Endmember mol. %										
Ca-Mg-Fe	98.41	99.95	98.03	99.86	99.73	97.97	100.00	99.95	99.97	97.81
Jd	0.05	0.00	0.05	0.00	0.00	0.08	0.00	0.00	0.00	0.04
Aeg	1.54	0.05	1.92	0.14	0.26	1.95	0.00	0.05	0.03	2.15
En	43.56	69.83	44.24	69.95	69.42	42.94	71.52	69.12	70.30	45.82
Fs	11.22	28.43	8.78	28.07	28.74	9.72	26.33	29.05	27.90	4.35
Wo	45.22	1.74	46.98	1.97	1.84	47.34	2.14	1.83	1.81	49.83

Pyroxene Analyses cont'd

Sample ID	**067-2**	**067-3**	**067-4**	**68-1**	**68-2**	**68-3**	**68-4**	**68-5**	**6100-1**	**6100-2**
Rock Type	Plag. Cum.	Plag. Cum.	Plag. Cum.	Plag. Cum.	Plag. Cum.	Plag. Cum.	Plag. Cum.	Plag. Cum.	Plag. Cum.	Plag. Cum.
Map Unit	WCC	WCC	WCC	WCC	WCC	WCC	WCC	WCC	WCC	WCC
Oxide wt. %										
SiO_2	52.755	52.005	50.311	52.416	55.714	53.212	53.243	52.768	49.838	49.587
TiO_2	0.191	0.336	0.428	0.097	0.061	0.090	0.108	0.028	0.220	0.680
Al_2O_3	0.781	1.753	3.532	1.092	1.057	0.950	1.052	0.730	4.371	4.244
FeO	4.280	5.595	7.729	19.059	16.675	20.514	19.778	20.114	16.283	7.751
MnO	0.214	0.241	0.179	0.523	0.515	0.565	0.556	0.617	0.462	0.170
MgO	16.171	15.673	14.759	25.069	22.560	24.720	24.785	24.916	13.409	14.905
CaO	24.732	23.467	20.943	0.970	0.970	0.476	0.957	0.495	11.512	21.855
Na_2O	0.101	0.164	0.469	0.029	0.139	0.005	0.004	0.021	0.451	0.261
Cr_2O_3	0.000	0.024	0.034	0.016	0.018	0.000	0.000	0.000	0.000	0.108
NiO	0.000	0.022	0.037	0.002	0.057	0.000	0.000	0.032	0.023	0.022
Total	**99.225**	**99.278**	**98.421**	**99.272**	**97.764**	**100.531**	**100.483**	**99.719**	**96.568**	**99.582**
Morimoto Class.	**Diopside**	**Diopside**	**Diopside**	**Enstatite**	**Enstatite**	**Enstatite**	**Enstatite**	**Enstatite**	**Augite**	**Diopside**
DHZ Class.	**Diopside**	**Diopside**	**Diopside**	**Hypersthene**	**Bronzite**	**Hypersthene**	**Hypersthene**	**Hypersthene**	**Augite**	**Diopside**
Endmember mol. %										
Ca-Mg-Fe	99.26	98.78	96.40	99.79	98.91	99.97	99.97	99.85	96.34	97.97
Jd	0.00	0.02	0.24	0.00	0.00	0.00	0.00	0.00	0.00	0.06
Aeg	0.74	1.20	3.36	0.21	1.09	0.03	0.03	0.15	3.66	1.96
En	46.07	45.45	45.24	71.96	69.18	69.82	69.93	71.21	43.51	45.42
Fs	3.28	5.63	8.62	26.04	28.68	29.22	28.13	27.78	29.64	6.72
Wo	50.64	48.92	46.14	2.00	2.14	0.97	1.94	1.02	26.85	47.86

Pyroxene Analyses cont'd

Sample ID	**6100-3**	**6100-4**	**6100-5**	**6100-6**	**105-1**	**105-2**	**105-3**	**516-1**	**516-2**	**516-3**
Rock Type	Plag. Cum.	Plag. Cum.	Plag. Cum.	Plag. Cum.	Plag. Cum.	Plag. Cum.	Plag. Cum.	Qtz. WCC	Qtz. WCC	Qtz. WCC
Map Unit	WCC	WCC	WCC	WCC	WCC	WCC	WCC	WCC	WCC	WCC
Oxide wt. %										
SiO_2	50.363	50.474	49.783	49.786	53.228	50.564	53.320	51.241	52.277	51.244
TiO_2	0.642	0.612	0.784	0.614	0.162	0.576	0.128	0.104	0.176	0.110
Al_2O_3	4.301	2.129	3.799	3.799	3.150	4.076	1.791	0.950	1.400	0.536
FeO	7.320	12.608	9.333	8.258	9.209	6.597	19.708	26.561	10.001	26.941
MnO	0.172	0.516	0.282	0.246	0.151	0.208	0.682	0.816	0.322	0.741
MgO	14.520	13.034	14.255	14.624	18.340	16.705	19.176	19.388	13.335	19.432
CaO	21.683	19.799	20.583	20.674	12.082	20.111	2.063	0.753	22.220	0.631
Na_2O	0.249	0.229	0.306	0.388	0.327	0.276	0.245	0.002	0.223	0.008
Cr_2O_3	0.117	0.017	0.042	0.049	0.040	0.600	0.008	0.000	0.025	0.002
NiO	0.022	0.008	0.025	0.067	0.000	0.012	0.047	0.000	0.000	0.003
Total	**99.388**	**99.425**	**99.191**	**98.506**	**96.689**	**99.725**	**97.168**	**99.814**	**99.980**	**99.647**
Morimoto Class.	**Diopside**	**Augite**	**Diopside**	**Diopside**	**Augite**	**Augite**	**Enstatite**	**Enstatite**	**Diopside**	**Enstatite**
DHZ Class.	**Diopside**	**Augite**	**Salite**	**Diopside**	**Augite**	**Endiopside**	**Hypersthene**	**Hypersthene**	**Salite**	**Hypersthene**
Endmember mol. %										
Ca-Mg-Fe	98.10	98.24	97.63	96.99	97.42	97.90	98.03	99.99	98.34	99.94
Jd	0.14	0.05	0.12	0.17	0.00	0.10	0.00	0.00	0.06	0.00
Aeg	1.76	1.71	2.25	2.84	2.58	2.01	1.97	0.01	1.60	0.06
En	43.54	39.17	43.43	44.97	56.97	50.06	60.46	57.10	38.77	57.17
Fs	9.74	18.06	11.50	9.34	16.05	6.62	34.86	41.31	14.79	41.49
Wo	46.73	42.77	45.07	45.69	26.98	43.32	4.67	1.59	46.43	1.33

Pyroxene Analyses cont'd

Sample ID	**516-4**	**516-5**	**516-6**	**516-8**	**020-1**	**020-2**	**020-3**	**020-4**	**020-5**	**020-6**
Rock Type	Qtz. WCC	Qtz. WCC	Qtz. WCC	Qtz. WCC	Qtz. WCC	Qtz. WCC	Qtz. WCC	Qtz. WCC	Qtz. WCC	Qtz. WCC
Map Unit	WCC	WCC	WCC	WCC	WCC	WCC	WCC	WCC	WCC	WCC
Oxide wt. %										
SiO_2	51.420	51.562	51.716	51.657	51.319	51.752	52.117	52.008	51.832	51.306
TiO_2	0.103	0.099	0.102	0.217	0.370	0.088	0.161	0.141	0.116	0.158
Al_2O_3	0.934	0.876	1.091	1.740	1.981	0.975	1.549	0.940	1.036	0.943
FeO	26.571	26.619	26.228	11.000	9.722	24.098	9.234	24.678	9.077	24.778
MnO	0.721	0.760	0.747	0.345	0.279	0.629	0.353	0.700	0.319	0.696
MgO	19.630	19.422	19.745	13.225	13.344	20.407	13.581	20.196	13.429	19.947
CaO	0.761	0.738	0.978	21.595	21.843	0.761	22.327	0.776	22.995	0.735
Na_2O	0.006	0.011	0.020	0.335	0.348	0.000	0.306	0.033	0.215	0.027
Cr_2O_3	0.000	0.000	0.010	0.017	0.013	0.000	0.009	0.016	0.056	0.000
NiO	0.000	0.037	0.012	0.000	0.005	0.074	0.009	0.030	0.000	0.000
Total	**100.146**	**100.122**	**100.648**	**100.130**	**99.224**	**98.784**	**99.644**	**99.517**	**99.075**	**98.591**
Morimoto Class.	**Enstatite**	**Enstatite**	**Enstatite**	**Diopside**	**Diopside**	**Enstatite**	**Diopside**	**Enstatite**	**Diopside**	**Enstatite**
DHZ Class.	**Hypersthene**	**Hypersthene**	**Hypersthene**	**Salite**	**Salite**	**Hypersthene**	**Salite**	**Hypersthene**	**Salite**	**Hypersthene**
Endmember mol. %										
Ca-Mg-Fe	99.96	99.92	99.85	97.48	97.37	100.00	97.72	99.75	98.39	99.79
Jd	0.00	0.00	0.00	0.07	0.11	0.00	0.08	0.00	0.02	0.00
Aeg	0.04	0.08	0.15	2.45	2.51	0.00	2.20	0.25	1.59	0.21
En	57.53	56.86	57.63	39.25	39.78	59.38	39.90	58.61	39.40	58.62
Fs	40.87	41.59	40.32	14.68	13.42	39.02	12.96	39.77	12.12	39.83
Wo	1.60	1.55	2.05	46.07	46.80	1.59	47.14	1.62	48.48	1.55

Pyroxene Analyses cont'd

Sample ID	**6027-1**	**6027-2**	**6027-3**	**6027-4**	**6027-5**	**6027-6**	**6027-7**	**6027-8**	**6027-9**	**6027-10**
Rock Type	Basalt dyke	Basalt dyke	Basalt dyke	Basalt dyke	Basalt dyke	Basalt dyke	Basalt dyke	Basalt dyke	Basalt dyke	Basalt dyke
Map Unit	Bon. Volc.	Bon. Volc.	Bon. Volc.	Bon. Volc.	Bon. Volc.	Bon. Volc.	Bon. Volc.	Bon. Volc.	Bon. Volc.	Bon. Volc.
Oxide wt. %										
SiO_2	47.388	49.317	51.113	50.487	50.079	50.613	50.003	49.399	49.782	46.456
TiO_2	1.178	0.647	0.553	0.444	0.495	0.554	0.533	0.560	0.594	1.271
Al_2O_3	6.526	4.050	2.658	3.064	4.060	2.584	4.183	4.281	4.005	6.956
FeO	7.882	7.299	8.563	6.926	6.479	9.131	6.913	6.550	6.850	9.402
MnO	0.168	0.174	0.262	0.192	0.090	0.329	0.133	0.111	0.170	0.190
MgO	13.694	15.021	15.124	14.969	15.155	15.281	15.129	15.060	15.061	12.785
CaO	21.823	22.015	20.900	22.791	22.482	20.803	22.698	22.718	22.253	21.566
Na_2O	0.312	0.227	0.221	0.227	0.172	0.164	0.184	0.220	0.216	0.268
Cr_2O_3	0.025	0.176	0.000	0.170	0.266	0.025	0.098	0.121	0.094	0.053
NiO	0.003	0.000	0.019	0.044	0.000	0.000	0.029	0.005	0.000	0.005
Total	**99.000**	**98.926**	**99.411**	**99.315**	**99.280**	**99.484**	**99.902**	**99.025**	**99.024**	**98.951**
Morimoto Class.	**Diopside**	**Diopside**	**Augite**	**Diopside**	**Diopside**	**Augite**	**Diopside**	**Diopside**	**Diopside**	**Diopside**
DHZ Class.	**Diopside**	**Diopside**	**Augite**	**Diopside**	**Diopside**	**Augite**	**Diopside**	**Diopside**	**Diopside**	**Diopside**
Endmember mol. %										
Ca-Mg-Fe	97.48	98.23	98.33	98.26	98.67	98.74	98.58	98.28	98.33	97.80
Jd	0.14	0.05	0.05	0.04	0.04	0.02	0.03	0.04	0.05	0.10
Aeg	2.38	1.72	1.62	1.70	1.29	1.24	1.39	1.67	1.62	2.09
En	43.51	45.91	44.70	44.86	45.45	45.46	45.51	45.94	45.59	41.25
Fs	6.65	5.73	10.90	6.05	6.09	10.07	5.41	4.25	6.00	8.75
Wo	49.84	48.36	44.40	49.09	48.46	44.48	49.08	49.81	48.41	50.00

Pyroxene Analyses cont'd

Sample ID	**6027-11**	**6027-12**
Rock Type	Basalt dyke	Basalt dyke
Map Unit	Bon. Volc.	Bon. Volc.
Oxide wt. %		
SiO_2	49.153	44.947
TiO_2	0.609	1.589
Al_2O_3	5.022	7.961
FeO	6.809	10.279
MnO	0.150	0.198
MgO	14.930	12.283
CaO	22.401	21.013
Na_2O	0.214	0.298
Cr_2O_3	0.183	0.015
NiO	0.000	0.000
Total	**99.471**	**98.582**
Morimoto Class.	**Diopside**	**Diopside**
DHZ Class.	**Diopside**	**Diopside**
Endmember mol. %		
Ca-Mg-Fe	98.33	97.49
Jd	0.05	0.13
Aeg	1.62	2.38
En	45.74	40.86
Fs	4.93	8.91
Wo	49.33	50.23

Spinel Analyses

Sample ID	**005-1**	**005-4**	**005-3**	**005-5**	**21-1**	**21-2**	**030-1**	**030-2**
Rock Type	Ol. Hblite	Ol. Hblite	Ol. Hblite	Ol. Hblite	Ol. Hblite	Ol. Hblite	Ol. Hblite	Ol. Hblite
Map Unit	WCC	WCC	WCC	WCC	WCC	WCC	WCC	WCC
Oxide wt. %								
SiO_2	0.021	0.019	0.073	0.022	0.049	0.045	0.258	0.000
TiO_2	0.051	0.073	1.776	3.346	1.266	0.811	0.040	0.070
Al_2O_3	55.906	44.606	9.471	9.154	1.035	0.611	41.718	31.966
FeO(T)	21.891	27.337	61.476	58.726	88.692	88.720	29.801	35.873
MnO	0.085	0.221	0.362	0.366	0.133	0.119	0.151	0.197
MgO	15.607	11.756	2.527	2.669	0.443	0.375	10.783	7.297
CaO	0.007	0.011	0.022	0.004	0.041	0.016	0.023	0.011
Cr_2O_3	5.825	14.751	20.602	21.870	2.107	2.725	15.078	22.456
V_2O_3	0.048	0.070	0.550	0.183	0.384	0.423	0.061	0.043
NiO	0.218	0.135	0.169	0.172	0.025	0.080	0.155	0.123
Total	**99.658**	**98.979**	**97.027**	**96.512**	**94.175**	**93.924**	**98.068**	**98.034**
Species name	**Spinel**	**Spinel**	**Magnetite**	**Magnetite**	**Magnetite**	**Magnetite**	**Hercynite**	**Hercynite**
mol. % Usp			0.049	0.099	0.020	0.013		

Sample ID	**030-3**	**030-4**	**031-1**	**031-2**	**031-3**	**031-4**	**6031-1**	**6031-2**
Rock Type	Ol. Hblite	Ol. Hblite	Ol. Hblite	Ol. Hblite	Ol. Hblite	Ol. Hblite	Ol. Hblite	Ol. Hblite
Map Unit	WCC	WCC	WCC	WCC	WCC	WCC	WCC	WCC
Oxide wt. %								
SiO_2	0.009	0.009	0.044	0.013	0.372	0.028	0.000	1.091
TiO_2	2.770	0.136	3.205	3.696	4.772	3.389	0.081	2.131
Al_2O_3	3.714	37.904	3.376	5.003	3.699	3.954	53.201	3.035
FeO(T)	74.787	31.960	77.997	70.293	75.517	75.569	26.619	75.684
MnO	0.424	0.229	0.254	0.362	0.247	0.285	0.203	0.290
MgO	1.362	9.784	0.948	1.333	1.612	1.303	12.186	1.847
CaO	0.000	0.004	0.000	0.000	0.000	0.000	0.000	0.026
Cr_2O_3	12.827	17.298	9.752	15.146	9.228	11.583	7.767	9.378
V_2O_3	0.140	0.172	0.254	0.072	0.172	0.275	0.095	0.438
NiO	0.288	0.213	0.204	0.299	0.133	0.298	0.311	0.216
Total	**96.320**	**97.707**	**96.034**	**96.215**	**95.751**	**96.684**	**100.462**	**94.136**
Species name	**Magnetite**	**Hercynite**	**Magnetite**	**Magnetite**	**Magnetite**	**Magnetite**	**Spinel**	**Magnetite**
mol. % Usp	0.055		0.061	0.082	0.094	0.067		0.042

Sample ID	**6031-3**	**6031-4**	**043-2**	**106-1**	**106-2**	**106-3**	**106-4**	**106-5**
Rock Type	Ol. Hblite	Ol. Hblite	Ol. Hblite	Ol. Hblite	Ol. Hblite	Ol. Hblite	Ol. Hblite	Ol. Hblite
Map Unit	WCC	WCC	WCC	WCC	WCC	WCC	WCC	WCC
Oxide wt. %								
SiO_2	0.004	0.000	0.000	0.028	0.017	0.022	0.089	0.241
TiO_2	4.235	4.133	0.989	0.007	0.220	1.503	0.184	1.857
Al_2O_3	3.765	4.346	1.009	59.920	32.336	5.623	31.062	3.550
FeO(T)	75.372	72.742	91.795	21.520	36.816	71.816	38.729	77.786

Spinel Analyses cont'd

Sample ID	**6031-3**	**6031-4**	**043-2**	**106-1**	**106-2**	**106-3**	**106-4**	**106-5**
MnO	0.324	0.327	0.056	0.212	0.314	0.464	0.392	0.541
MgO	1.053	1.247	0.565	15.146	7.924	1.769	7.432	1.442
CaO	0.009	0.007	0.000	0.019	0.001	0.015	0.029	0.000
Cr_2O_3	9.376	11.320	0.057	0.018	19.214	14.498	19.793	9.393
V_2O_3	0.213	0.184	0.209	0.000	0.062	0.066	0.073	0.000
NiO	0.218	0.201	0.016	0.261	0.107	0.260	0.129	0.183
Total	**94.568**	**94.505**	**94.695**	**97.131**	**97.010**	**96.036**	**97.914**	**94.991**
Species name	**Magnetite**	**Magnetite**	**Magnetite**	**Spinel**	**Hercynite**	**Magnetite**	**Hercynite**	**Magnetite**
mol. % Usp	0.083	0.086	0.015			0.032		0.035

Sample ID	**011-1**	**011-4**	**011-6**	**011-8**	**067-1**	**067-3**	**067-5**	**067-7**
Rock Type	Plag. Cum.	Plag. Cum.	Plag. Cum.	Plag. Cum.	Plag. Cum.	Plag. Cum.	Plag. Cum.	Plag. Cum.
Map Unit	WCC	WCC	WCC	WCC	WCC	WCC	WCC	WCC
Oxide wt. %								
SiO_2	0.017	0.039	0.033	0.030	0.000	0.052	0.034	0.019
TiO_2	0.302	0.164	0.214	0.239	0.247	0.099	0.151	0.103
Al_2O_3	0.261	0.269	0.256	0.303	0.361	0.180	0.327	0.613
FeO(T)	93.277	92.930	91.961	92.801	92.909	92.819	92.787	92.340
MnO	0.000	0.000	0.054	0.043	0.000	0.000	0.041	0.092
MgO	0.124	0.111	0.121	0.149	0.165	0.111	0.142	0.208
CaO	0.071	0.009	0.015	0.004	0.034	0.049	0.009	0.021
Cr_2O_3	0.063	0.002	0.034	0.012	0.027	0.111	0.085	0.100
V_2O_3	0.675	0.754	0.864	0.766	0.545	0.768	0.527	0.667
NiO	0.027	0.000	0.090	0.000	0.034	0.009	0.080	0.000
Total	**94.816**	**94.277**	**93.642**	**94.347**	**94.322**	**94.199**	**94.183**	**94.162**
Species name	**Magnetite**	**Magnetite**	**Magnetite**	**Magnetite**	**Magnetite**	**Magnetite**	**Magnetite**	**Magnetite**
mol. % Usp	0.004	0.002	0.003	0.003	0.004	0.001	0.002	0.002

Sample ID	**68-1**	**68-3**	**6100-1**	**105-2**	**105-4**	**516-1**	**516-3**	**516-6**
Rock Type	Plag. Cum.	Plag. Cum.	Plag. Cum.	Plag. Cum.	Plag. Cum.	Qtz. WCC	Qtz. WCC	Qtz. WCC
Map Unit	WCC	WCC	WCC	WCC	WCC	WCC	WCC	WCC
Oxide wt. %								
SiO_2	0.050	2.800	0.038	0.036	0.029	0.066	0.063	0.046
TiO_2	2.986	2.006	2.504	0.160	0.092	1.783	1.417	1.940
Al_2O_3	1.943	0.668	0.474	0.349	0.107	1.563	1.066	1.592
FeO(T)	85.653	84.219	89.912	91.894	92.561	87.905	90.016	88.156
MnO	0.405	0.082	0.088	0.000	0.017	0.135	0.093	0.110
MgO	0.148	0.608	0.093	0.109	0.129	0.236	0.209	0.295
CaO	0.092	1.570	0.042	0.008	0.008	0.047	0.065	0.030
Cr_2O_3	0.391	0.382	0.041	0.065	0.058	0.240	0.216	0.098
V_2O_3	0.371	0.457	0.819	0.927	1.105	1.194	1.117	0.831
NiO	0.042	0.037	0.039	0.052	0.046	0.056	0.000	0.020
Total	**92.081**	**92.829**	**94.049**	**93.600**	**94.152**	**93.225**	**94.261**	**93.118**
Species name	**Magnetite**	**Magnetite**	**Magnetite**	**Magnetite**	**Magnetite**	**Magnetite**	**Magnetite**	**Magnetite**
mol. % Usp	0.048	0.034	0.038	0.002	0.001	0.028	0.022	0.030

Spinel Analyses cont'd

Sample ID	**020-2**	**020-4**	**6066-1**	**6066-2**	**6066-3**	**6027-2**
Rock Type	Qtz. WCC	Qtz. WCC	Qtz. WCC	Qtz. WCC	Qtz. WCC	Bas. Dyke
Map Unit	WCC	WCC	WCC	WCC	WCC	Bon. Volc.
Oxide wt. %						
SiO_2	0.052	0.000	0.032	0.034	0.044	1.203
TiO_2	1.043	1.106	0.253	0.233	0.214	11.432
Al_2O_3	0.894	1.583	0.265	0.135	0.427	0.080
FeO(T)	90.414	89.445	92.728	92.395	92.394	78.868
MnO	0.017	0.056	0.081	0.070	0.062	0.676
MgO	0.198	0.357	0.065	0.150	0.070	0.149
CaO	0.006	0.002	0.015	0.018	0.107	1.085
Cr_2O_3	0.604	0.588	0.081	0.116	0.130	0.121
V_2O_3	1.321	1.259	0.575	0.570	0.546	0.000
NiO	0.042	0.075	0.051	0.000	0.079	0.048
Total	**94.590**	**94.471**	**94.145**	**93.721**	**94.071**	**93.662**
Species name	**Magnetite**	**Magnetite**	**Magnetite**	**Magnetite**	**Magnetite**	**Magnetite**
mol. % Usp	0.016	0.017	0.004	0.003	0.003	0.211

Table 4 – Thermobarometry results

Sample ID	Max Amph. P (Mpa)	Avg. Amph P (Mpa)	Std. Deviation (1-σ)	Thermocalc P (Mpa)	QUILF Temp (°C)
JL06-005	750	640	150		
JL06-021	970	880	80		
JL06-030	840	650	200		
JL06-031	830	470	180	571 +/- 126	1058 +/- 91
JL06-043	790	710	120		
JL06-106	920	780	100		
JL06-011				208 +/- 117	898 +/- 36
DC05-016				171 +/- 44	843 +/- 29

Table 5 – Synthesis of Sample Data

Sample #	UTM Easting*	UTM Northing	Map Unit	Rock Type	Thin Section	WR Chem	Mineral Chem
JL06-001	403673	5389127	WCC	Gabbrodiorite	x	x	
JL06-002	403707	5389526	IPS	Granite	x	x	
JL06-003	403699	5389566	WCC	Gabbrodiorite	x	x	
JL06-005	403501	5388596	WCC	Olivine hornblendite	x	x	x
JL06-006	403629	5387463	WCC	Gabbrodiorite	x	x	
JL06-007	405723	5384694	WCC	Amphibolite			
JL06-008	412556	5385656	WCC	Cumulate gabbro	x	x	
JL06-009	412720	5387075	WCC	Cumulate gabbro	x	x	
JL06-010	412720	5387075	WCC	Gabbrodiorite	x	x	
JL06-011	412334	5386105	WCC	Cumulate gabbro	x	x	x
JL06-012	402525	5391344	WCC	Gabbrodiorite			
JL06-013	404212	5390800	WCC	Gabbrodiorite	x	x	
JL06-014	405063	5386424	WCC	Gabbrodiorite	x		
JL06-015	405084	5385889	WCC	Cumulate gabbro	x	x	
JL06-016	393453	5387734	WCC	Pyroxenite			
JL06-017	392804	5388843	WCC	Gabbrodiorite		x	
JL06-018	393933	5391834	IPS	Granite			
JL06-019	393874	5387227	WCC	Gabbrodiorite	x		
JL06-020	393392	5385237	WCC	2 pyroxene gabbrodiorite	x	x	x
JL06-021	390494	5386212	WCC	Olivine hornblendite	x	x	x
JL06-022	392435	5386793	WCC	Gabbrodiorite	x	x	
JL06-023	392332	5387705	WCC	Cumulate gabbro	x		
JL06-024	414195	5386734	WCC	Cumulate gabbro	x	x	
JL06-025	415781	5385266	WCC	Gabbrodiorite	x	x	
JL06-026	416217	5392098	IPS	Plagioclase porphyry			
JL06-027	408959	5392773	Bonanza	Mafic dyke	x	x	x
JL06-028	408412	5391025	WCC	Gabbrodiorite			
JL06-029	405110	5385995	WCC	Olivine hornblendite		x	
JL06-030	404511	5387000	WCC	Olivine hornblendite	x	x	x
JL06-031	404319	5386734	WCC	Olivine hornblendite	x	x	x
JL06-032	403711	5387008	IPS	Granodiorite			
JL06-033	407666	5393351	IPS	Granite			
JL06-034	400858	5395160	IPS	Granite	x	x	
JL06-035	399520	5395109	WCC	Gabbrodiorite			
JL06-036	396902	5397476	IPS	Granodiorite			
JL06-037	397143	5398820	Bonanza	Andesite			
JL06-038	415057	5390142	Bonanza	Basaltic andesite	x	x	
JL06-039	414470	5392680	Karmutsen	Basalt			
JL06-040	418621	5392761	IPS	Granodiorite	x	x	
JL06-041	398191	5393513	IPS	Granodiorite	x	x	
JL06-042	406520	5390645	WCC	Hornblendite	x	x	
JL06-043	391021	5386186	WCC	Olivine hornblendite	x	x	x
JL06-044	391400	5386446	WCC	Gabbrodiorite	x	x	
JL06-045	389013	5385584	WCC	Cumulate gabbro	x	x	
JL06-046	388030	5399134	IPS	Granodiorite			

Sample #	UTM Easting*	UTM Northing	Map Unit	Rock Type	Thin Section	WR Chem	Mineral Chem
JL06-047	386377	5396396	**Bonanza**	Dacite			
JL06-049	386138	5394057	**Bonanza**	Andesite			
JL06-050	385254	5391473	**Bonanza**	mafic dyke	x	x	
JL06-051	384093	5390017	**IPS**	Granite			
JL06-052	384961	5395873	**Bonanza**	Basalt	x	x	
JL06-053	385589	5398648	**Bon. Volc.**	mafic dyke	x	x	
JL06-054	385589	5398648	**IPS**	Granite	x	x	
JL06-055	384474	5399038	**Bonanza**	wacke			
JL06-056	377867	5407516	**Bonanza**	Andesite			
JL06-057	379035	5411705	**Bonanz**	Wacke			
JL06-058	378951	5413045	**Bonanza**	Andesite			
JL06-059	385977	5416780	**Karmutsen**	Basalt			
JL06-060	386784	5418171	**Bonanza**	Basaltic andesite			
JL06-061	387233	5418628	**Bonanza**	Basalt	x		
JL06-063	374783	5404199	**Bonanza**	Basaltic andesite			
JL06-064	374847	5403497	**IPS**	Granodiorite			
JL06-065	374343	5402150	**IPS**	Granite			
JL06-066	372623	5395509	**WCC**	Gabbrodiorite	x	x	x
JL06-067	371930	5394121	**WCC**	Cumulate gabbro	x	x	x
JL06-068	371538	5393252	**WCC**	Cumulate gabbro	x	x	x
JL06-069	371183	5390137	**WCC**	Cumulate gabbro	x	x	
JL06-070	384877	5414266	**WCC**	Gabbrodiorite			
JL06-071	385476	5414922	**Bonanza?**	Basalt			
JL06-072	389427	5413878	**Bonanza**	Basalt			
JL06-073	390803	5413207	**Bonanza**	Andesite			
JL06-074	417448	5405242	**Karmutsen**	Basalt			
JL06-075	421087	5397049	**IPS**	Gdiorite			
JL06-076	421738	5387048	**IPS**	Granodiorite	x	x	
JL06-077	423043	5384583	**Bonanza**	Andesite			
JL06-078	420624	5385436	**Bonanza?**	Basaltic andesite			
JL06-079	411658	5396344	**Karmutsen**	Basalt			
JL06-080	410404	5393089	**Karmutsen**	Volcanic breccia			
JL06-081	400728	5403704	**Karmutsen**	Basalt			
JL06-082	415647	5405435	**IPS**	Granodiorite			
JL06-083	403664	5406632	**Karmutsen**	Basalt			
JL06-084	400361	5400772	**Bonanza**	Andesite			
JL06-085	398906	5400310	**Bonanza**	Basalt			
JL06-086	395999	5394989	**WCC**	Gabbrodiorite			
JL06-087	396905	5397518	**IPS**	Granodiorite			
JL06-088	397149	5398817	**Bonanza**	Andesite			
JL06-089	392974	5410037	**Karmutsen**	Basalt			
JL06-090	396953	5416048	**Bonanza**	Andesite	x	x	
JL06-091	396676	5415855	**Bonanza**	Dacite (?)			
JL06-092	396437	5415837	**Bonanza**	Basalt	x	x	
JL06-093	400758	5414266	**Bonanza**	Basalt	x	x	
JL06-094	403588	5405970	**Karmutsen**	Volcanic breccia			
JL06-095	390866	5406516	**Bonanza**	Intermediate dyke			
JL06-096	390914	5406380	**Bonanza**	Basaltic andesite			
JL06-097	390998	5409029	**Bonanza**	Ash tuff			
JL06-098	393691	5409208	**Karmutsen**	Basalt			

Sample #	UTM Easting*	UTM Northing	Map Unit	Rock Type	Thin Section	WR Chem	Mineral Chem
JL06-099	389123	5408146	**Bonanza**	Dacite (?)			
JL06-100	409315	5390155	**WCC**	Cumulate gabbro	x	x	x
JL06-101	390187	5388291	**WCC**	hornblendite	x	x	
JL06-102	393023	5386699	**WCC**	Gabbro			
JL06-103	393105	5386920	**WCC**	Gabbrodiorite		x	
JL06-104	393105	5386920	**WCC**	Gabbrodiorite	x	x	
JL06-105	393135	5386903	**WCC**	Cumulate gabbro	x	x	x
JL06-106	404168	5389078	**WCC**	Olivine hornblendite	x	x	x
JL06-107	412336	5386098	**WCC**	Granite dyke	x	x	
JL06-108	411744	5388666	**WCC**	Gabbrodiorite	x	x	
JL06-109	413319	5390355	**WCC**	Gabbrodiorite			
JL06-113	397432	5386029	**WCC**	Olivine hornblendite			
JL06-114	397303	5386033	**WCC**	Layered gabbro	x		
JL06-115	397539	5385582	**WCC**	Gabbrodiorite			

* UTM Zone 10, NAD 83
WR; whole rock

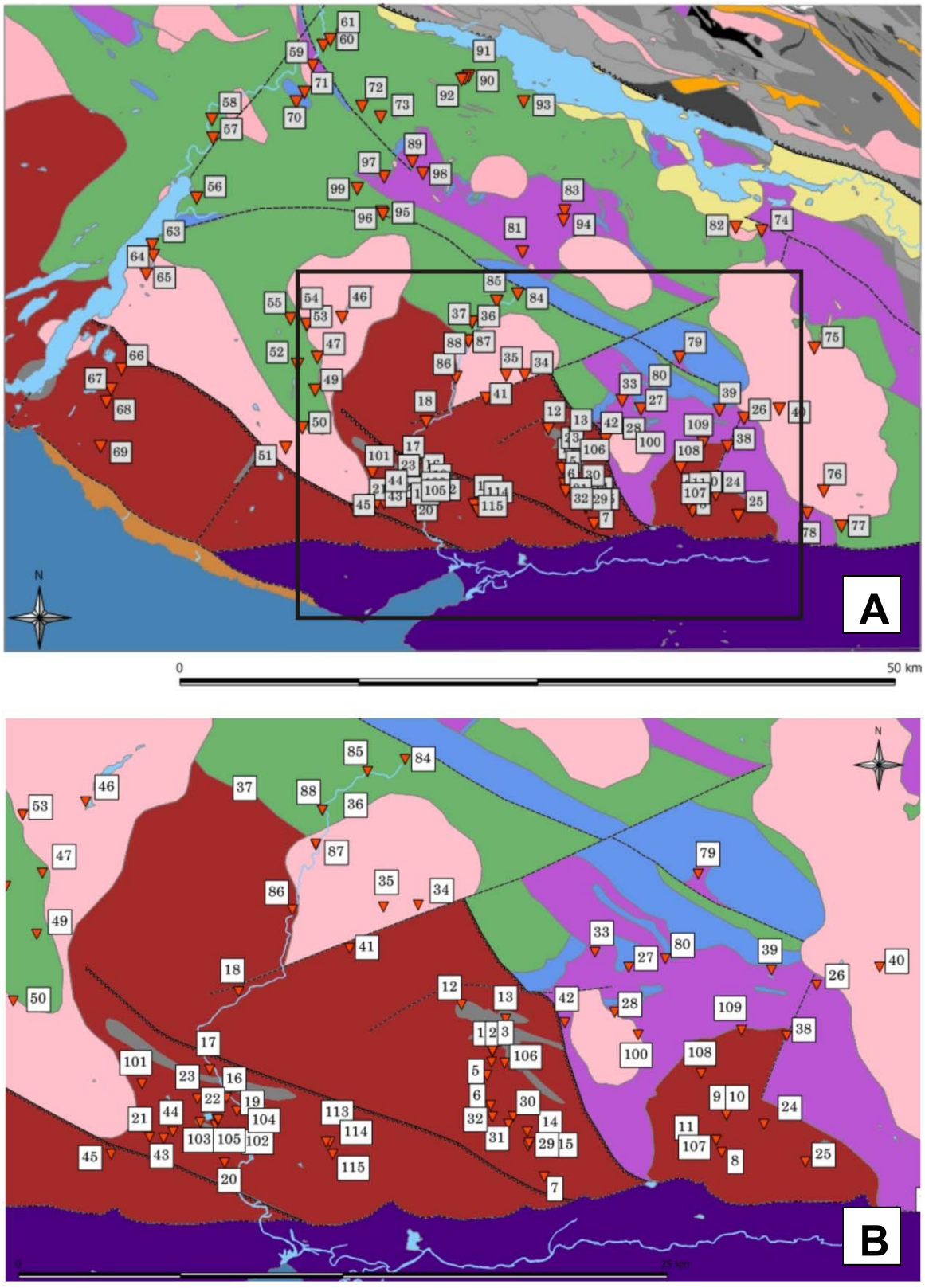

Figure 20. Sample locations for all samples collected during 2006 field mapping. Location of B is outlined in A.